

Design for Additive Manufacturing

Marcus Moe Johansen

Stian Andre Løvås

Bachelor's thesis in Mechanical Engineering

Bergen, Norway 2022



Design for Additive Manufacturing

Marcus Moe Johansen

Stian Andre Løvås

Department of Mechanical- and Marine Engineering

Western Norway University of Applied Sciences

NO-5063 Bergen, Norway

Høgskulen på Vestlandet
Fakultet for Ingeniør- og Naturvitskap
Institutt for maskin- og marinfag
Inndalsveien 28
NO-5063 Bergen, Norge

Cover and backside images © Norbert Lümmen

Norsk tittel: Design for additiv tilvirkning.

Author(s), student number: Marcus Moe Johansen, 582417
Stian Andre Løvås, 579581

Study program: General Mechanical Engineering

Date: June 2022

Report number: IMM 2022-M07

Supervisor at HVL: Saeed Bikass

In cooperation with: Bergen Engines

Contact person: Sjur Herheim

Antall filer levert digitalt: None

Preface

This bachelor thesis was written in the Department of Mechanical and Marine Engineering at Western Norway University of Applied Sciences (WNUAS) and it was created in cooperation with Bergen Engines, which provided relevant cases for the case studies performed and provided supervision during the design process. The supervisor for the thesis was Associate professor Saeed Bikass. The thesis was written by students of mechanical engineering.

We would like to thank Associate professor Saeed Bikass for his great communication and good supervision during the whole thesis. We would also like to thank Sjur Herheim and Svein Eidsvik from Bergen engines, for supervising us and contributing to the content of the thesis. We would also like to thank Frode Jansen for helping us produce the test equipment needed and Harald Moen for helping us set up the test instrument to perform the lab tests.

Abstract

This report aims to give a good understanding of how to design for additive manufacturing, as the technology requires different considerations than for example casting or machining. It has been completed in cooperation with Bergen Engines, which provided interesting engine parts they wanted to adapt for additive manufacturing and possibly print as a proof of concept. These parts were key engine components and most of them required high stiffness to maintain the timing of the engine cycle. The goal of the redesign was to reduce weight, and maintain the stiffness of the parts while adapting them for 3D printing. The report includes information and key aspects of the most relevant 3D printers for prototyping and metal printing currently available, Powder bed fusion, binder jetting, and direct energy deposition. The design aspects of this thesis focus on the Powder bed fusion technology as it is regarded as the best for the case studies in this report.

The redesign of parts was done using Creo Parametric CAD software which has tools and possibilities to create topology optimized geometries and lattice structures. These advanced geometries were analysed in ANSYS finite element analysis software, which provided the anticipated strength and stiffness of the parts. To confirm the software's calculation an experimental test was done to verify the designed geometries. Destructive tests were conducted to test the maximum strength and deflection of the new geometries compared to the originals.

The redesign using generative design made it possible to save considerable weight on the parts. This design is based on Michell structures which have the strongest shapes known and helped maintain the stiffness in the parts. The completed lab tests confirmed the simulations of the complex geometry in Ansys were correct.

Sammendrag

Denne oppgaven skal gi en god forståelse av hvordan man kan tilpasse design til additiv tilvirking, siden denne teknologiens krever andre hensyn en støping eller konvensjonelle tilvirknings metoder. Oppgaven ble laget i samarbeid med Bergen Engines som kom med interessante motor deler de ville tilpasse til additiv tilvirkning, for å se om man kan beholde stivhet samtidig som man reduserer vekten på delene. Stivheten er viktig for timing på forbrennings syklusen til motorene. Denne oppgaven handler om hvordan man kan tilpasse et design til å benytte seg av fordelene additiv tilvirkning byr på og hvilke begrensninger teknologien har. En beskrivelse av de mest relevante teknologiene blir gitt, powder bed fusion, binder jetting og direct energy depositing. Teknologien som er mest relevant for prototype deler og metall printing er powder bed fusion, som denne oppgaven baserer seg på å bruke.

Redesign av delene ble gjort med Creo Parametric CAD programvare, som inneholder avanserte funksjoner som topologi optimalisering og lattice strukturer. Geometriene lagd ved hjelp av disse metodene ble kontrollert med ANSYS element metode analyse, som gir et estimat av hvordan geometrien vil oppføre seg gitt de laster som er definert. For å bekrefte svaret fra ANSYS ble det utført en lab test som strakk og presset delene til destruksjon, og sammenliknet de originale geometriene med de nye og ga oss maks krefter og defleksjon før brudd.

De nye geometriene klarte å spare betydelig med vekt samtidig som de bevarte stivheten til delene. Dette ble oppnådd ved hjelp av geometri basert på Michell strukturer som er den sterkeste strukturen kjent. Lab testen ga gode resultater og styrket analysen gjort med ANSYS og bekrefter at delene oppfører seg som forventet.

Table of contents

Preface	V
Abstract	VII
Sammendrag	IX
Nomenclature	XV
1. Introduction	1
1.1 Background	1
1.2 Objective	1
2. Literature Review	2
2.1 Available Technologies	2
2.1.1 PBF – Powder Bed Fusion	2
2.1.2 Binder Jetting	2
2.1.3 DED - Direct Energy Deposition	3
2.2 Material selection	3
2.3 Designing for additive manufacturing	4
2.3.1 Limitations	4
2.3.2 Advantages	6
2.4 Nondesign aspects of additive manufacturing	7
2.5 Companies in Norway	8
3. Method	8
3.1 Optimization using lattice structures	8
3.1.1 Basic setup	8
3.2 PTC CREO Generative design	9
3.2.1 Basic setup	10
3.2.2 Advanced use	12
3.2.3 Bugs and instability	12
3.3 Price calculation With AmoTools	12
4. Case studies	13

4.1	Case 1: Bracket.....	13
4.1.1	Original Bracket GJS-500-7.....	14
4.1.2	Redesigning the Bracket.....	17
4.2	Case 2: Rocker Arm	23
4.2.1	Original Rocker Arm GSJ-500-7.....	23
4.2.2	Redesigning the Rocker Arm	26
4.3	Case 3: Toolholder	28
4.3.1	Original Tool Holder	28
4.3.2	Redesigning Tool Holder	30
4.4	Case 4: Pressure indicator	31
4.4.1	Original Pressure Indicator S235JR	32
4.4.2	Redesigning the Pressure Indicator	34
5.	Results and Discussion	35
5.1	Numerical Results	35
5.1.1	Case 1: Redesigned Bracket.....	35
5.1.2	Case 2: Redesigned Rocker Arm.....	44
5.1.3	Case 3: Toolholder	50
5.1.4	Case 4: Pressure Indicator valve.....	52
5.2	Experimental test.....	55
5.2.1	Stretch Test.....	55
5.2.2	Estimated results.....	57
5.2.3	Test Set-up.....	57
5.2.4	Test results.....	58
5.2.5	Sources of error	60
5.3	Discussion	61
5.3.1	Comparing case 1, Bracket.....	61
5.3.2	Comparing case 2, Rocker arm	61
5.3.3	Comparing case 3, Toolholder	62

5.3.4	Comparing case 4, Pressure Indicator Valve.....	63
5.3.5	Experimental test result	63
6.	Conclusion	64
	List of figures	65
	List of tables	69
	References	70
	Attachments.....	71

Nomenclature

PBF	Powder Bed Fusion
FDM	Fused Material Deposition
DED	Direct Energy Deposition
FE	Finite Element
FEA	Finite Element Analysis
CAD	Computer-Aided Design
M	Moment
F	Force
L	Length
STEP	The Standard for the Exchange of Product Data
PLA	Polylactic Acid
E-PLA	Easy Polylactic Acid
SLM	Selective Laser Melting
SLS	Selective Laser Sintering
RPD	Rapid Plasma Deposition

1. Introduction

Additive manufacturing is still a relatively new concept, usually referred to as 3D printing. Which is a process of selectively adding or melting thin layers of material on top of each other to create advanced geometry and functional assemblies. The concept is continually developed to use different techniques to increase speed and quality, while minimizing the cost, constraints, and post-processing of parts. The current most used printer technologies will be explained in detail with a focus on metal printing technology. Additive manufacturing can bring some advantages to companies which include lowered cost and delivery time, easier logistics, and rapid prototype manufacturing, which leads to a shorter design phase.

1.1 Background

Most engineers and production managers have heard of the possibilities of additive manufacturing, but there are also some little-known limits and constraints to the technology. Some of these limitations are the print size, material quality, thermal stress, shrinkage, and the surface quality achieved. There are several factors affecting these components, which could be the purity of material and its standardized size of grains, the shape of grains and the composition, build temperature and pressure, shielding gas used, wavelength and energy of the laser, and tolerances on the machine hardware.

The main objective was to redesign a rocker arm and its bracket so that it is optimized for additive manufacturing, the goal was to decrease the weight while maintaining stiffness. A detailed explanation for why design choices were made has been provided, and an expanded look at the more challenging decisions. To obtain more experience, case studies of a Toolholder and a Pressure indicator valve were redesigned as well. The relevant drawing and boundary conditions for the parts were provided by Bergen Engines.

The project's first phase was reading the newest literature, finding relevant sources on the subject, and practising and testing the computational tools needed to redesign the parts. The next phase was to create multiple iterations of the parts, while looking at different ways that the objectives could be met, focusing on the advantages that additive manufacturing gives.

1.2 Objective

In this thesis, the objective is to understand the general design aspects of using different metal additive manufacturing methods. It will focus on the details of the capabilities and limits, which features are possible and not possible. It will also look at the different capabilities and limits of some of the relevant computational tools, predominantly Creo Parametric and ANSYS. The theory will mainly be obtained through the newest available literature and scientific papers.

Central in the thesis will be redesigning four parts supplied by Bergen Engines for metal additive manufacturing. These parts have some advanced features which will demand a good understanding of how additive manufacturing works and its limits. These parts will be redesigned, and then printed and tested with a method for static tension and compression.

2. Literature Review

In the thesis, some important aspects will be considered and explained to determine the full benefits and possibilities of metal additive manufacturing. This includes the most relevant metal printing technologies, different materials, and design limitations.

2.1 Available Technologies

Much research has been done in the field since the first printers were unveiled, and there have become many variations of the technology, some of the most relevant for metal production are described in the next subchapters. Power bed fusion would be the preferred choice for the thesis as it is easy to compare to the existing parts' strengths and the build orientation of the bracket arm benefits from a low anisotropy in the z-axis. (Diegel, Nordin, & Motte, 2020, p. 33)

2.1.1 PBF – Powder Bed Fusion

This technology consists of three main different laser types and technologies. Laser sintering (LS) for polymers, Selective laser melting (SLM), and Electron Beam Melting (EBM) for metals, as higher temperatures are needed. Commonly for all these are that a laser hits an angled mirror and steers the beam on the surface of the print bed. The print bed is a platform that lowers as a Material roller takes the material powder from the adjacent chamber over to the platform. The mirror steers the beam to the desired coordinates and sinters the desired material particles for each layer, which builds a cross-section. Then a new layer is added, and the next cross-section is sintered to the previous, layer upon layer creates a part. (Diegel, Nordin, & Motte, 2020, p. 33)

Materials available are stainless steel, aluminium, titanium, cobalt chrome alloy, tool steel, tungsten, nickel alloys, copper, and precious metals, such as gold. Some polymers are also available. (Toyserkani, et al., 2022, p. 86). The powder is of preferably grain sizes between 30 and 40 μ m, some smaller grains are also useful as they will interlock between the larger ones and prevent empty pockets in the material. (Diegel, Nordin, & Motte, 2020, p. 124)

The strength and quality of the parts are comparable to cast components, given good grain quality to avoid imperfections and voids. Some small anisotropy is anticipated, but small compared to other technologies

2.1.2 Binder Jetting

This technology uses a printer head, which deposits a binder onto the surface of a traditional print bed. The binder could be of many different materials and adhesives, and one of the most used cases of this technology is creating gypsum (ceramic) moulds and investment casting patterns. Ceramics would need to be treated with a special glue afterwards to keep their strength. Metal powders have been applied to a binder in the same way and make it possible to brush off the excess powder until we have a fragile “green” part, consisting of powder and binder. Then this green part will be heated in a furnace to sintering temperature to create a functional metal part.

Many materials can be used as the binding of powder applies to most materials. For metal materials sintering would be needed to create a functional part. Sintering in an oven could impose its own difficulties and a shrinkage of 3-20% can be expected for some materials, and this is difficult to anticipate as it vary on both material and geometry. Handling the fragile green part imposes some risks of damage during movment. Considering this technology would be best suited for serial production, as it would be difficult to anticipate the shrinkage of a prototype. (Diegel, Nordin, & Motte, 2020, p. 23)

2.1.3 DED - Direct Energy Deposition

There are some differences in the practical solution to this technology. In common the solutions have a laser which is feed material powder or wire that melts on impact. Like some welding techniques, DED builds upon the existing layer and gives much freedom of design, and can print on existing geometries, for maintenance and altering old designs. The process is much faster than print bed technologies as the layers are much coarser and larger, reducing the total layers and the height of the build. The technology is known to be less accurate than print bed technologies and usually requires CNC machining afterwards for surface finish and regular dimensions.

Known different variations of the technology consist of LENS (Laser Engineered net shaping), DMD (direct metal deposits), CLAD (3D laser cladding) (Diegel, Nordin, & Motte, 2020, p. 36)

2.2 Material selection

Additive manufacturing has a lot of different technologies offering different materials. This thesis focuses on metal AM, but a lot of the design challenges are similar to plastic AM. Ferrous AM materials consists of a lot of different alloys, which can be tailored to specific tasks. Ranging from 316L to H13 tool steel.

Because of the low material cost of printing, compared to the price of using the printer, a lot of studies and R&D have been put into the more commonly expensive materials, which can be challenging to work with using traditional manufacturing methods. This includes titanium and nickel-based alloys.

Nickel-based alloy is mostly used in the aerospace industry, because of its high strength even at high temperatures. Mostly used in nozzles and rocket parts, these are hard to make with traditional manufacturing methods. The metals with the most research currently available are Inconel 625 and Inconel 718. These alloys have a high Yield strength to weight ratio and a medium young modulus. Which makes these alloys relevant for high strength parts in corrosion environments and with minimal stiffness requirements. While materials like 316L lose most of their mechanical strength at around 400 degrees Celsius, Inconel 625 can maintain its strength up to 700 degrees Celsius due to its high melting point. (Desu, 2015) and (Mauro M. de Oliveira, 2018)

Titanium alloys are known for having the highest strength to weight ratio, for this reason, it is mostly used in aerospace and in machines where the moment of inertia must be reduced. The most commonly used titanium alloy is Ti-6Al-4V also known as Grade 5 titanium. Most titanium alloys are about 40% lighter than most ferrous alloys. The main weakness of these alloys is their low Young's modulus, which leads to the need for extra material to maintain the stiffness of the redesigned part. When stiffness is not a requirement, titanium alloys are a great choice. Companies like General Electric are now studying new powders which make Titanium-Aluminium alloys, these maintain low weight while increasing Young's modulus. Because this new alloy is not in use today, it will not be focused on during the case studies. In this thesis, it is vital to reduce the moment of inertia as much as possible on the rocker arms, and as the goal is to reduce the weight of the bracket as much as possible, titanium alloys are expected to be a good choice as shown in Table 1.

Table 1. Comparison of different alloys for additive manufacturing. Properties for Inconel 625 from (Zhihua Tian, 2019) and (Fábio Gustavo Lima Pereiraa, 2018). Properties for GJS-500-7 from (dijkkamp, 2022). for Ti-6AL-4V from (Shunyu Liu, 2019) and (Galinak Asperovicha, 2015). Also for 316L from (Rakish Shrestha, 2021).

	<i>GJS-500-7</i> <i>(original material)</i>	<i>Ti-6Al-4V</i>	<i>Inconel 625</i>	<i>316L</i>
<i>Density [g/cm³]</i>	7,3	4.4	8,3	8
<i>Yield Strength [MPa]</i>	320	990	743	485-535
<i>Ultimate Strength [MPa]</i>	500	1095	1043	594-697
<i>Young Modulus [GPa]</i>	169	112	165-207	165-196
<i>Fatigue Limit [MPa]</i>	165	500	240	340-440

As can be seen in the table above. The preferred material for high strength to weight ratio is titanium. It also has a high fatigue limit, though it lacks stiffness. This makes the usability somewhat limited. Nickel alloys are better at stiffness, while maintaining a good strength to weight ratio, but have a lower fatigue limit. They are also the most corrosion-resistant material in the selection. Stainless steel has high strength and fatigue values but its young modulus to weight is a bit lower than casting steel.

From the data above, it has been concluded that only Grade-5 titanium and 316L are relevant for the case study concerning the parts from Bergen Engines. Since Inconel 625 has a lower Young’s modulus to weight ratio than 316L and there is no need for high-temperature resistance, including this material in the case study would be a waste of time. Instead, the third material in the case study will be GJS-500-7. Even though this material is not printable, it is a great way to compare the advantages additive manufacturing provides when only changing the geometry of the part.

2.3 Designing for additive manufacturing.

There are several limitations to additive manufacturing and it’s important to have a design that is adapted to the technology and method that is going to be used to print the parts. During the design period, it is also important to plan the possible post-processing and understand which quality can be anticipated from the final part.

2.3.1 Limitations

This chapter considers powder bed printers, as that is the technology that will be used in this thesis. Due to the function of the printers, some design limitations need to be considered.

The biggest limitation is that there can be no overhanging material, it would collapse if it’s not built with support material. A general rule is that the printer can print in 45° degree expanding angles. (Diegel, Nordin, & Motte, 2020, p. 141) If this is not possible, changing the design to include support and create an accepted angle is preferred, as it often increases the strength of the part and would be free compared to having excess support material. If weight or volume is important removable support material could

be made temporarily to support the print. Support is often generated in the printer's own software and is something the operator of the printer usually decides.

Secondly, there needs to be sand shaker holes for hollow structures. Using PBF, the powder is filled in each layer and will be trapped inside internal volumes if there are no holes to extract it through, two holes are usually needed as air pressure is applied to push out the powder through a venting hole.

Tolerances can be expected to vary between different printers and the settings they operate on. Generally, a tolerance of 0.5 mm can be expected. (Diegel, Nordin, & Motte, 2020, p. 111) If post-machining is planned 0.5mm extra material is recommended, and the double of that on diameters. Different problems could cause lower tolerances, like warping of the part due to different cooling rates of the material, usually because of uneven thickness of the part. A printer with a closed environment for printing helps solve this. The surface roughness that can be expected is comparable to a roughcast part. It will need polishing if low roughness is vital. Polishing can also increase the strength of the part by removing micro-notches.

Temperature differences could also impose internal stress on the part, and an even thickness is preferred to reduce internal stress and the risk of cracks. If internal stress is anticipated, post-heating the part in an oven to recrystallization temperature will relieve the stress.

Powder bed fusion is recognized as the technology which has the most isotropic strength of the print given print direction. There is expected to be a small weakness in the z-direction, in the height of the build. This is often small enough to neglect. (Diegel, Nordin, & Motte, 2020)

It's possible to print assemblies with 3D printing technology, in PBF this is somewhat limited due to the powder which will fill every tolerance and coarse surface roughness. The joint will be a loose fit and too coarse to move smoothly. It could have some uses but for high-frequency movement, it will not be a good option.

After the print, the supports will need to be removed by milling or grinding and will be included in the post-processing of the part. A polish is usually needed after this removal. If post-machining is needed a square or circular shape is preferred to be able to fix the part during machining.

2.3.2 Advantages

The main advantage of additive manufacturing is that complexity becomes “free”, which means that the design engineer can add complex features without this adding to the price of the part. When designing for conventional manufacturing, all features like chamfers, rounds, and holes add cost from setting up and machining time. When using additive manufacturing, for example, chamfered edges lead to less material needed, which again actually leads to a slightly cheaper part.

This makes it possible to use complex geometry in parts, the most promising method for this is generative design, also known as topology optimization. This is the process of optimizing the stiffness to weight ratio, removing unnecessary material, given a load case. The remaining material usually mimics the complex geometry of Michell structures seen in Figure 1, which can be near impossible to manufacture with machining or casting. Earlier, the optimized geometry was used as a template for inspiration, and a new part that is easier to produce was made.

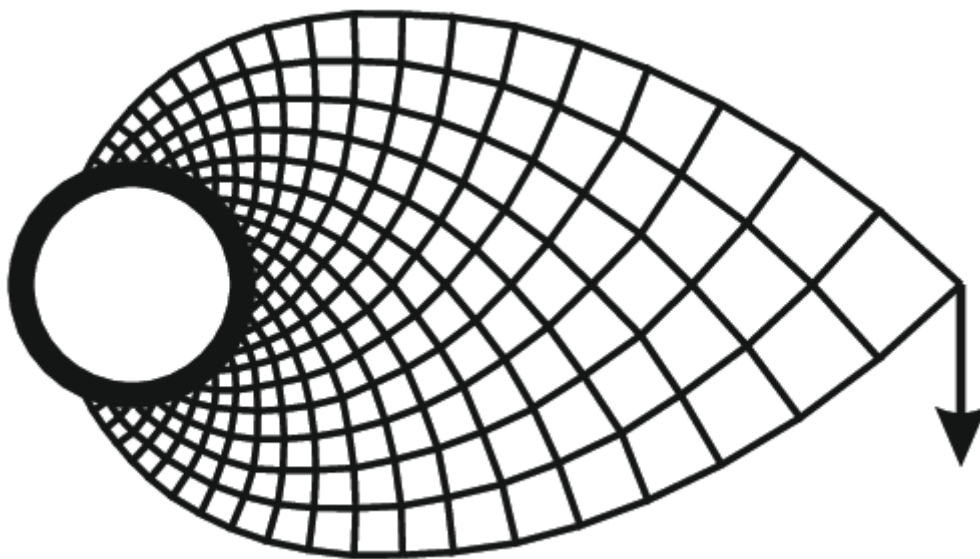


Figure 1. Michell structure (Picelli, 2015)

Today it is possible to directly convert these optimized geometries into STEP or STL files which can be printed directly. More modern software also can control the optimization, for instance, one can specify the build direction so that there is no expansion larger than 45° degrees. This can save a lot of weight on the part and save time for the design engineer. This will be one of the main focuses of the case study in the thesis.

Another example of complex geometry that can be added is the possibility to add small internal complex channels, and thin walls. For example, oil channels in a part that usually had to be straight can now bend around inside the complex topology optimized geometry. This is hard to do with casting, as that has limitations on how small details can be because of the cohesive forces in the melted material.

Another design element that can be used when designing is the use of lattices, usually used in parts when there is no load requirement, but some stiffness is wanted. The reason that the parts must not have any critical load requirement is the complexity of validating the lattices in FEA software. Some lattice structures can be simplified for use in simulation, but these are limited to simple structures where all the cells are complete.

There are possibilities to print complete working assemblies. The tolerances will be coarse, and the bending of the parts is only available when printing in plastic or with thin ductile metals. This makes the use cases limited, but for low force, slow movements it's possible to print it directly. This opens the possibilities for machines with internal movable parts, which would not be possible with traditional manufacturing.

2.4 Nondesign aspects of additive manufacturing

The capabilities of this manufacturing method can lead to more efficient parts with less waste of material. New design possibilities will lead to new machines and new technologies to further increase the efficiency and function of existing machines.

The key aspect of this production method is its availability, if you have the 3D file of the part, it can be printed from all around the world. The transportation cost and emissions could be eliminated in the supply chain, and the delivery time can be cut to under a day for prioritized parts. If a vital part breaks for a ship, which is in port somewhere in the world, it could be locally printed using their design and file. This could revolutionize delivery time and the need for spare part storage.

Additive manufacturing also opens the door for digital warehouses. For large companies, the warehouses alone are a huge expense. If you could produce on need, rather than for the expected demand, storage facilities could be greatly reduced thus saving cost.

2.5 Companies in Norway

Additech is located in Bergen and is an innovative additive manufacturing and design company currently using a Lasertech 30 SLM printer for Inconel 625 parts. They have multiple nonmetal printers and provide engineering and consultant services to adapt a design to additive manufacturing or complete the design of new parts to the customer's specifications. They are one of Aker solutions innovation businesses and get funding from them.

In Oslo, Norsk Titanium is using a proprietary RPD printer that prints with a very high layer height that needs a lot of post-processing. Because of the high layer height and bad tolerances, this is not comparable to technologies like SLM and SLS. They are one of the first additive manufacturing companies that produce parts for the civil aviation sector, now they have contracts with Boeing.

In 2018, Onesubsea was one of the first companies in Norway to start using the advantages additive manufacturing provides. As they needed complex geometry for the impeller of their multi-phase compressor, they had to resort to additive manufacturing.

3. Method

Because of the special limitations present when designing for additive manufacturing, manual design of the parts is usually not plausible. In this chapter, the tools available for this thesis will be described.

3.1 Optimization using lattice structures

An interesting option to save weight and material in additive manufacturing is using lattice structures. Lattices are structures using thin arms or webs as infill in a body to create a volume with low density and are in some cases considered a good choice for weight saving. This requires the body to be wide, since the sides of the lattice structure usually do not provide any strength, the preferred design choice is to have an almost closed volume with an infill of lattice, in PBF, binder jetting and all printer technologies using powder beds, this design would require "salt shaker holes" to remove internal powder material.

3.1.1 Basic setup

To create a lattice structure in a part, a multi-body part should be created. The area that should contain the lattice structure has to be its own body. It's possible to create it as an infill or generate it in the whole body. In Creo Parametrics there are multiple native cell types to choose from. 2D shapes are triangular, Square, Pentagonal, and 2D Octagonal as shown in Figure 2. And is possible to customize the height, length, and width of the cells.



Figure 2. 2D Cell shapes

The advanced 3D shapes possible to choose from are 3D octagonal and stochastic as shown in Figure 3.



Figure 3. 3D Cells shapes

These settings are somewhat limited. There are companies and software focusing on creating more advanced and better performing lattices than are possible with this software. The most advanced inbuilt option here is the stochastic cells, which are nodes with multiple connections to each other, Sizes and amount can be customized. Figure 4 is an example using stochastic cells in Creo Parametric.

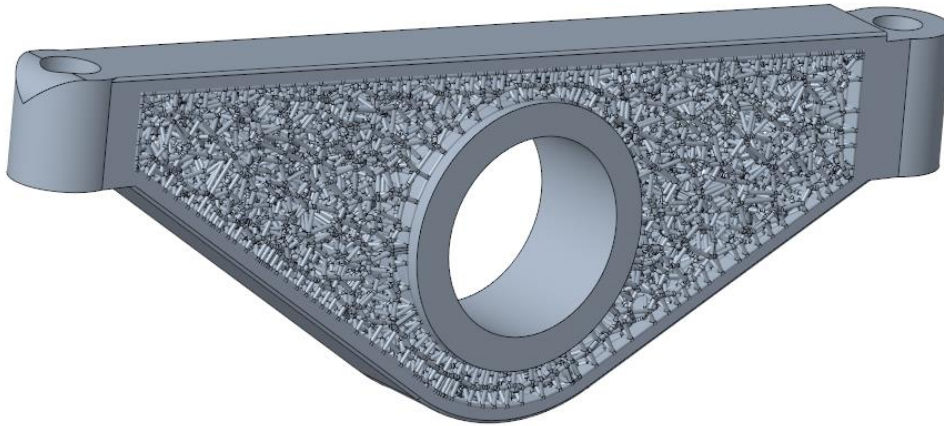


Figure 4. Rocker Arm design with lattice

Using lattice structures makes it difficult to analyse in finite element software. As the mesh setting needs to be extremely low size to be able to fit the nodes and bends in the part. This also increases computation time greatly. Physical testing of parts with lattice is recommended to obtain mechanical properties.

3.2 PTC CREO Generative design

The most powerful tool when designing for additive manufacturing is as mentioned earlier topology optimization, the software that is used in this thesis is specifically Creo Parametric 8 Generative design. the goal of topology optimization is to maximize the stiffness to weight ratio. Figure 5 below is an example of how the topology optimization mimics the Michell truss in Figure 1.

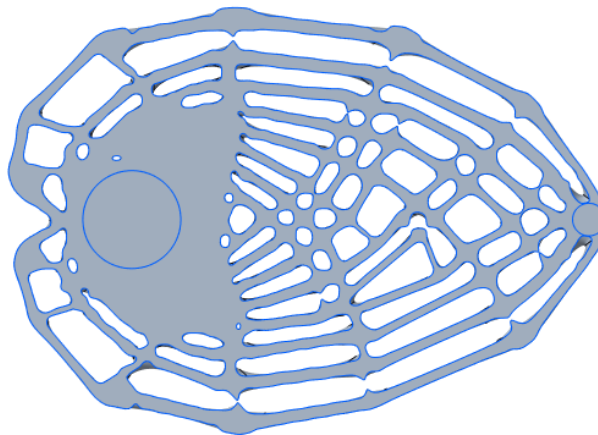


Figure 5. Example mimicking Michell structure

3.2.1 Basic setup

To perform a topology optimization with this tool the first step is to modify or recreate the part, splitting it into two or three main bodies. The first body is the starting geometry, this can be described as the outer boundaries of the part being generated. The original step file received can be set as starting geometry, but this is not recommended. To maximally utilize the advantages of the tool, it is recommended to expand this geometry to the outer boundaries allowed. This is dependent on the assembly provided with the part being designed. The second body needed is the preserved geometry, this geometry will not be modified in the analysis. This is also the body where all loads and boundary conditions will be applied. It is recommended to try to minimize this area as much as possible, only leaving the geometry that is needed to apply the boundary conditions if possible. The third body is the excluded body, this is an optional body that can be used to exclude geometry from being optimized. This is similar to the starting geometry but does not need to have loads and boundary conditions applied. Figure 6 shows the three different body options.

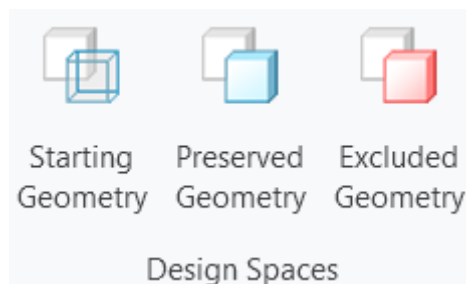


Figure 6. Generative Design options

The next step is to define all the loads and boundary conditions. This is done similarly to most FEA software but is somewhat limited. The constraints are limited to “Fixed”, “Displacement”, “Cylindrical” and “Planar”. The loads are as shown in Figure 7 and are limited to “Force”, “Moment”, “Pressure”, “Centrifugal”, and “Linear acceleration”. There is also the possibility to define contacts between the bodies, but this substantially increases computation time and was therefore avoided. In the newest version of Creo, it is also possible to define multiple design cases, it is important to state that this was not a possibility when this thesis was started.

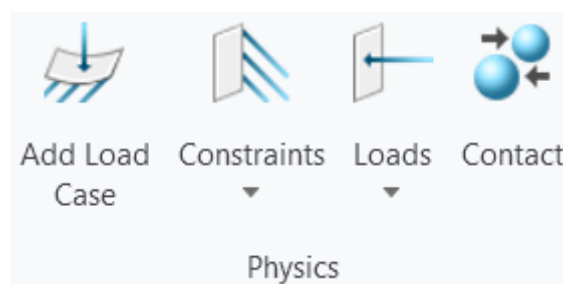


Figure 7. Different boundary conditions in Creo

The next part of the analysis is to define the design criteria, this is used to control the analysis in a specific direction. The main criteria that are mandatory to define are the percentage of material to conserve. The other optional settings include “Build Direction”, “Linear Extrude”, “Material Spreading”, “Parting Line”, “Planar Symmetry” and “Minimum Crease Radius”. “Linear extrude” is not directly relevant to this thesis, as it controls the analysis so that it outputs a 2D optimization that can be used in for example a plasma cutter. “Material Spreading” is one of the most important settings, as this controls how thin the struts of the geometry will be. As seen earlier, the Michell truss consists of many very thin struts, and even though this is the best topology available, this is not optimal for practical use.

This is mostly because the geometry becomes unnecessarily complex, and the thin geometry can lead to poor fatigue properties. The “Parting Line” criteria are also not relevant for this thesis, as this is used when designing for die casting. “Minimum Crease Radius” is an important criterion, this limit the design so that there are no sharp creases and therefore can help when trying to control the maximum stresses. Criteria like “Build Direction” and “Planar Symmetry” are self-explanatory. Figure 8 shows an overview of the different design options.

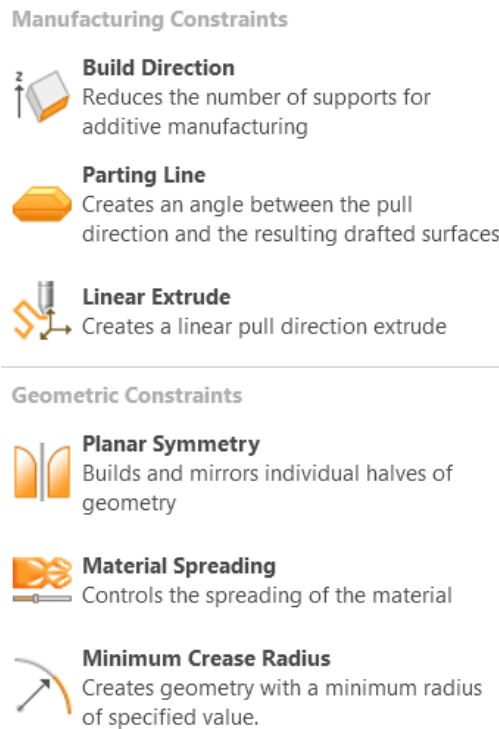


Figure 8. Generative Design options

After the topology optimization has been completed, the part needs to be generated. When generating the part, it is important to export it with as high precision as possible, different options are shown in Figure 9. The export settings that got the highest number of successful exports were when result output was set to “New Part” and “Reconstructed” and “copy only the result geometry” is selected. It is also important to select the highest resolution level, as the output solid part is not identical to the mesh from the analysis, but this makes it as similar as possible. To verify the analysis and the generated part, it is recommended to run a new simulation in another FEA software where it is easier to modify the mesh.

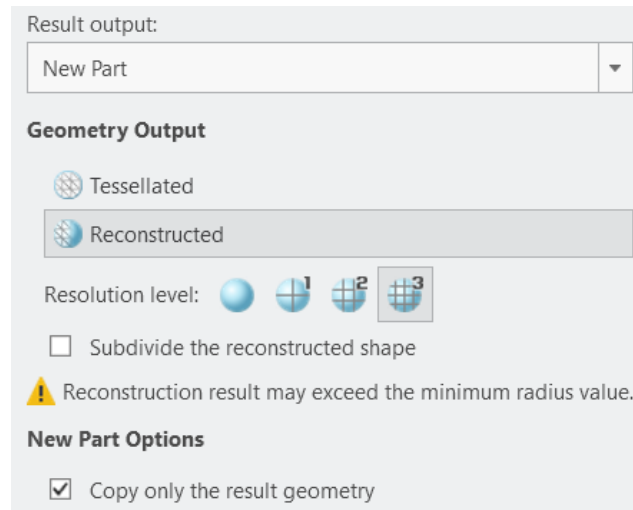


Figure 9. Generate options in Generative Design

3.2.2 Advanced use

The main weakness of the generative design is that the analysis optimizes the stiffness of the part, without regarding the stresses. Because of this, the most common method to find the best part possible is to run multiple analyses where the percentage of material conserved is slowly being raised until the stress is acceptable. Because of the nature of this thesis, where the goal was to minimize the weight while maintaining a specific stiffness, using this method would lead to a lot of extra unnecessary weight and an uneven distribution of the stress. This is naturally dependent on the material being used, as titanium has an extremely high yield strength while having a relatively low Young's modulus. One way to circumvent this flaw is to adjust the starting geometry so that there is already material present in the areas of high stress. This will control the analysis so that even more material will be added to the area, and therefore the stress will be lowered. This will be expanded more on in the relevant parts where this method was used.

3.2.3 Bugs and instability

This is a relatively new tool that was first implemented in Creo Parametric 7, and therefore has multiple bugs and suffers from instability. This was the biggest challenge in the thesis and led to the first part being designed taking a substantially longer time than planned. The main issue was that the topology optimized parts being output after an analysis is not solid geometry, but rather a mesh format. Creo then needs to convert the part to solid geometry using the freestyle tool. This tool is very sensitive to the inputs of the analysis, and most outputs end with an error message. Considering that each analysis took up to two hours, the first months of working on the thesis were therefore used to find a setting that would lead to a successful solid body. On the bracket for instance, it took over 60 attempts to get a successful part. When designing the two last two cases it only took around 5 attempts to get a successful part.

3.3 Price calculation With AmoTools

To calculate the expected price for the manufactured parts, Amotools was used. This is free software developed by Etteplan that estimates the price to 3D print parts in metal, based on geometric parameters. This is very useful as there is no need to upload the specific STEP files that can be classified. The tool requires the height, volume, and surface area of the part being manufactured.

Additech was contacted and they confirmed that the prices provided by Amotool are comparable to their own estimates.

4. Case studies

The data received from Bergen Engines did not give us any maximum stress or deformation limits. Different loads and geometry constrictions were provided including mechanical drawings and Step files of the parts. A stress and deflection limit were needed for the redesigned parts. This information was obtained by doing a finite element analysis of the original step file in ANSYS. The procedural method of this was to first define the given loads as accurately as possible. The loads were dynamic with the highest maximum reactive force of 18 000N on one of the sides on the rocker arm, the other force is not given but is not as relevant, as it's a motion and the force the resistance of it.

Bergen engines provided four parts for the case studies, a rocker arm, its bracket, a pressure indicator valve, and a tool holder for assembly of the engine cylinder. Throughout these case studies, we have obtained much information on which designs that work and not, what kind of weight savings that can be achieved and the cost of using this technology.

4.1 Case 1: Bracket

The bracket has two rocker arms and a shaft connected. The stiffness of this part is crucial for the timing of the exhaust and inlet to the cylinders. The part is today made by casting and is produced in GJS-500-7. The goal is to decrease the weight as much as possible while maintaining the stiffness. Good fatigue properties are also crucial, as the bracket is under a cyclic dynamic load with high spikes in force. The case study will be comparing the possible weight savings and price differences using GJS-500-7, 316L, and TI-6AL-4V. There are no material requirements from Bergen Engines, thus these were selected for their properties and usability in additive manufacturing. The original bracket can be seen in Figure 10.

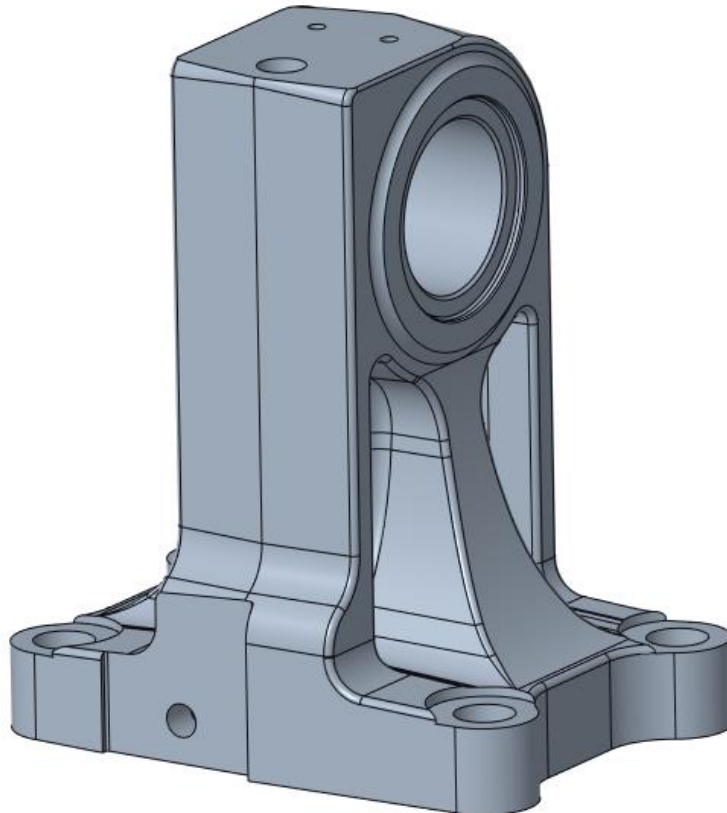


Figure 10. Original Bracket

4.1.1 Original Bracket GJS-500-7

From the values collected from the rocker arm calculations, it can be seen that the reaction force working on the bracket is 38500N. Using the dimension of the shaft, and the position of the rocker arm, the moment can be calculated. Both the force and the moment will be placed at the shaft hole as seen in Figure 11.

$$M = F * L = 38\,500\text{N} * 48\text{mm} = 1\,848\,000\text{Nmm}$$

A: Static Structural
Bearing Load
Time: 1. s
04/03/2022 22:44

A Bearing Load: 38500 N
B Moment: 1.848e+006 N-mm

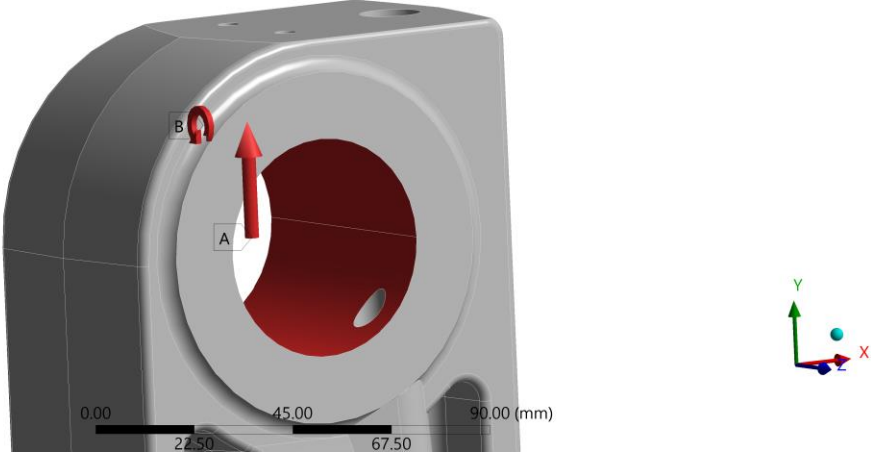


Figure 11. Bracket moment and bearing load

To simulate the four M18 bolts used to mount the bracket, 24mm circles around the holes are set to fixed in all directions except the Y direction. The bottom is set to fixed in the X and Z direction to simulate the friction. Boundary conditions are shown in Figure 12 and Figure 13.

A: Static Structural
Displacement
Time: 1. s
04/03/2022 22:52

A Displacement 2
B Displacement

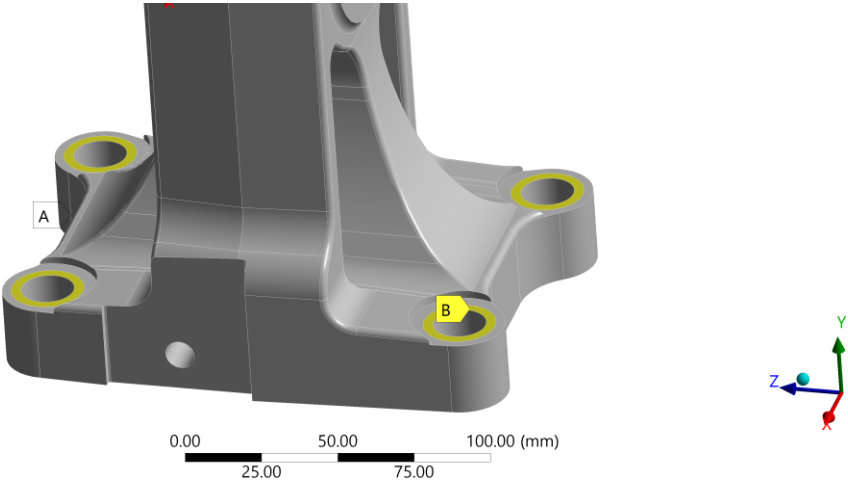


Figure 12. Bracket bolt pretention

A: Static Structural
 Displacement
 Time: 1. s
 04/03/2022 22:55

A Displacement 2
B Displacement

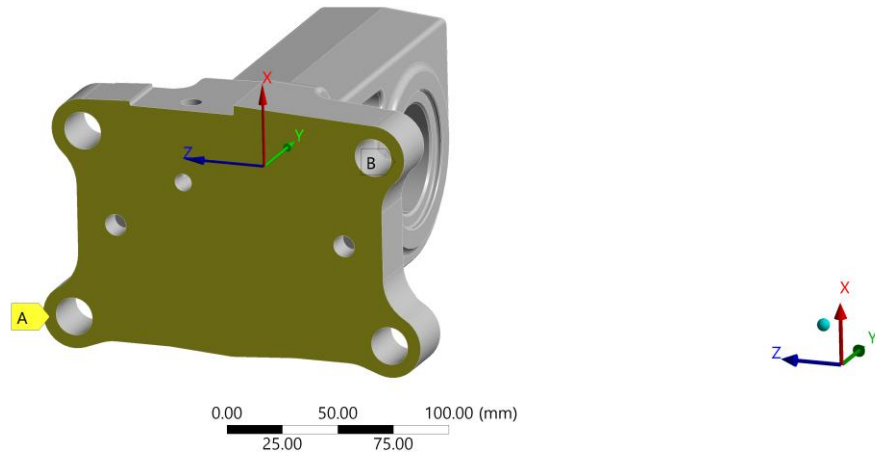


Figure 13. Bracket friction surface

The oil pressure is set to 4 bar and has been applied to the inner tubing as shown in Figure 14.

A: Static Structural
 Pressure
 Time: 1. s
 06/03/2022 14:12

Pressure: 0.4 MPa

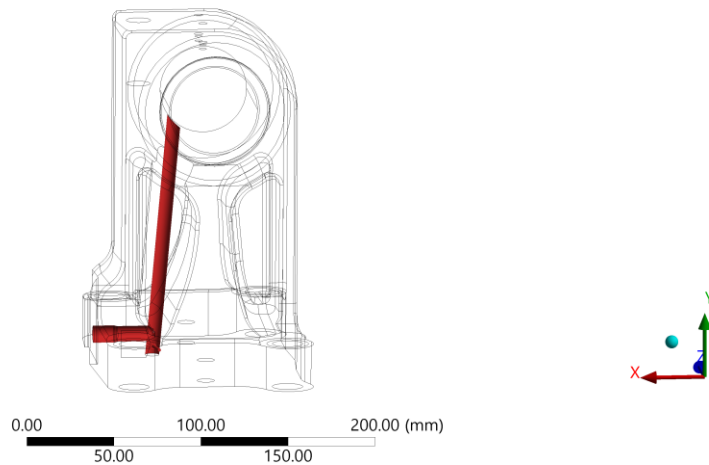


Figure 14. Original Bracket oil channel

Ignoring the singularities, the original part has a maximum equivalent von mises stress of approximately 95Mpa as shown in Figure 15, given that the maximum principal stress at the same area is 92Mpa as shown in Figure 16, we can see that this is mostly tension. Figure 17 shows that the maximum deformation is localized at the top of the part and is approximately 0.15mm. This means that the maximum deformation of the redesigned part cannot exceed this value. The safety factor for yield can be calculated using the formula:

$$SF = \frac{Yield\ strength}{\sigma_{Max}}$$

On the original bracket, the safety factor is 3.4.

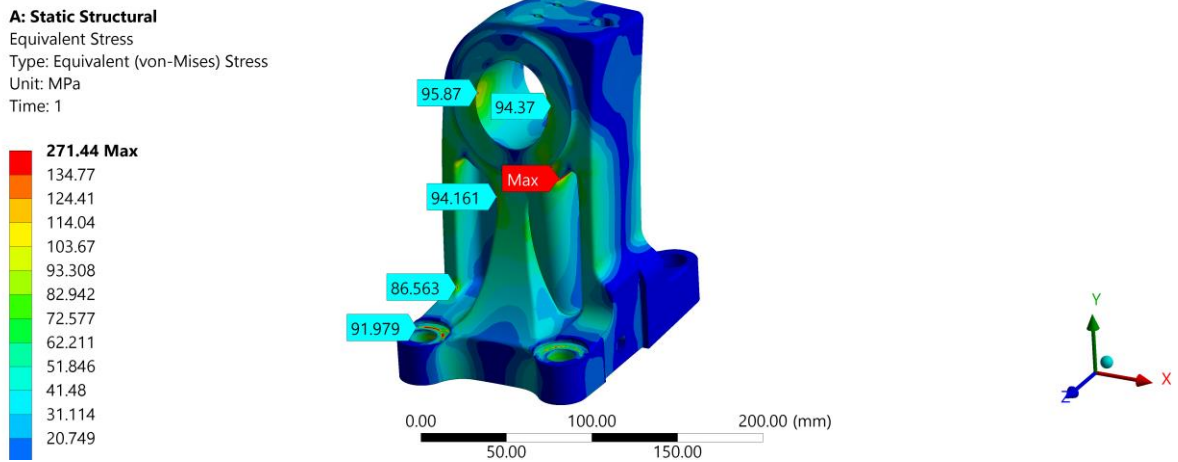


Figure 15. Original Bracket von mises stress

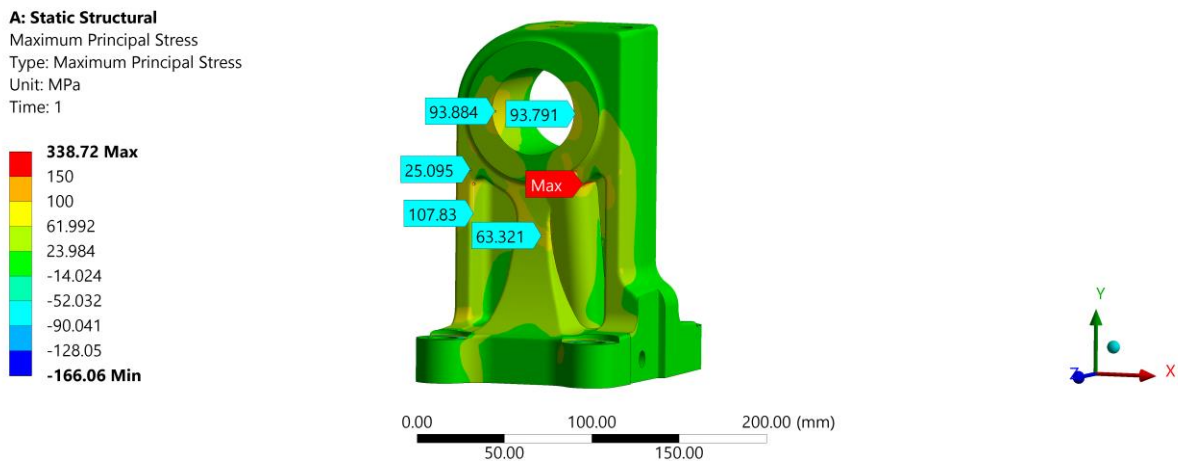


Figure 16. Original Bracket maximum principal stress

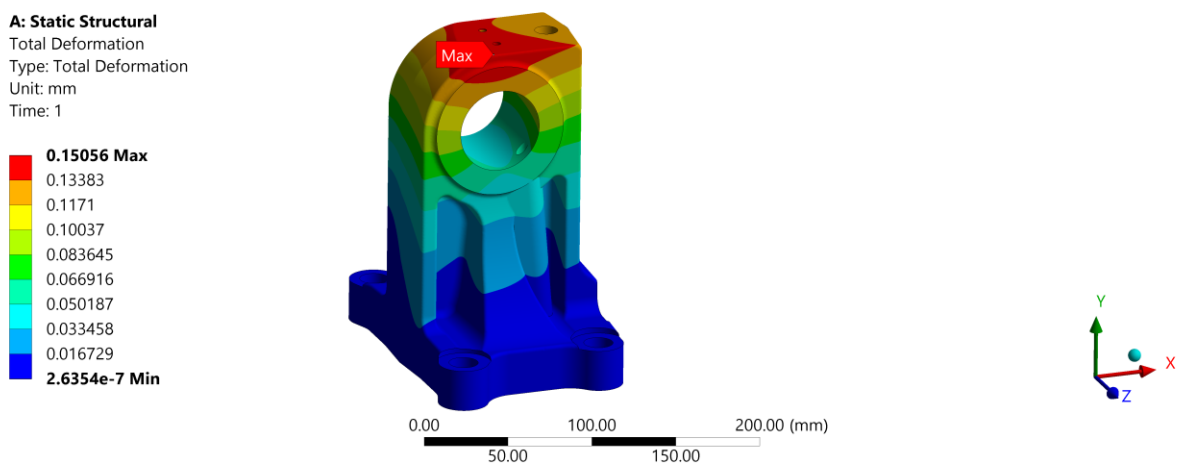


Figure 17. Original Bracket deformation

All the same boundary conditions will be set in the redesigned parts. The bracket is also subject to an alternative reversed load, there the moment is set to 720 000 Nmm and the bearing load is 16 000 KN.

4.1.2 Redesigning the Bracket

The first part of redesigning the bracket was to decide which method would be used. Lattice structures were quickly ruled out because of the high cyclic load and the importance of good fatigue properties. Because of the moment on the bracket, it is also hard to predict where material should be placed manually. Therefore, the best alternative was to use the generative design tool from Creo, because of its high customizability. From the results of the original test, it is noticeable that the part can be optimized a lot because of the low stresses, and it was expected that most of the material would be removed in the lower part of the bracket. Even though it is theoretically cheaper and better to design the part so that it is printed in the shortest direction, the amount of support needed in this example makes it more logical to print it standing up. This leads to the highest stresses being perpendicular to the print layers and because of the non-isotropic properties of 3D printed parts this is usually not recommended. Because SLM printing has better isotropic properties than other additive manufacturing methods, this should not be a too big issue, but there will be an extra safety factor applied.

First, the starting geometry was defined and expanded as much as possible. The outer boundaries of this were defined by a STEP-File provided by Bergen Engines. This file was a “negative” of the air surrounding the bracket and rocker arms when assembled. This makes it easy to maximize the starting geometry as much as possible, the starting geometry is shown in Figure 18. All sharp edges where the material is expected to be generated were rounded for better transitions and for avoiding notches.

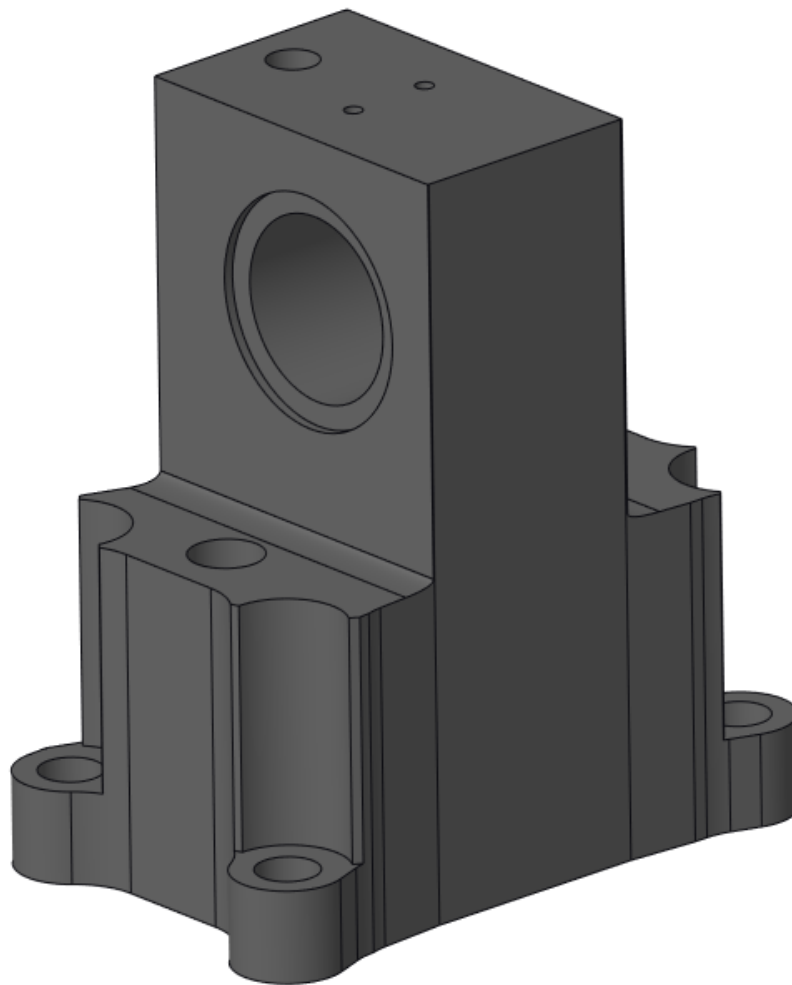


Figure 18. Starting geometry of bracket, based on negative step file of free space.

When setting up the preserved geometry of the analysis, it was first attempted to minimize them maximally. The Bolt, shaft, and positioning holes were replaced with simple cylinders, and all the mounting plates were replaced by simple plates as shown in Figure 19. This led to no material spreading to the positioning holes and mounting plates, as there was no load applied to them. This setup also quickly led to errors when trying to generate the solid geometry.

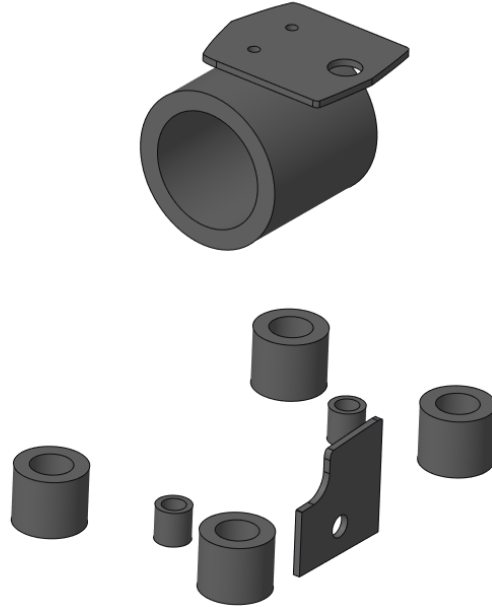


Figure 19. The original conserved geometry, this was too complicated to generate.

It was then decided to make the conserved geometry less complex. The lower part of the bracket would be included in the conserved geometry, and then be hollowed out later. The thickness of this “slice” is the same as the length of the bolts, this is to get a good distribution of the bolt pressure cone. The bottom surface will also help distribute the horizontal forces. The bottom surface is directly modelled after the contact surface from the bracket to the rest of the surface shown in Figure 20. The oil canal is also completely removed for simplicity.

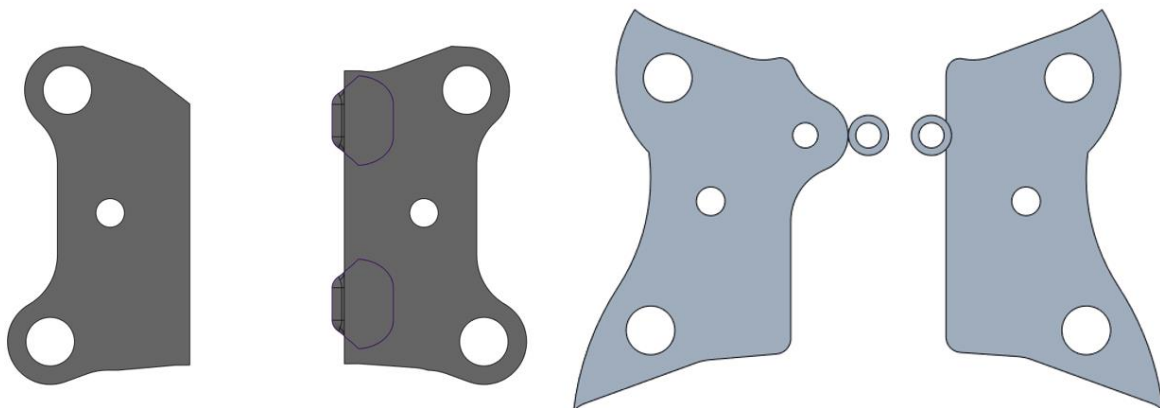


Figure 20. Bottom face of the available space

In the first analyses it was observed that the topology optimization would only get fixed to one of the lower fixtures as seen in Figure 21 (Left), to mitigate this, two extra support legs were added as seen in Figure 21 (Right). This led to geometry being added to both fixtures. This is also important for the lower alternative load case that is present on the bracket. The shaft cylinder was also made ecliptic to help distribute the stresses. Notice that all the sharp edges on the support legs are rounded for smoother transitions.

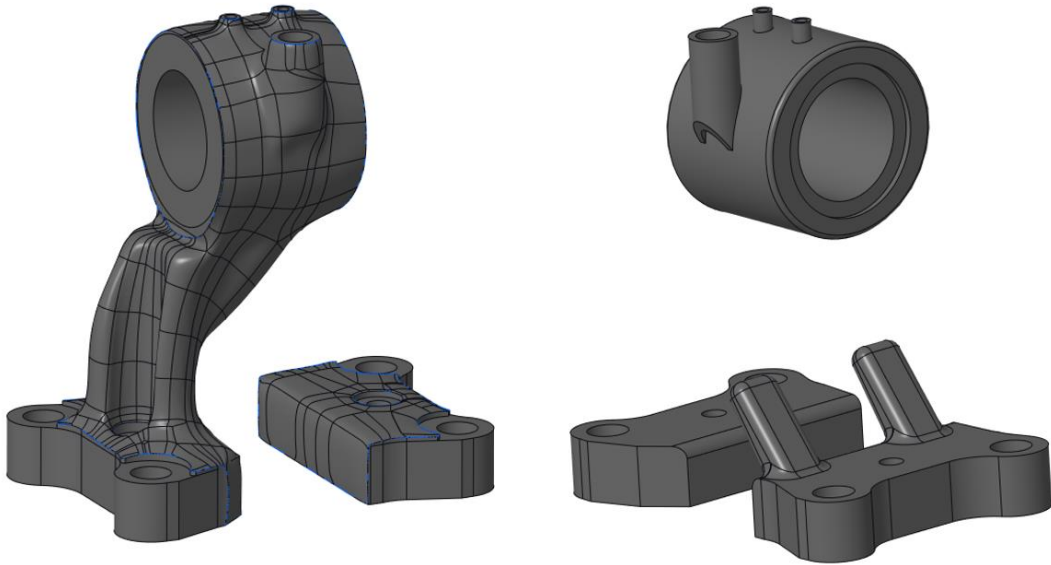


Figure 21. Initial results of generative design (Left). Fix to "seed" the geometry flow (Right).

Another issue that was leading to generation errors was the geometry around the bolt holes. One known bug with generative design is that it is a guaranteed error when there is geometry where a radial curve connects directly to a flat line, creating an infinitely small point. To mitigate this, cuts were made on all the geometry around the bolt holes as shown in Figure 22.

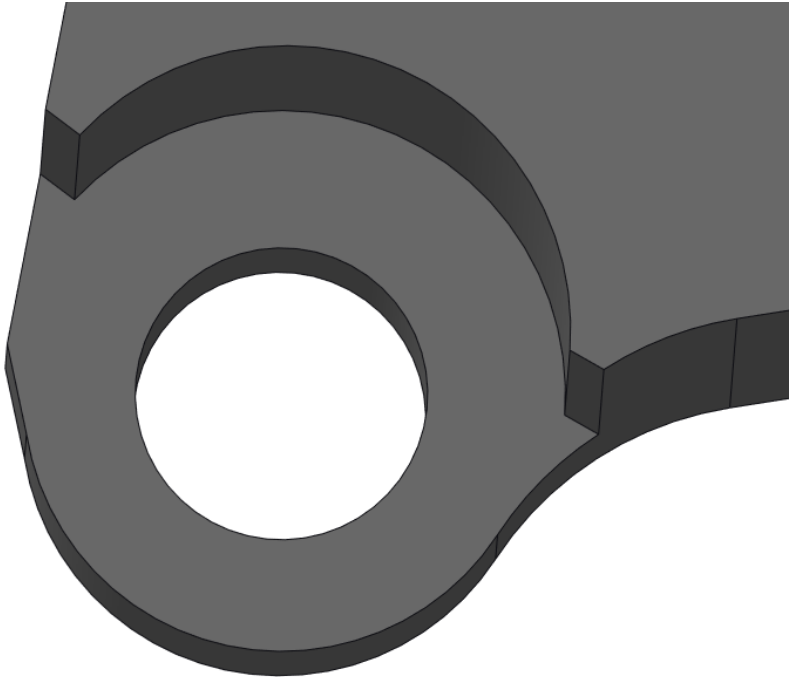


Figure 22. Cut outs of sharp corners on the edges of the bracket feet.

The most important design criteria for the bracket were “Print Direction”, “Material Spreading” and “Minimum Crease Radius”. The print direction was set so that the part would be printed as planned, this makes sure that the number of angles over 45% is limited, which again limits the amount of support needed. The material spreading was set to 35, this seemed to be to most stable setting when trying to generate the part, at the same time it made sure that there were not too many unnecessary struts. Minimum Crease Radius was set to 8 mm, this is again to make sure there are no sharp bends, which again makes the part easier to generate into solid geometry. The settings are shown in Figure 23

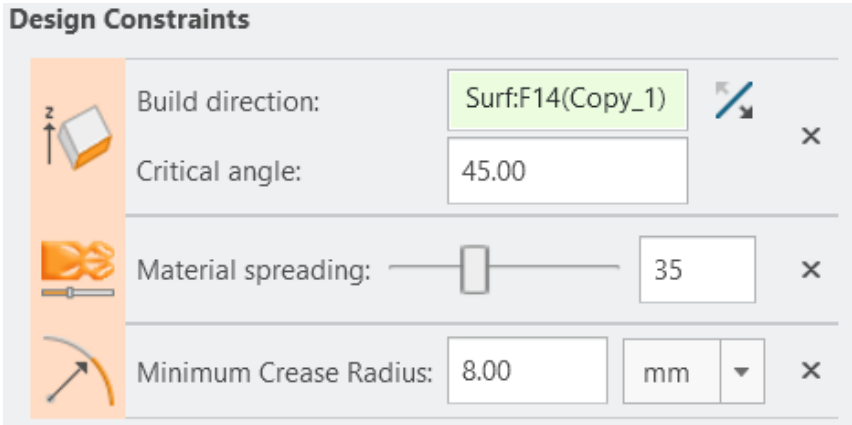


Figure 23. Design criteria used on redesigned Bracket

After a part had successfully converted into solid geometry and had acceptable results in Ansys Mechanical, the parts needed to be further modified in Creo. The first step was to make the oil channels

as Figure 24 (Left) illustrates. These were made by first making two perpendicular sketches that followed the geometry made by the topology optimization. Then the sketches were converted into a 3D sketch using the intersect tool, and this 3D sketch was used with a sweep to make the feature. The oil channel is made so that there is no expansion over 45° so that it can be printed without internal supports. The horizontal start of the channel has a tear-drop shape to avoid supports, this is seen in Figure 24 (Right).

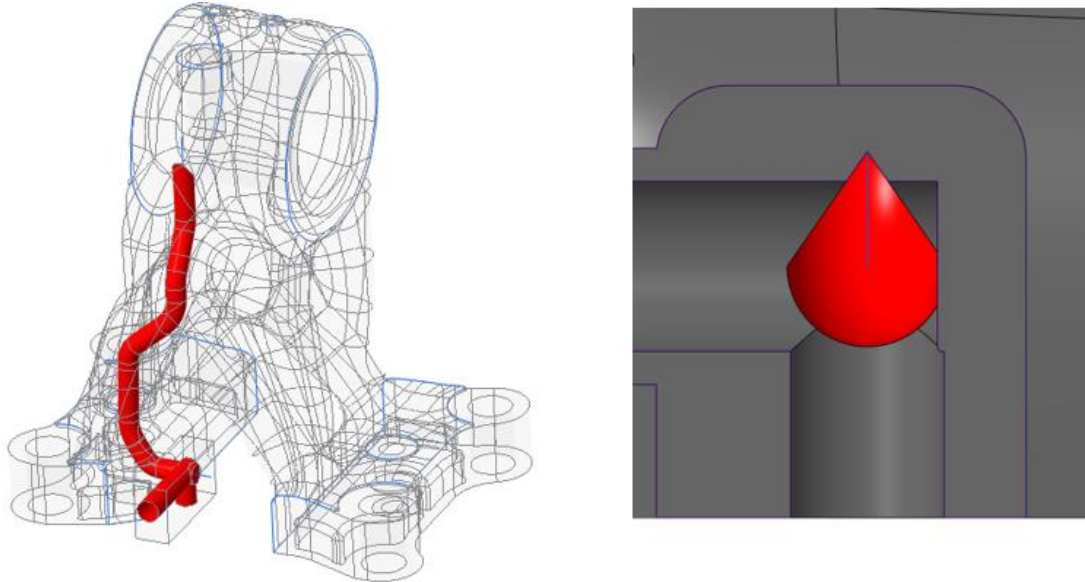


Figure 24. The internal oil channel is marked in red (Left). Notice the teardrop shape in the horizontal part of the channel (Right).

The final step in the redesign of the bracket is to hollow out the bottom part. Because the geometry was too complicated for the shell function to be used, it was done manually with a sketch. The thickness of the walls is set to 6 mm and the depth of the shell is dependent on the material being chosen. The correct depth was found by trying different depths in Ansys Mechanical, as the removal of too much material would lead to great deformations. The edges around the cut were then rounded for extra support. The final shape is shown in Figure 25.

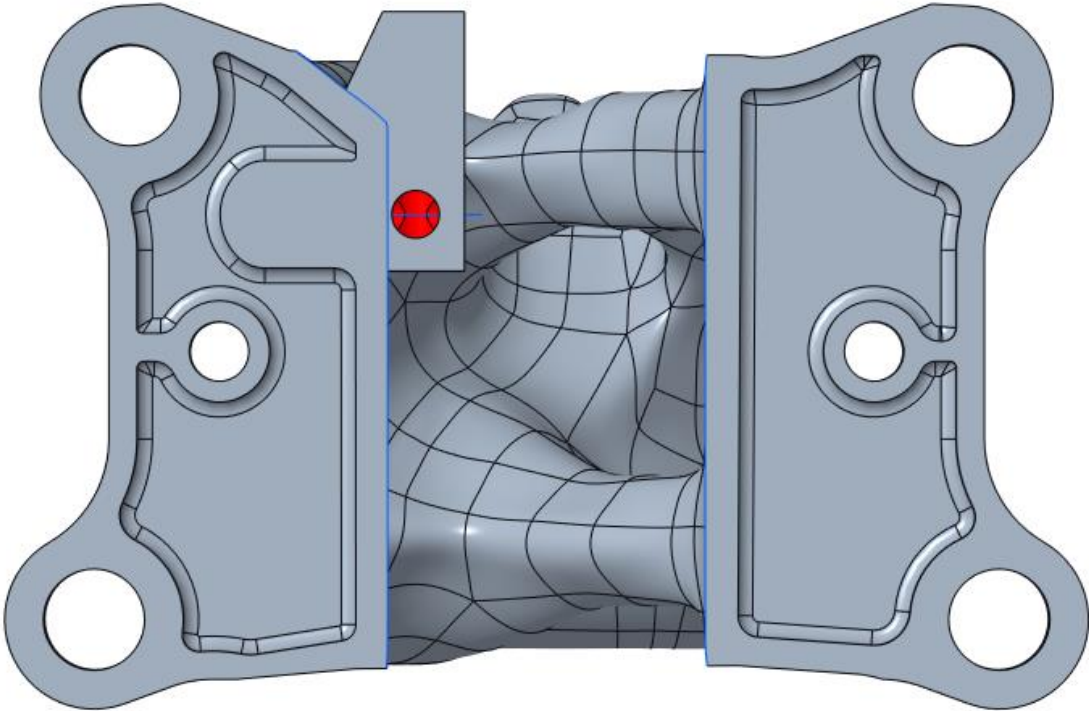


Figure 25. The hollowing out of the bottom of the bracket.

The final parts were then verified in Ansys mechanical using the same loads and boundary conditions that were used on the original part. This is a necessary step as the removal of the material from the bottom plate and the material removed in the oil channel can weaken the part.

4.2 Case 2: Rocker Arm

The Rocker Arm case study was one of the parts provided by Bergen Engines. A rocker arm is a part of an engine that opens and closes either the exhaust or suction valves to the cylinder chamber, these are being pushed by a rod coming up from the lower camshaft, pushing the rocker arm to rotate, opening the spring-loaded valve downwards in the top cylinder. The stiffness of this part is critical since a deflection creates a delay from camshaft rotation to valve opening, making it difficult to anticipate the timing of the combustion cycle.

4.2.1 Original Rocker Arm GSJ-500-7

The simulation of the rocker arm was best represented using cylindrical support on one-third of the shaft surface and a remote displacement on the exhaust valve side to stop the rotation which would have occurred due to the load at the pushrod side. This load had a peek at 18000N upwards due to the engine pushrod as shown in Figure 26.

E: Original step file Displacement

Static Structural
Time: 1, s
19.05.2022 17:29

- A** Cylindrical Support: 0, mm
- B** ShockRod: 18000 N
- C** Displacement

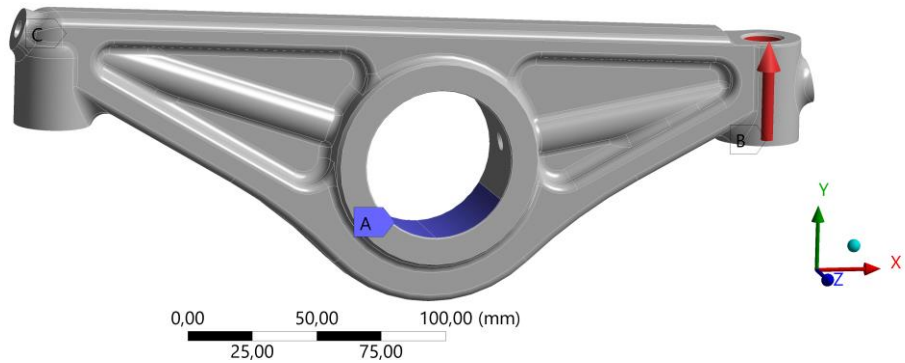


Figure 26. Rocker Arm boundaries

As shown in Figure 27, the highest stress in this arc is not affected by singularities since there is no sharp angle of the elements.

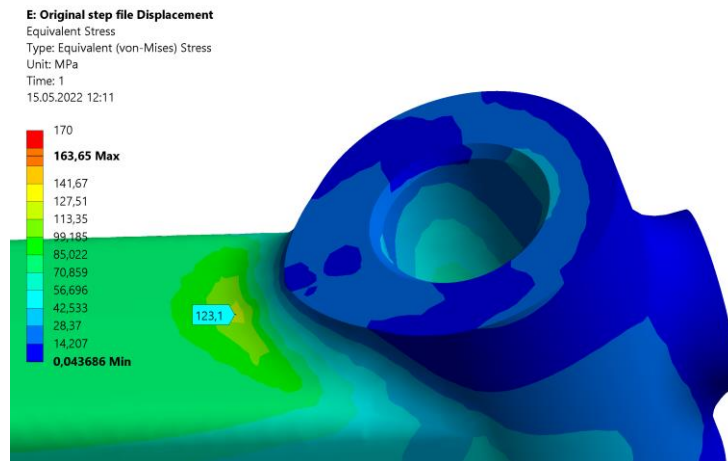


Figure 27. Original Rocker Arm highest stress

The highest von mises stress obtained excluding singularities in the FE model, was 123,1 MPa at the initial angle of force, zero degrees, Z direction, in the arc near the exhaust valve piston. the stress on that arc is not realistic as the angle will never be 0 degrees simultaneously as the force is high. There is a spring that is compressed and generates the highest force at a lower point, which translates to a degree of rotation in the part, which gives less stress on that specific arc. The stress inside the oil tube is not considered as the load-carrying area, as its cross-section is quite small and a deflection here is not vital. The biggest cross-section and the area designed to take loads are the arms of the part, which had a maximum of 77,5MPa with a force of 18000N in the z-direction (zero degrees) as shown in Figure 28.

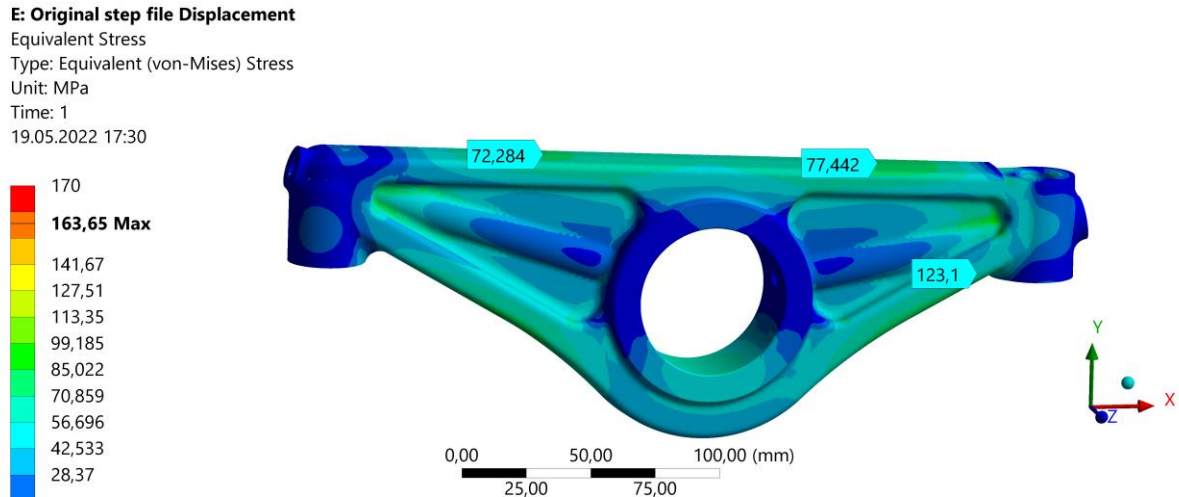


Figure 28. Original Rocker Arm von mises stress

The highest principal stress found was 134,6MPa in the same point as the von mises were highest. The principal stress describes the actual load in an area better and should be used to calculate fatigue which is shown in Figure 29.

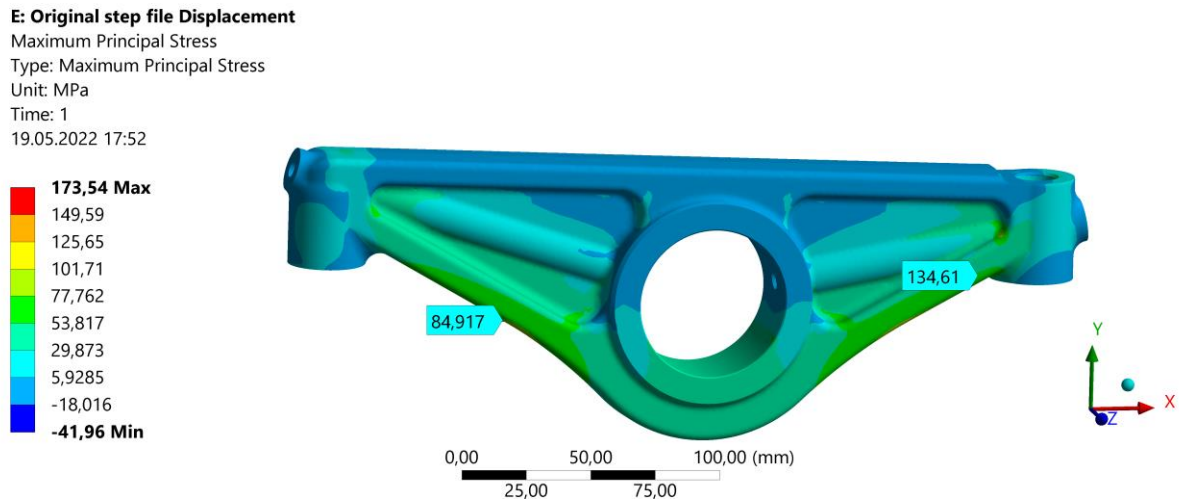


Figure 29. Original Rocker Arm maximum Principal Stress

At the beginning of the thesis, a lower load was expected. A table was created to test which direction that exposed the part for the highest stress, it was discovered to be at the initial angle of zero degrees as seen in Table 2. Through further conversations with Bergen Engines the loading was increased later on, so the values in the table below are not current. But the conclusion is the same, the highest stress is obtained when the force is perpendicular to the part, straight up. As described in the boundaries earlier.

Table 2. Simulation results of original STEP file Rocker Arm

Angle[deg]	Stress Arms[Mpa]	Stress Arc[Mpa]	max deformation Y [mm]	max total deformation [mm]
-20	65,071	113,910	0,223	0,219
-10	82,764	123,080	0,296	0,289
0	100,420	137,420	0,371	0,361
5	88,847	120,670	0,344	0,334
10	78,482	101,680	0,316	0,308
20	63,660	66,826	0,265	0,256
30	59,291	10,839	0,216	0,208
40	50,667	9,678	0,172	0,164
50	43,211	48,514	0,131	0,123

Considering that this part is not optimized completely, the stress level could be somewhat increased, the number for max principal stress is set to 165 MPa, due to fatigue limits of the current material that has been given by Bergen Engines and will be used in the project. The first design will be a redesign of the part considering the same material to optimize weight conserving stiffness in the part, Using the freedom of the additive manufacturing capabilities. The weight of the original part is 3kg.

The deflection of the part is vital, and the original rocker arm had a deflection of 0.29mm as shown in Figure 30. The deflection is important in this case study and the redesigned parts should have the same stiffness.

E: Original step file Displacement

Directional Deformation
 Type: Directional Deformation(Y Axis)
 Unit: mm
 Global Coordinate System
 Time: 1
 19.05.2022 17:31

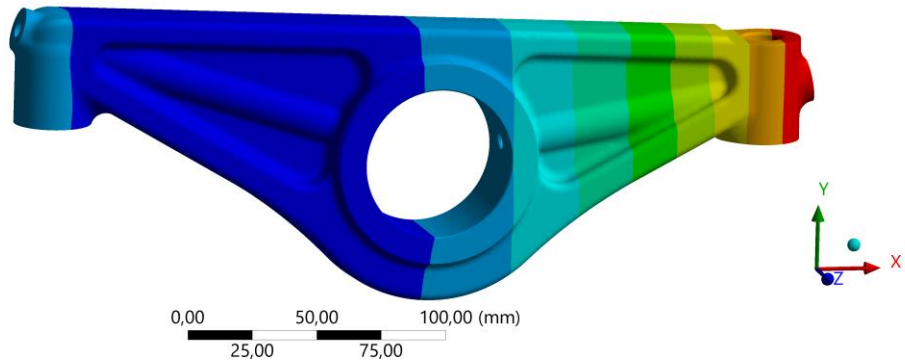
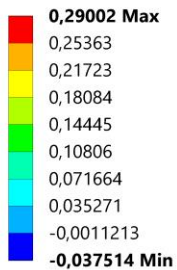


Figure 30. Original Rocker Arm deflection

4.2.2 Redesigning the Rocker Arm

Initially, three options emerged to decrease weight: topology optimization, using a lattice structure, designing the part with traditional methods and creating advanced geometry, or a combination of these methods together.

The loads on a rocker arm are cyclic and have a peak load of 18 000 N, where the average load is very low. Taking this into account the part is designed with fatigue in mind and the stress limits are for a long fatigue life of the part.

Topology optimization was discovered to be the best solution as it's easier to create than manual design and comes up with more advanced geometry. A lattice structure would be too thin and have a lot of unused strings. To create a part in a CAD program with topology optimization the preserved bodies of the design had to be added first as a separate body, as these are the features that would be kept unchanged and are designed from the mechanical drawings of the original part. For the rocker arm design the preserved bodies are as shown in Figure 31.

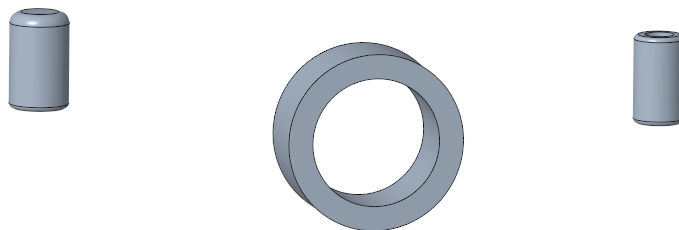


Figure 31. Rocker Arm preserved geometry

And a frame for the topology optimization design would need to be added, the starting geometry is shown in Figure 32. Which defined the outer material boundaries for the software. There were some issues with generating the part, rounding all the outer edges on the boundary fixed this. The boundary of the starting geometry is based on the original design and a “negative” volume step file, supplied by Bergen Engines.

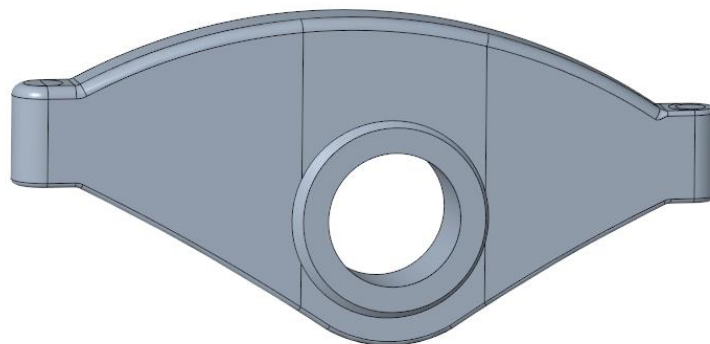


Figure 32. Rocker Arm starting geometry

The angle difference from the shaft hole to the rest of the body makes it impossible to print the part without supports in FDM and PBF printers, this is shown in Figure 33. It's better to have asymmetric design than to try to reduce the support. This is not avoidable as the function of the part requires this feature.

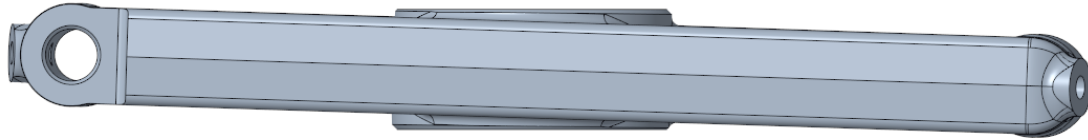


Figure 33. The slanted design of the Original Rocker Arm

As described in chapter 4.2.2. There could not be any circular features creating a tangent with any of the geometry walls, as this made the software fail to generate the solid geometry. This was relevant for the vertical holes, and thus the starting geometry had to be increased around them.

After the topology optimized geometry is created, internal oil channels are extruded to make oil flow through the part from the main mounting shaft hole outwards to the arms. These oil channels were created with teardrop cross-sections shown in Figure 34, to be able to print it without internal support.

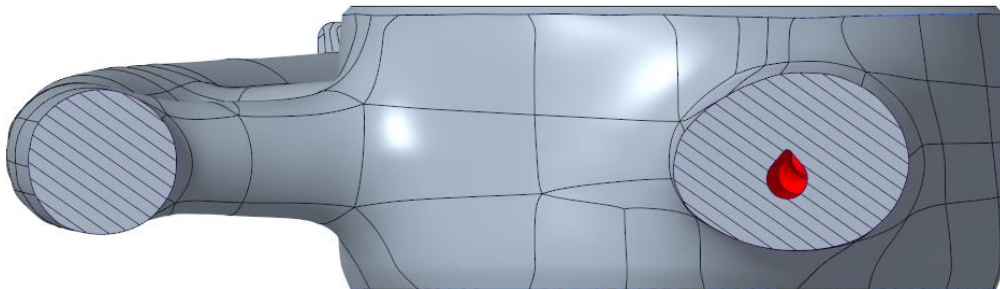


Figure 34. Cross-section of Rocker Arm 316L, teardrop-shaped internal oil channel

4.3 Case 3: Toolholder

The next part to be redesigned was the toolholder, which is an assembly tool needed to keep the piston in place for an exchange of cylinder liner. This is a tool used by technicians for maintenance. The current toolholder weighs 3.2 Kg. Which is considered a heavy tool. The main task here is to reduce the weight and reduce the two-part assembly to one part, which is easier to produce, as it's now currently made in a large CNC lathe.

4.3.1 Original Tool Holder

The original Toolholder is shown below in Figure 35.

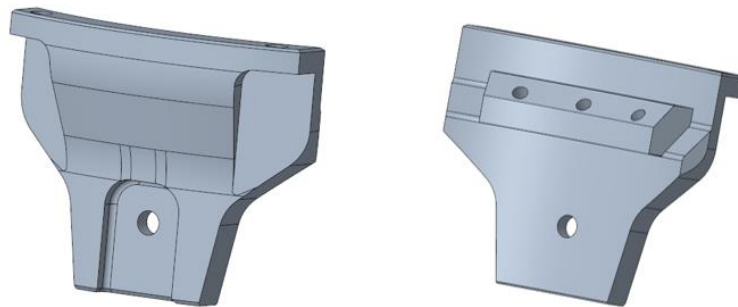


Figure 35. Original Toolholder overview

This is an assembly of two parts both currently turned separately and then assembled as shown in Figure 36.

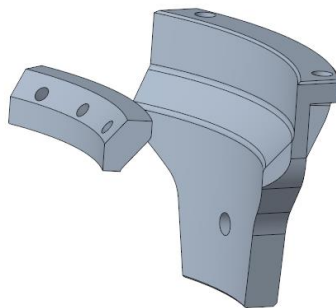


Figure 36, Original Toolholder exploded view

The key feature of this part is a large contact surface to reduce the forces from the mounted cylinder liner to tension on the middle bolt, the shear forces should be eliminated by the geometry. There was no provided stress limit for the part, only that no plastic deformation was allowed. The part is designed to withstand 46 385 N of static force, this includes a safety factor. The boundaries are shown in Figure 37.

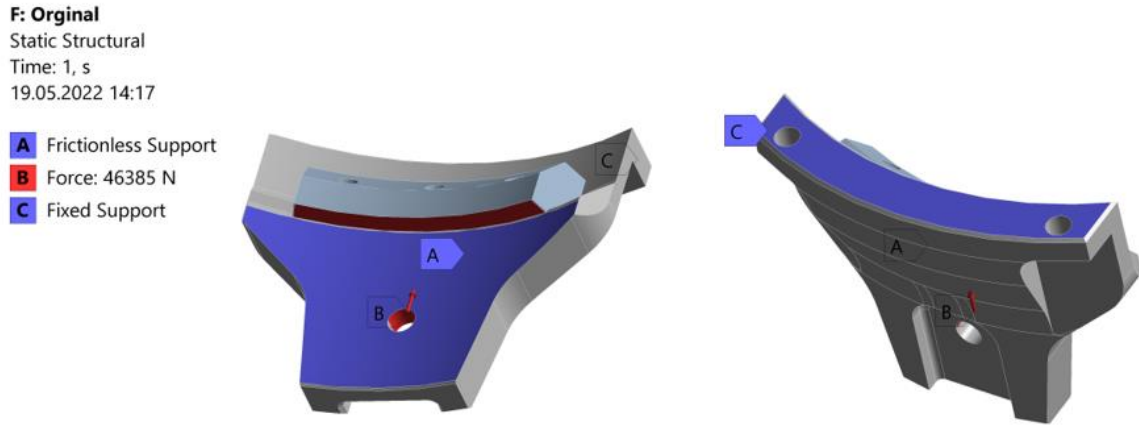


Figure 37. Original Toolholder boundaries

The values obtained in the analysis performed are shown in Figure 38. The highest stress obtained is 132 MPa. Which is quite low considering the S355JR has a yield strength of approximately 355 MPa.

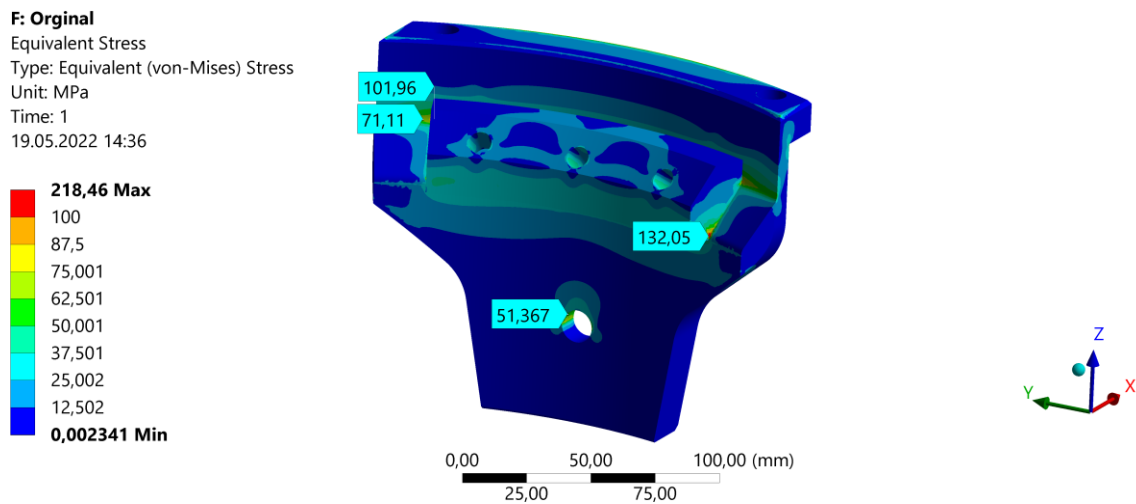


Figure 38. Original Toolholder von mises stress

The total deformation is shown in Figure 39. The maximum deformation is on the lip and is 0.02 mm which is considered a low value.

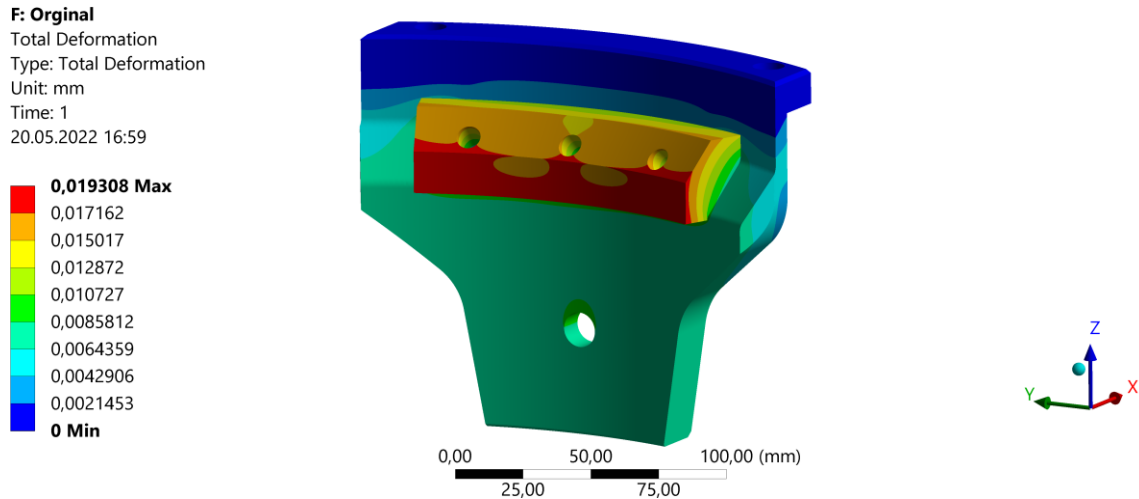


Figure 39. Original Toolholder total deformation

4.3.2 Redesigning Tool Holder

The new design was done using topology optimization as it's the best option for thin parts. The starting geometry was limited to the same shape so it's not possible to expand the part more.

To save as much weight as possible the part will be printed using Ti-6Al-4V. This material has high strength but low young modulus. The deflection here is not that important and shown in later analysis the deformation is still minimal. The starting and preserved geometry are shown in Figure 40. The starting geometry is expanded in circumference to increase the freedom of the generative design.

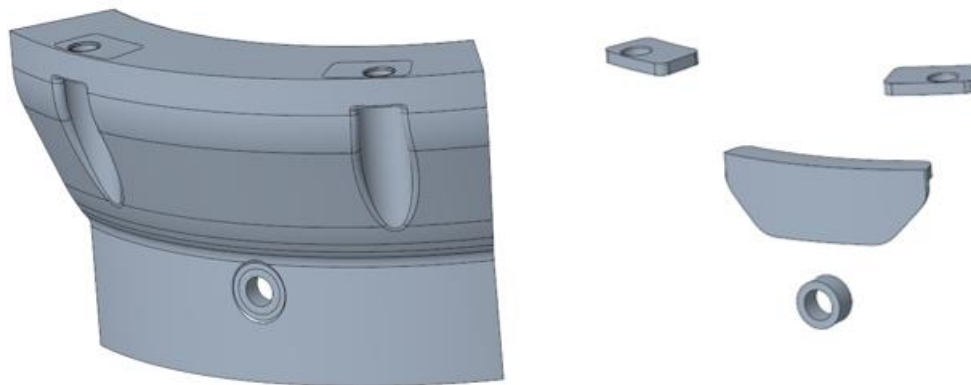


Figure 40. Toolholder starting geometry (Left). Toolholder preserved geometry (Right).

The upper surface of the preserved geometry shown in Figure 40 (Right), was reduced since the only feature is to support the cylinder liner. This does not require the whole surface from the initial part. And a support surface was added to increase support and obtain the moment induced.

4.4 Case 4: Pressure indicator

The pressure indicator valve is used to mount a pressure sensor to the engine. It is today made up of five parts, not including the valve assembly. The goal is to minimize the number of parts needed in this assembly, while at the same time making it lighter and keeping as much of the stiffness as possible. The valve and valve-contact cylinder which can be seen in yellow and red respectively, in Figure 41. These are standard parts that are purchased; therefore, these will not be modified. The goal was to reduce the assembly into a three-part assembly.

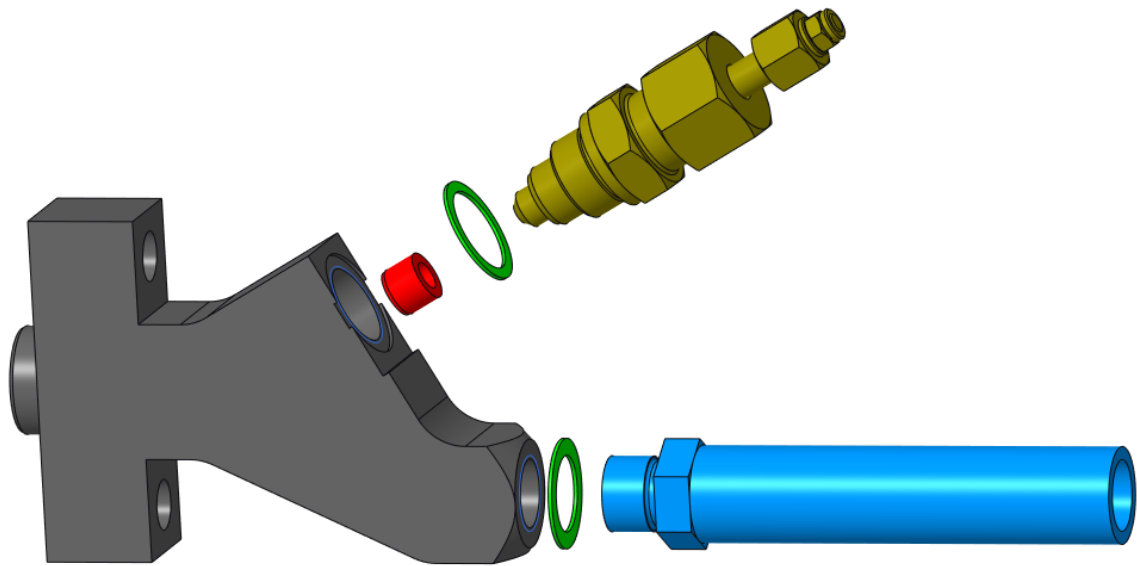


Figure 41. Original Pressure Indicator Valve exploded assembly

4.4.1 Original Pressure Indicator S235JR

The requirements given by Bergen Engines specify that the part must withstand 150 °C and a static pressure of 240 Bar. The bolt holes are set as fixed and a pressure of 24 MPa is applied to all surfaces subject to the pressure, as shown in Figure 42.

U: Originalindicatorvalve S235JR
 Static Structural
 Time: 1. s

- A** Pressure: 24. MPa
- B** Fixed Support

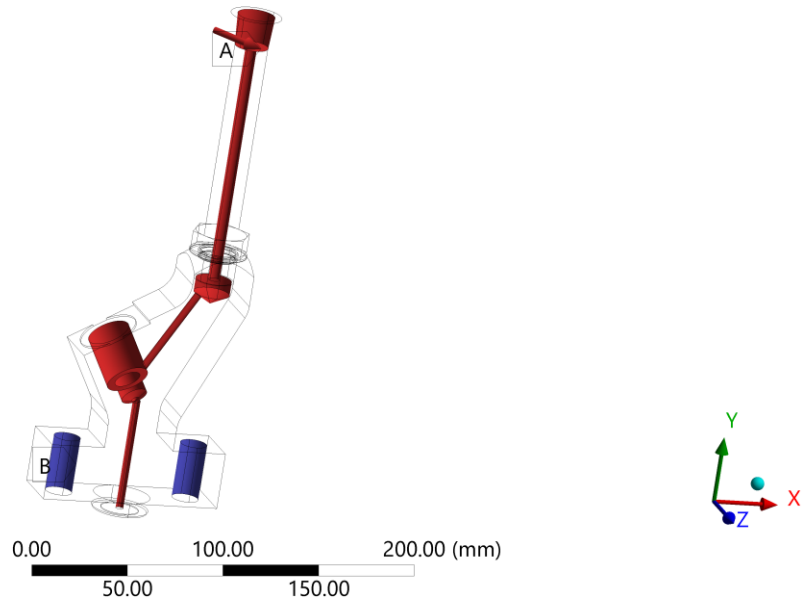


Figure 42. Pressure Indicator Valve boundary conditions

The stress on the original part was as expected low, with a maximum stress of approximately 108 MPa. This is well below the fatigue strength of all the relevant materials for additive manufacturing, and therefore a good weight reduction was expected. All the probed stresses shown in Figure 43, are on the inside of the model, as this is where the stresses are the highest.

U: Originalindicatorvalve S235JR
 Equivalent Stress
 Type: Equivalent (von-Mises) Stress
 Unit: MPa
 Time: 1

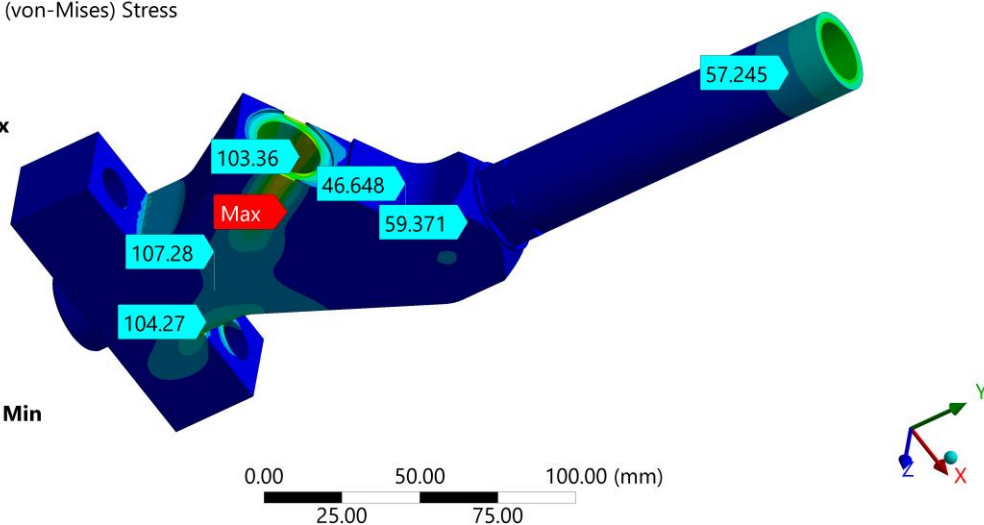
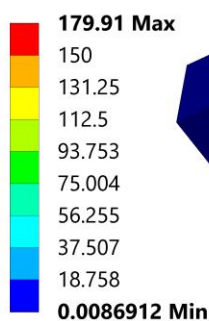


Figure 43. Original Pressure Indicator Valve von mises stress

Figure 44 shows the deformation of the part is due to the uneven distribution of the pressure, this deforms the part the same way a Bourdon tube works.

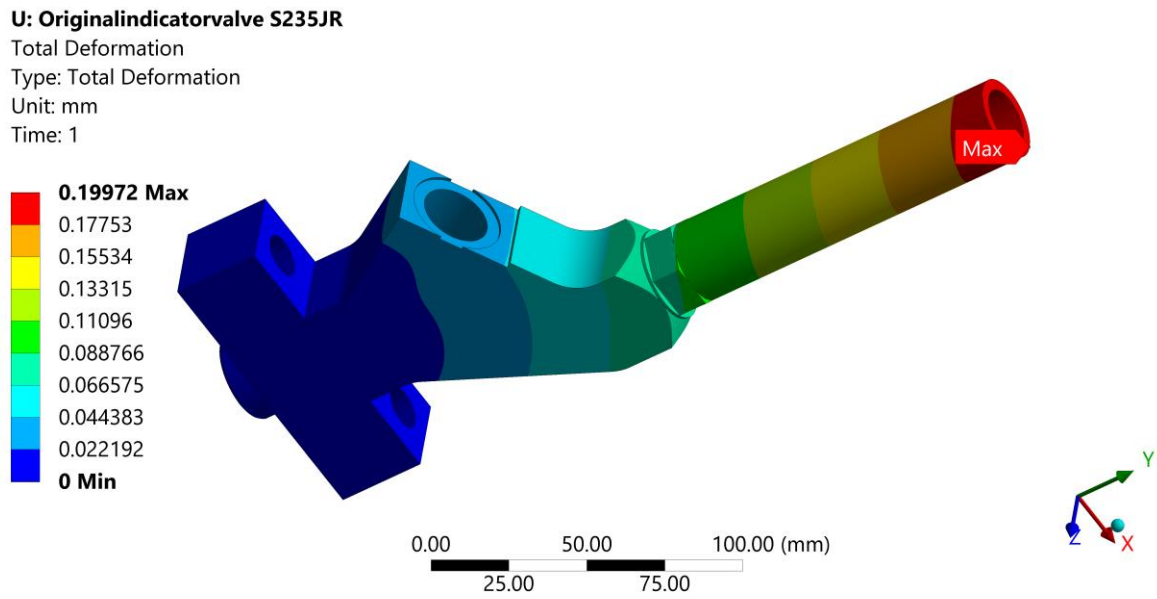


Figure 44. Original Pressure Indicator Valve deformation

4.4.2 Redesigning the Pressure Indicator

The starting geometry was expanded as much as possible as shown in Figure 45, the main limiting factor was that there needed to be space to mount the bolts, so the boundary could only be expanded in two directions. The sharpest corners were also rounded for better stress distribution.

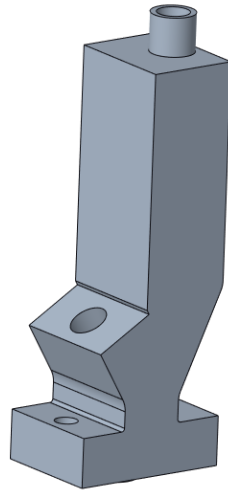


Figure 45. Pressure Indicator Valve starting geometry

Given the limited amount of information available on the surroundings of the indicator valve, the conserved geometry was based directly on the original tract, as shown in Figure 46. This was done to make sure that the part would fit. This conserved geometry was way more complicated than the one used earlier, but because a lot of space was left around it, and there were no places where radial and straight lines converged, it generated quickly.

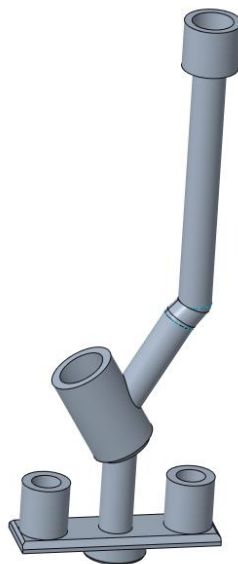


Figure 46. Pressure Indicator Valve conserved geometry

Most of the design criteria were set to the same as the bracket for stability, but this time asymmetry requirement was set as well for lower computation time.

5. Results and Discussion

In this chapter, the design results and analysis plots of the different case studies are presented. As well as experimental tests.

5.1 Numerical Results

To find different options, prices, and performances, the main cases Bracket and Rocker Arm were redesigned three times. One redesign with each of the materials GJS-500-7, Ti-6Al-4V and 316L. The indicator valve was redesigned for 316L and Ti-6Al-4V. The Toolholder was only redesigned for Ti-6Al-4V. This provided a broader comparison basis.

5.1.1 Case 1: Redesigned Bracket

The bracket was redesigned in three different versions because of the uncertainty of which material would be the best. All the models had the same design criteria, except for material properties and weight remained.

Bracket GJS-500-7

The first redesign was made using the same material as the original part and is shown in Figure 47. Even though this part is not manufacturable, it indicates the possibilities of using topology optimization alone, not being dependent on the material. The original part in GJS-500-7 weighed 10.62 Kg, and redesigned using the same material, the weight is reduced to 6.38 Kg. This is a weight saving of approximately 40% and clearly shows the possibilities of generative design.

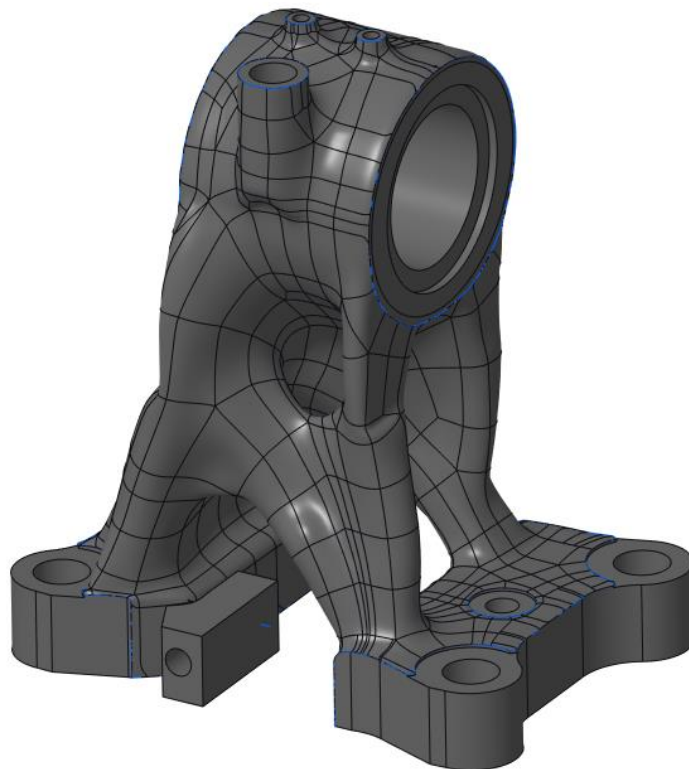


Figure 47. Bracket GJS-500-7

The simulations in Figure 48 and Figure 49 show that the highest stress area is around the shaft as expected, because of this, very little material has been removed in this area. Both the equivalent stress

and the maximum principal stress is approximately 130 MPa, showing that this is pure tension. The biggest removal of material is in the bottom of the bracket, as it has been split into three distinct legs. There is also an increase in stress around the “notch” approximately in the middle of the part. This is because this is where the starting geometry ends and was not removable. It was attempted to modify the transition, but the stress remained constant. This leads to a safety factor of 2.5.

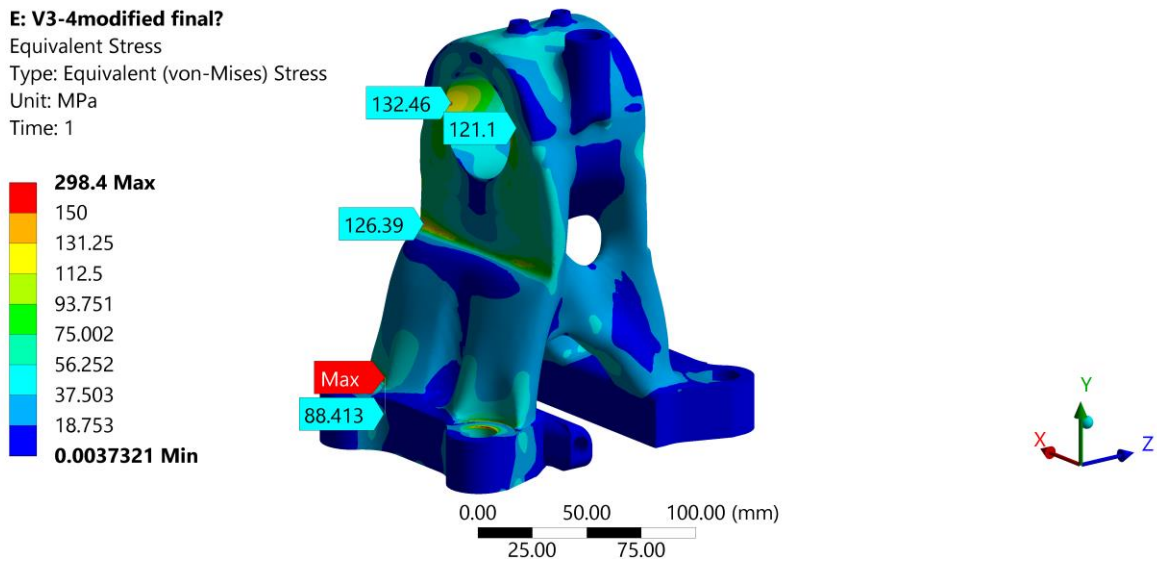


Figure 48. Bracket GJS-500-7 von mises stress

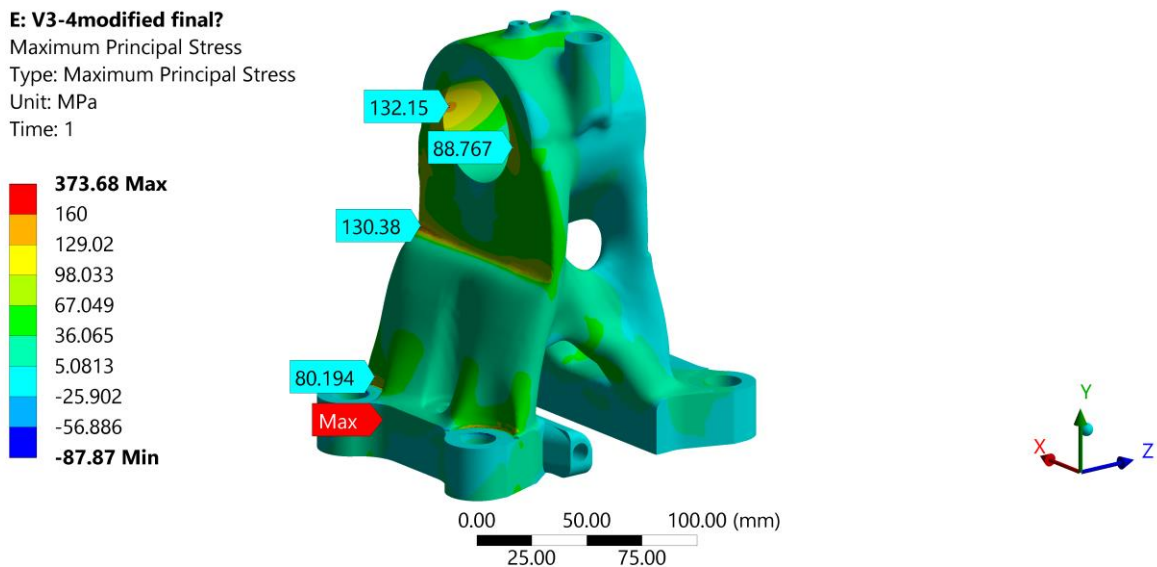


Figure 49. Bracket GJS-500-7 maximum principal stress

The maximum deformation is 0.124 mm, this is 0.026 mm less than the original part. As can be seen in Figure 51. the alternative load case has a maximum principal stress of 144 MPa, this is well below the fatigue strength limit of 165 MPa and is shown in Figure 50.

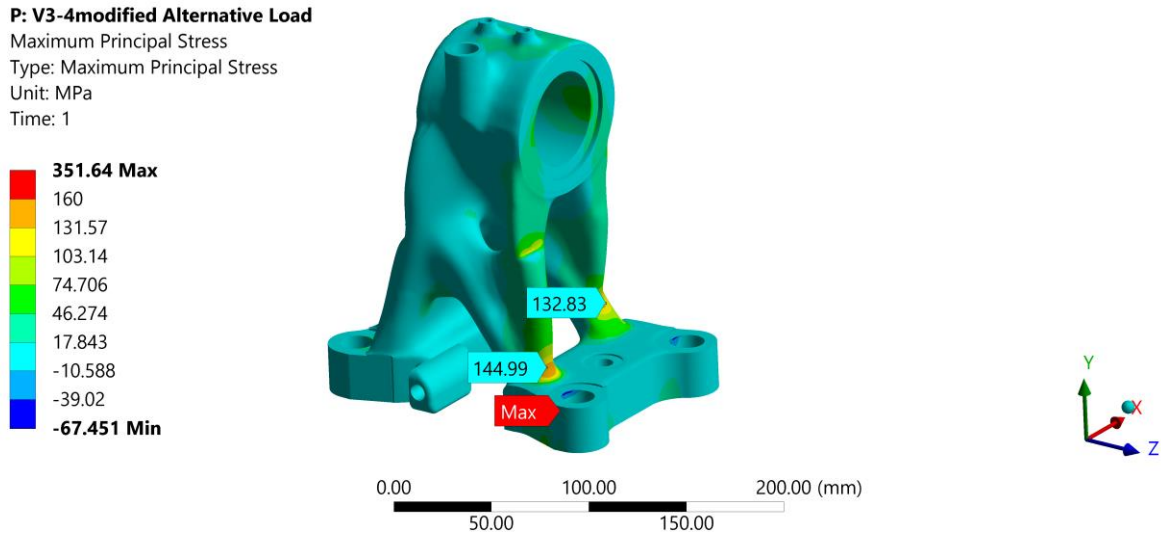


Figure 50. Bracket GJS-500-7 alternative load case maximum principal stress

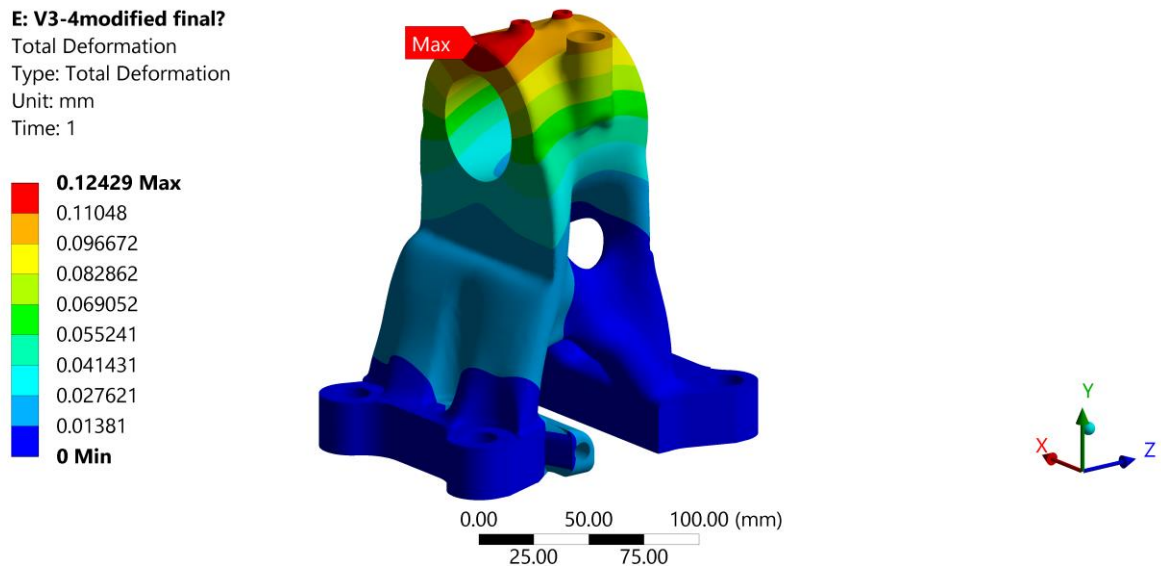


Figure 51. Bracket GJS-500-7 deformation

Bracket 316L

As the results from the GJS-500-7 version showed that there was much weight to be saved, the first test was to redesign the part with another ferrometal, for additive manufacturing, the natural choice is 316L. As can be seen in Figure 52 the results look similar, but because of the increased stiffness and yield strength, the model is thinner. The 316L variant weights 5.88 Kg, which is approximately a 45 % reduction in weight.

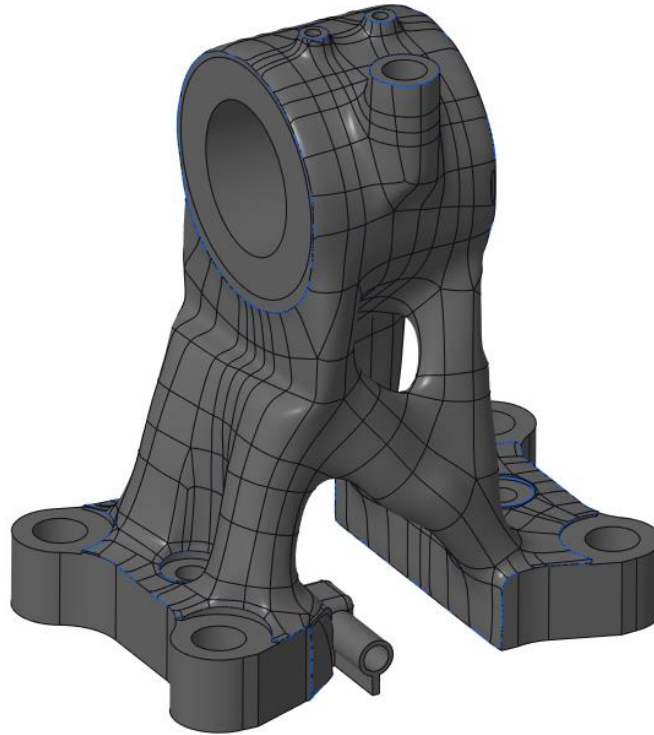


Figure 52. Bracket 316L

The stresses are very similar to the GJS-500-7 version but are increased because of the better material and less material present. Figure 53 shows maximum stresses of approximately 142 MPa in tension as the principal stress shown in Figure 54 confirms. This stress leads to a safety factor of 3.4, which is the same as the GJS-500-7 version. Amotools estimates that the part costs 3141 € to produce.

L: 316Lv1-1 finished

Equivalent Stress
 Type: Equivalent (von-Mises) Stress
 Unit: MPa
 Time: 1

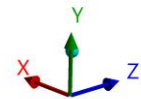
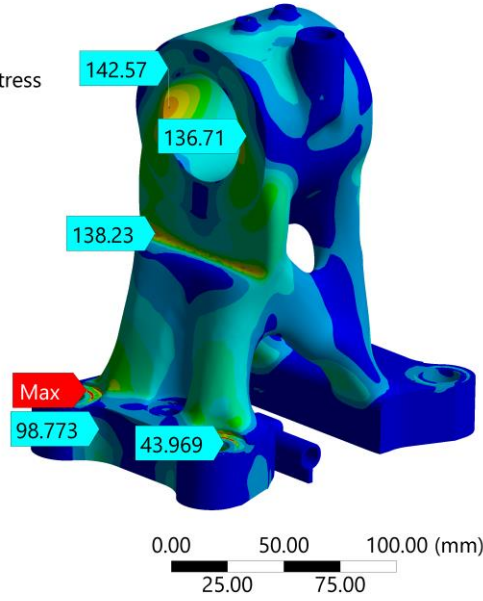
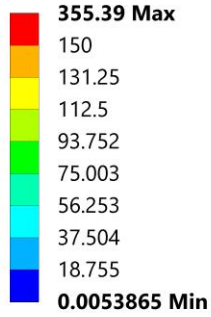


Figure 53. Bracket 316L von mises stress

L: 316Lv1-1 finished

Maximum Principal Stress
 Type: Maximum Principal Stress
 Unit: MPa
 Time: 1

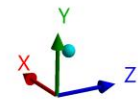
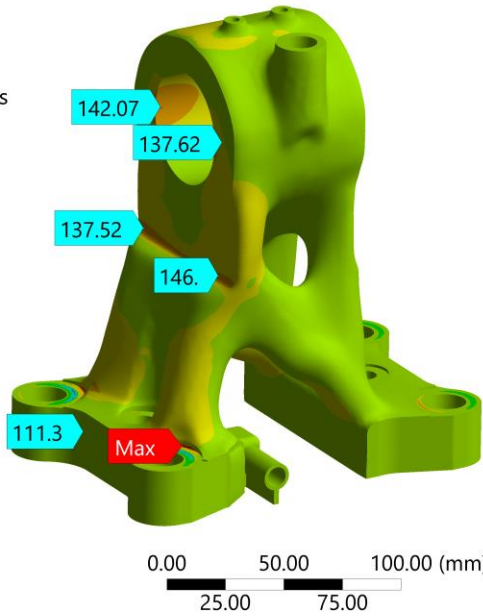
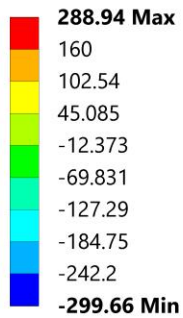


Figure 54. Bracket 316L maximum principal stress

As seen in Figure 55 the maximum deformation of the part is 0.152 mm, which is a negligible amount higher than the original part. On this part, the design was limited by the young modulus of the material, as removing more material could make the part lighter without breaking the part, but then the stiffness requirement would not be upheld.

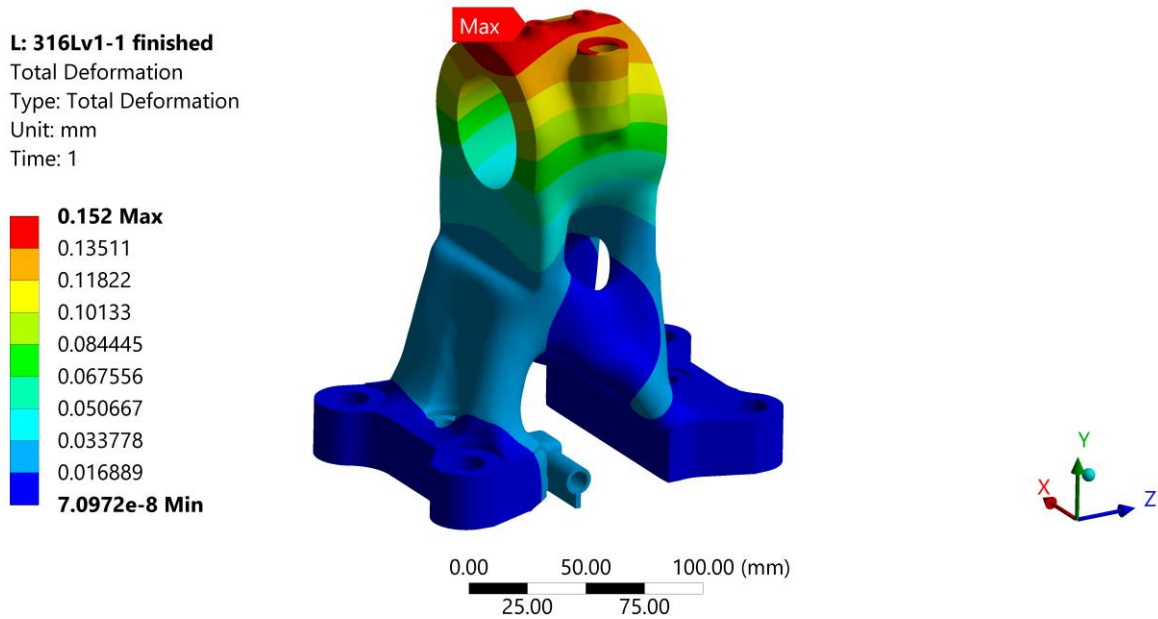


Figure 55. Bracket 316L deformation

The same is noticeable in the alternative load case shown in Figure 56, which has a maximum stress of approximately 160 MPa.

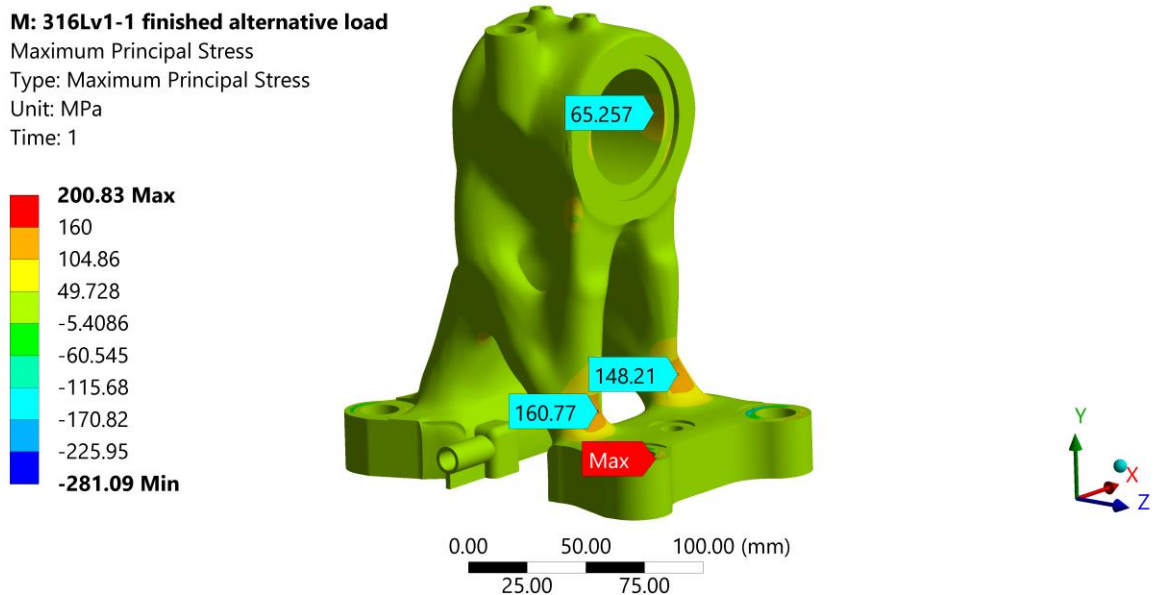


Figure 56. Bracket 316L maximum principal stress alternative load case

Bracket Ti-6Al-4V

The final version being made is the Ti-6Al-4V version, also known as Grade 5 Titanium. As expected, this was the lightest version at only 4.81 Kg, which has a total weight saving of approximately 55%. This model is noticeably thicker than the other versions as shown in Figure 57, because of the very low Young's modulus. The estimated price to produce this part is 6522 €, this is the most expensive and is over double the price of the 316L version.



Figure 57. Bracket Ti-6Al-4V

Because of the very low and limiting Young's modulus, Figure 58 shows that this version has very low stresses, only a maximum of approximately 122 MPa. Figure 59 confirms the results and describes it as mostly tension stresses.

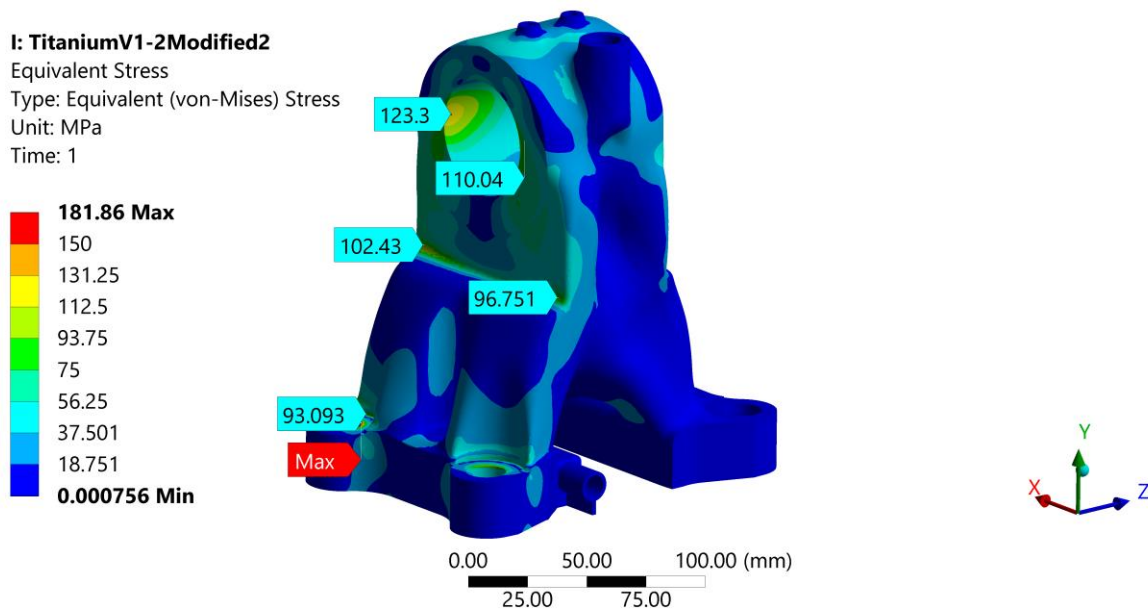


Figure 58. Bracket Ti-6Al-4V von mises stress

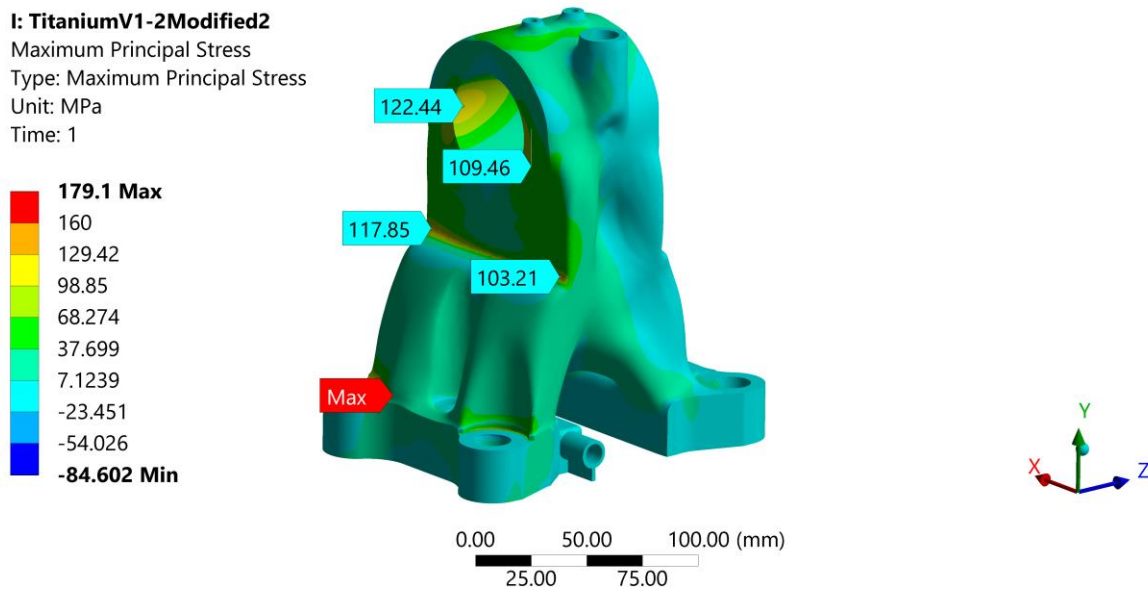


Figure 59. Bracket Ti-6Al-4V maximum principal stress

Figure 60 shows that this version has a maximum deformation of 0.156 mm, which again is a negligible amount higher than the original part. Because of all the extra material needed to fulfil the stiffness requirement, this version has a safety factor of 8.1 which is the highest of all versions. The alternative load also only has maximum stress of 60 MPa shown in Figure 61, which is the lowest of all the versions.

I: TitaniumV1-2Modified2

Total Deformation
 Type: Total Deformation
 Unit: mm
 Time: 1

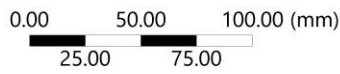
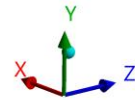
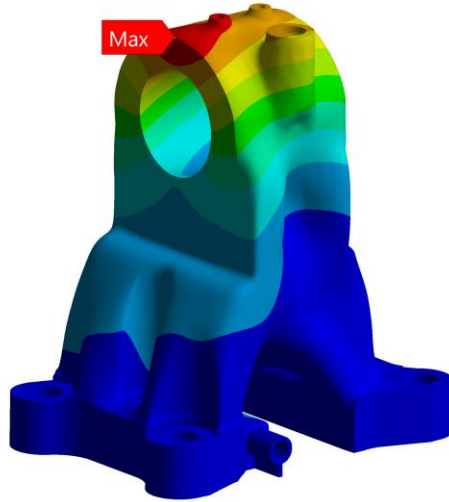
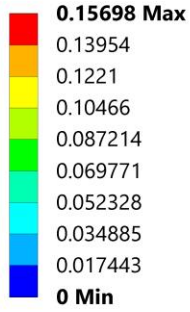


Figure 60. Bracket Ti-6Al-4V deformation

N: TitaniumV1-2Modified2 Alternative load

Maximum Principal Stress
 Type: Maximum Principal Stress
 Unit: MPa
 Time: 1

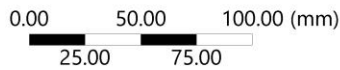
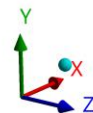
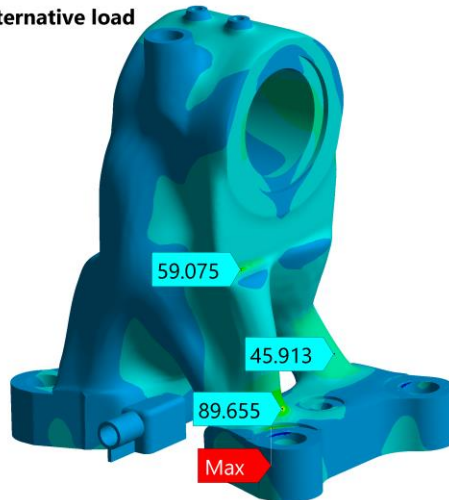
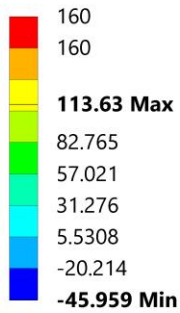


Figure 61. Bracket Ti-6Al-4V alternative load maximum principal stress

It is also important to mention, that because of the high amount of material and the uneven thickness of the titanium model, warping might be an issue during printing.

5.1.2 Case 2: Redesigned Rocker Arm

In this case study, three designs were created to see how much different material properties affect the design and which solution is cheapest and saves the most weight.

Rocker Arm GJS-500-7

The optimized part for cast iron was made using a crease radius of 8mm and a material spreading of 30. This produced an acceptable result as shown in Figure 62.

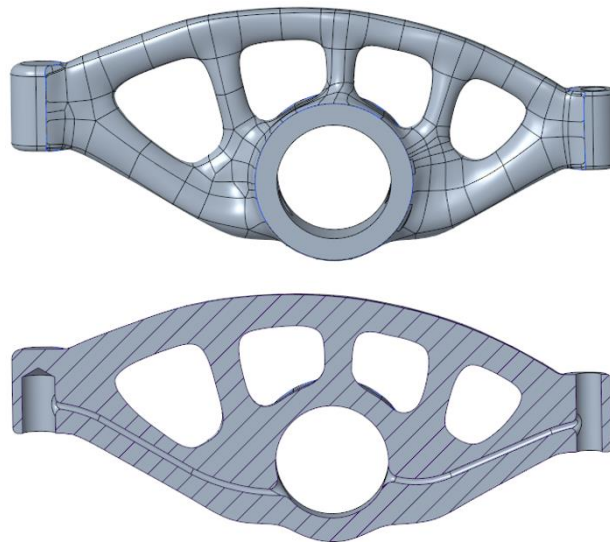


Figure 62. Rocker Arm GJS-500-7 external and internal overview.

Avoiding singularities, the results received were within the desired max of 165 MPa given in Table 1 due to fatigue, Figure 63 shows a von mises stress max of 183 MPa which were above the limit.

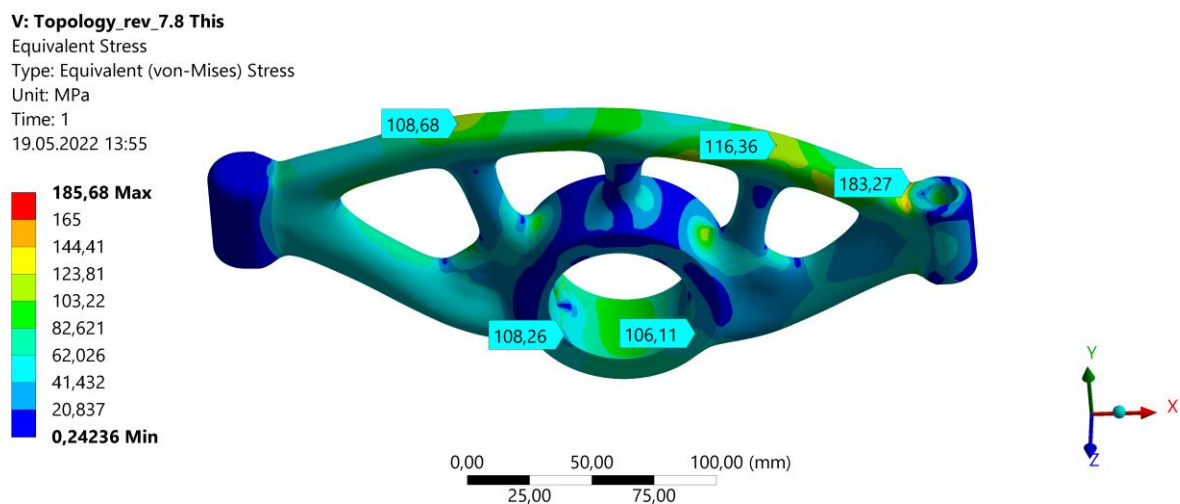


Figure 63. Rocker Arm GJS-500-7 von mises stress

The maximum principal stress is 115 MPa shown in Figure 64, which describes the tension stress in the area, not combined, which is the most important direction and affects fatigue the most. Thus the part is within the accepted limit.

V: Topology_rev_7.8 This

Maximum Principal Stress
 Type: Maximum Principal Stress
 Unit: MPa
 Time: 1
 19.05.2022 13:56

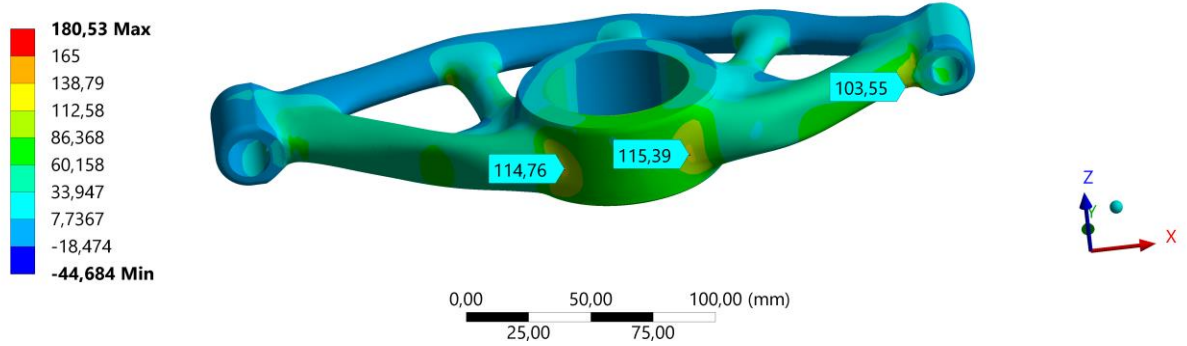


Figure 64. Rocker Arm GJS-500-7 maximum principal stress

Figure 65 shows a minimum principal stress of 189 MPa, this is compression and is less critical than tension, which is considered acceptable.

V: Topology_rev_7.8 This

Minimum Principal Stress
 Type: Minimum Principal Stress
 Unit: MPa
 Time: 1
 19.05.2022 13:56

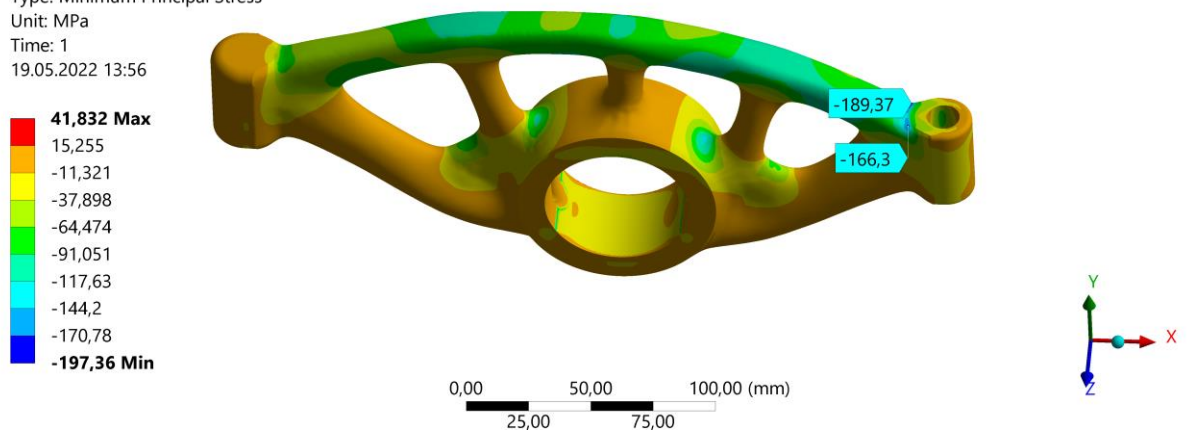


Figure 65. Rocker Arm GJS-500-7 minimum principal stress

The deformation is shown in Figure 66, and has a maximum of 0.286 mm, The new weight of the part is 2.3 Kg, which is a 24% reduction compared to the original part.

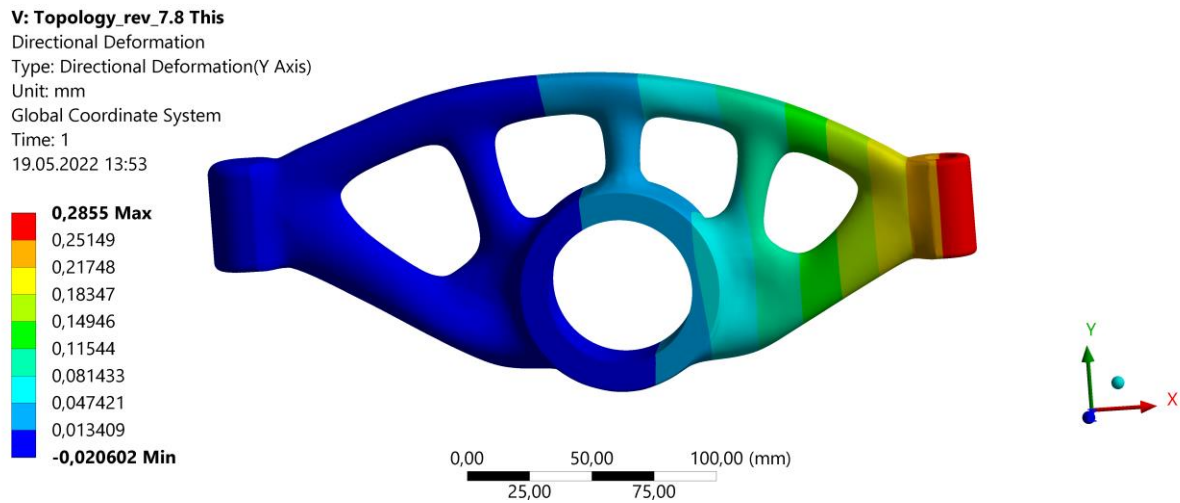


Figure 66. Rocker Arm GJS-500-7 deformation

Rocker Arm Ti-6Al-4V

The optimized part for titanium Ti-6Al-4V was made using a crease radius of 8mm and a material spreading of 47 in generative design. This produced an acceptable result as shown in Figure 67. The part was designed with internal oil channels in a teardrop shape.

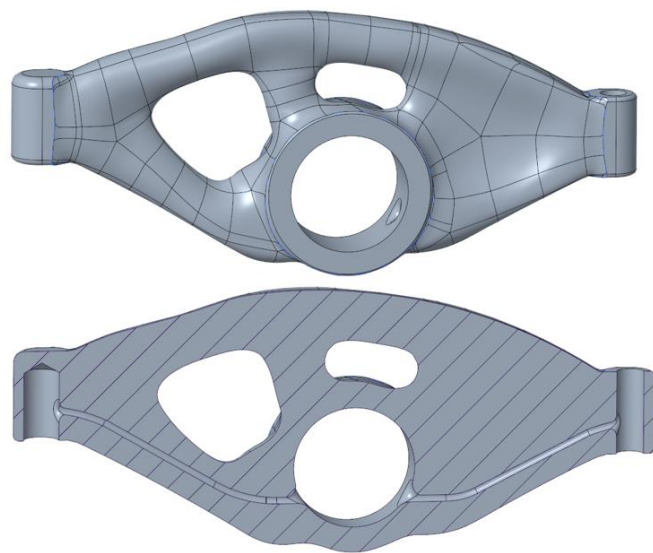


Figure 67. Rocker Arm Ti-6Al-4V titanium external and internal overview.

The Von Mises stress is shown in Figure 68, the maximum values are well within the limits of this material and as shown in Table 1 the fatigue limit is 500 MPa for Ti-6Al-4V. This creates a high safety factor for critical failure of the part. Since this alloy has a low young modulus the deformation is of importance.

AB: Titanium_rev_9_5 This

Equivalent Stress

Type: Equivalent (von-Mises) Stress

Unit: MPa

Time: 1

19.05.2022 13:35

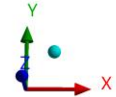
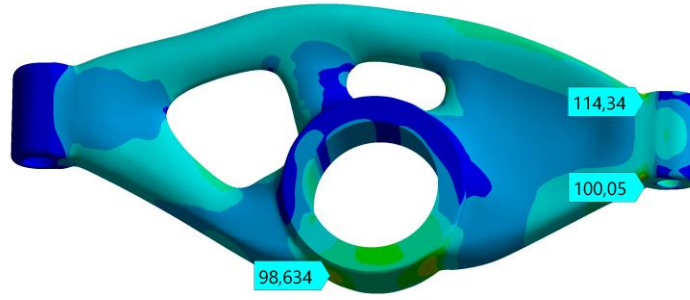
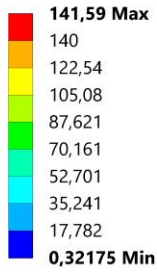


Figure 68. Rocker Arm Ti-6Al-4V von mises stress

From Figure 69 the deflection of the part is 0.32mm and is a bit high. but 0.03mm more deflection than the original should not introduce much latency in the system.

The new weight of the part is 1.8 Kg, which is a weight saving of 40% compared to the original part. Amotool provided an estimated cost of 3225€.

AB: Titanium_rev_9_5 This

Directional Deformation

Type: Directional Deformation(Y Axis)

Unit: mm

Global Coordinate System

Time: 1

19.05.2022 13:35

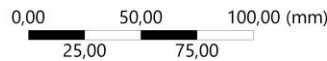
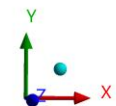
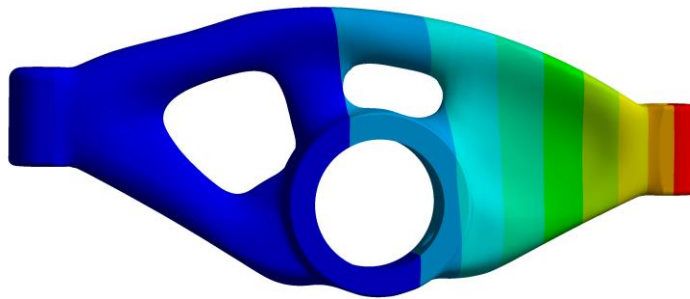
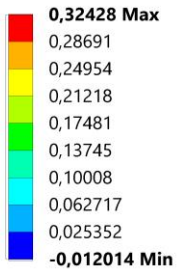


Figure 69. Rocker Arm Ti-6Al-4V deformation

Rocker Arm 316L

The part designed for 316L main limiting factor was the young modulus, and therefore a topology optimisation provided the best results. The design is shown in Figure 70. The part was designed with internal oil channels in a teardrop shape.

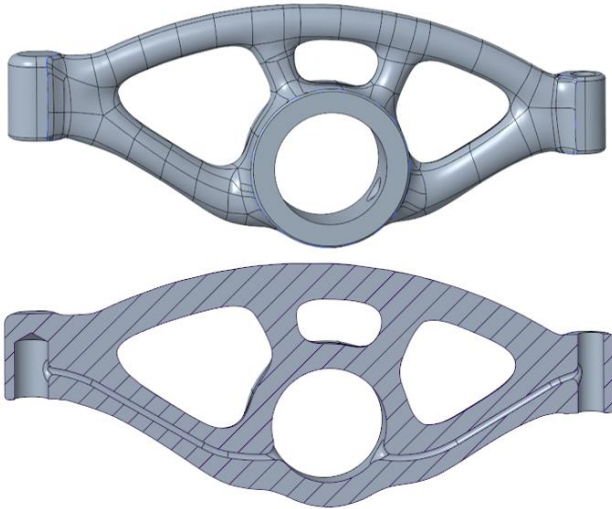


Figure 70. Rocker Arm 316L internal and external overview

The von mises stress is shown in Figure 71 and has a maximum of 174 MPa. This is well within the fatigue value from Table 1 at 340 MPa.

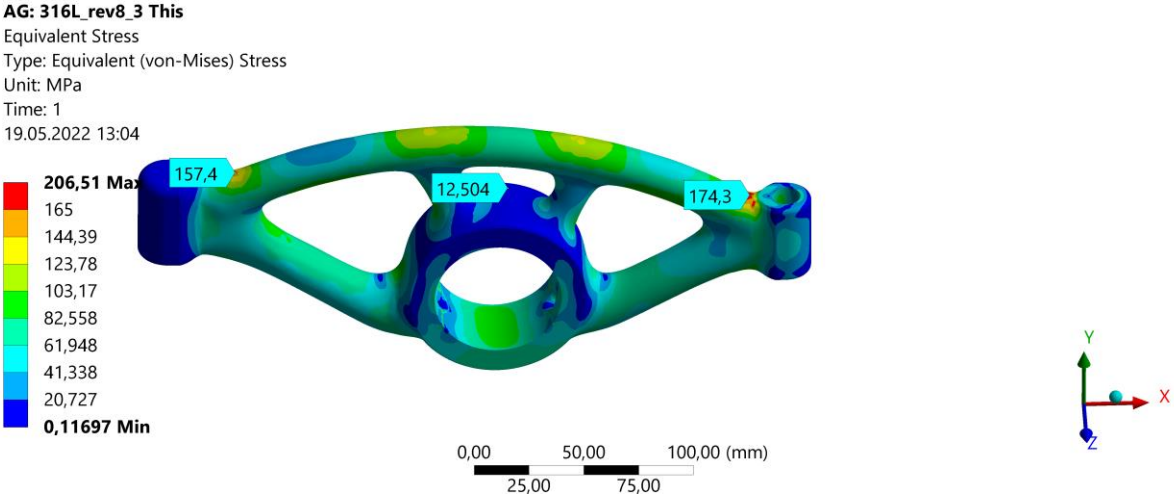


Figure 71. Rocker Arm 316L von mises stress

Figure 72 and Figure 73 confirm that the tension and compression stresses are within the limits as well. The part has a mass of 2.34 Kg. This is a reduction in weight of 21% while keeping the stresses within acceptable limits.

AG: 316L_rev8_3 This

Maximum Principal Stress
 Type: Maximum Principal Stress
 Unit: MPa
 Time: 1
 19.05.2022 13:03

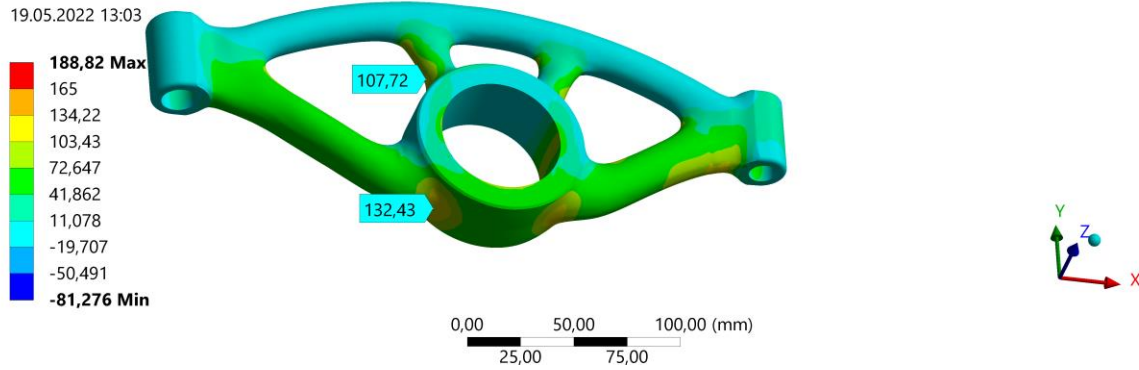


Figure 72. Rocker Arm 316L maximum principal stress

AG: 316L_rev8_3 This

Minimum Principal Stress
 Type: Minimum Principal Stress
 Unit: MPa
 Time: 1
 19.05.2022 13:26

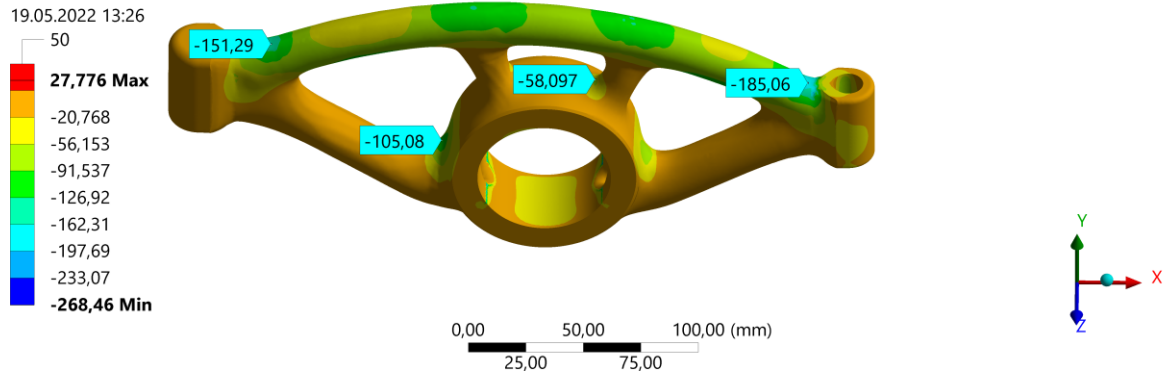


Figure 73. Rocker Arm 316L minimum principal stress

The deflection of the part is shown in Figure 74, the largest deflection is 0.28mm. Amotool provided an estimated cost of 1127€.

AG: 316L_rev8_3 This

Directional Deformation
 Type: Directional Deformation(Y Axis)
 Unit: mm
 Global Coordinate System
 Time: 1
 19.05.2022 13:11

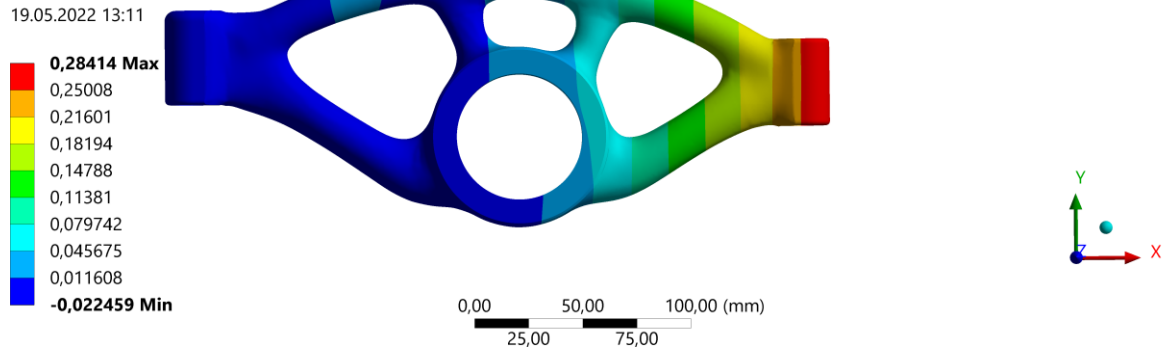


Figure 74. Rocker Arm 316L deformation

5.1.3 Case 3: Toolholder

The Toolholder was designed for TI-6AL-4V as it showed the best performance in the previous parts. From the bodies described in chapter 4.3.2 a topology optimized part was created, and the results are shown in Figure 75.

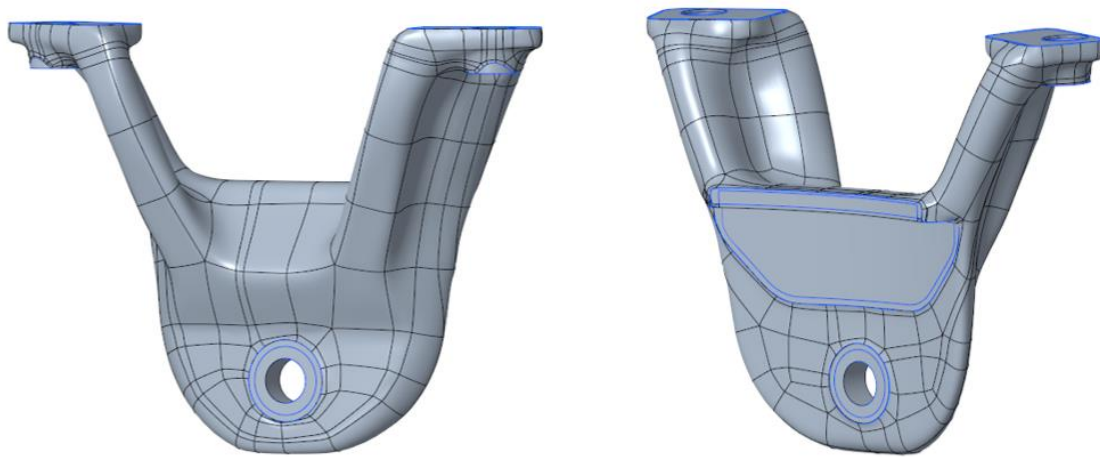


Figure 75. Toolholder Ti-6Al-4V front and back view

The new design reduces mass where it is not needed and distributes the forces onto the surface of the piston rod. The new lip takes up the vertical forces and removes shear forces on the bolt which is preferable. The stress obtained is shown in Figure 76 and Figure 77 and the maximum von mises stress is 633 MPa which is far under the yield strength of titanium described in Table 1.

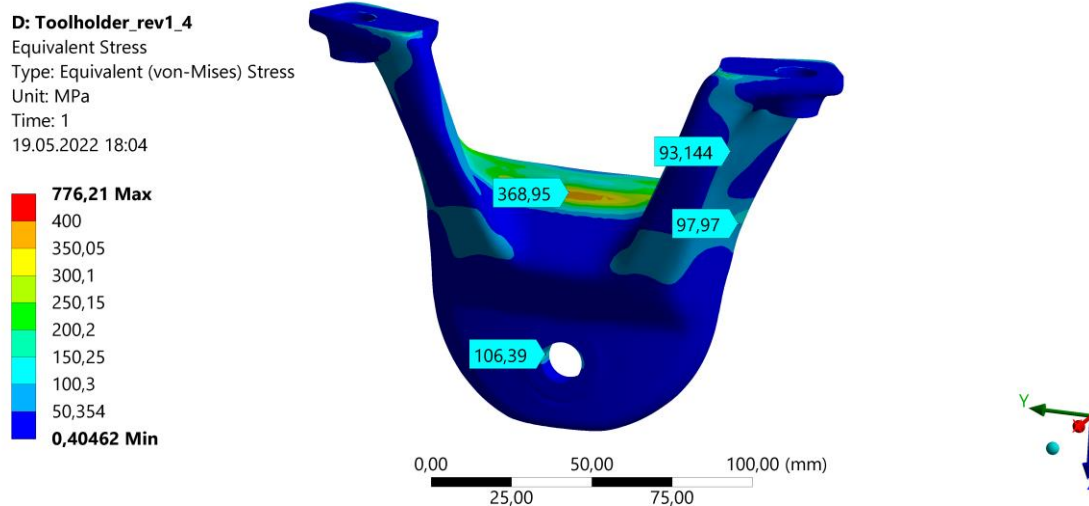


Figure 76. Toolholder Ti-6Al-4V front von mises stress

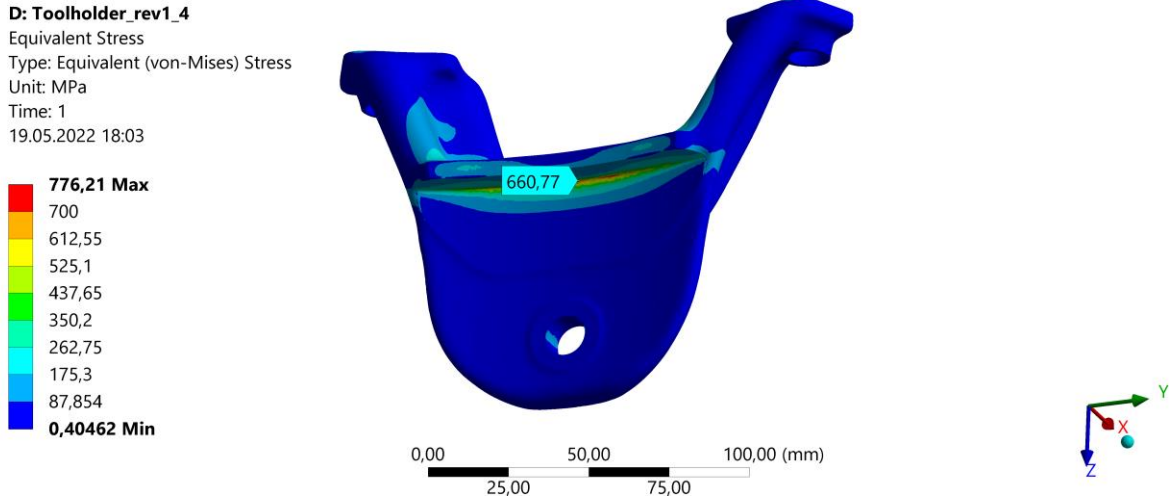


Figure 77. Toolholder Ti-6Al-4V back von mises stress

Deflection is elastic if the forces are below the yield strength, the Figure 78 shows a total deformation of 0.24 mm. The new design weighs 0.63 kg and has a production cost of approximately 1289 € by Amotools calculation. This is a weight reduction of 80%.

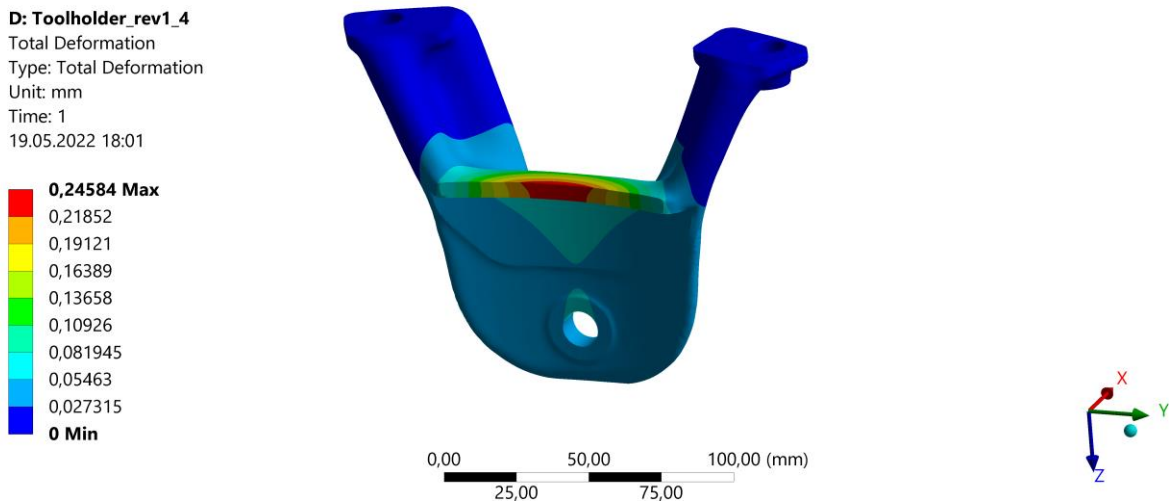


Figure 78. Toolholder Ti-6Al-4V deformation

5.1.4 Case 4: Pressure Indicator valve

The indicator valve was originally redesigned for 316L, but the same model was also tested in Ti-6Al-4V.

Pressure Indicator Valve 316L

Because of the results from the earlier cases and the limited time left, the first redesign was made in 316L as it had great weight reduction while being cheaper than Ti-6Al-4V. The redesigned model shown in Figure 79 shows that even though a lot of material could be removed, a lot was added in the largest bend as well. The redesigned Valve weighs 1.74 kg which is a 23% weight saving compared to the original weight of 2.25 Kg. The 316L version cost 1397 € to produce.

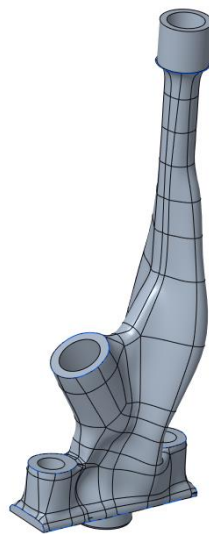


Figure 79. Redesigned Pressure Indicator Valve

The redesigned part showed a maximum equivalent von mises stress of 145 MPa. All the probes seen in Figure 80 are set on the inside of the valve as these stresses were higher than the ones on the outside.

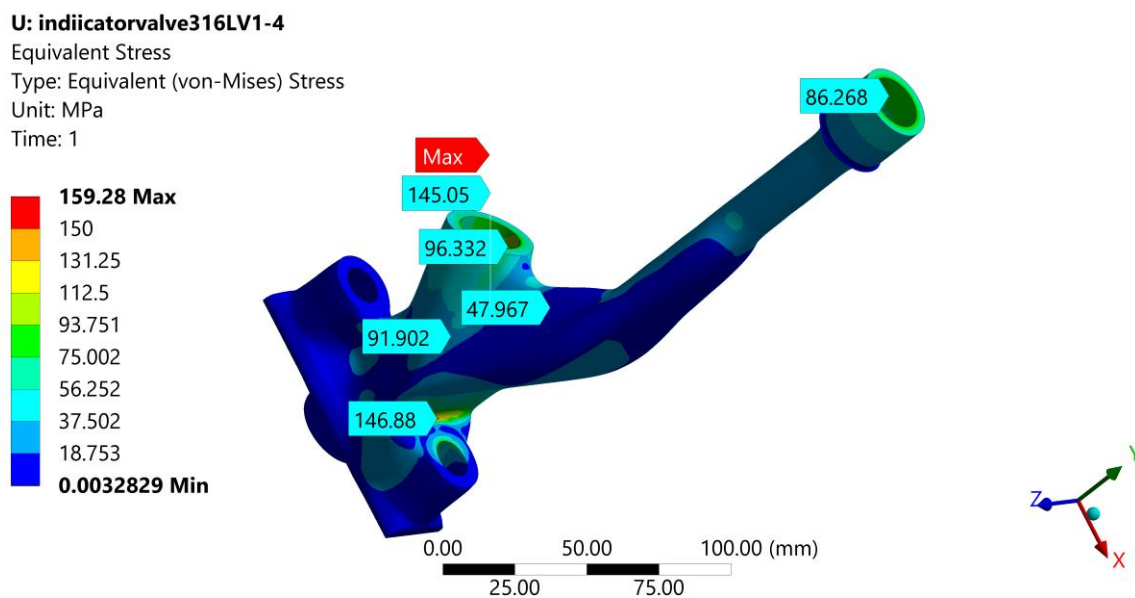


Figure 80. Redesigned Pressure Indicator Valve 316L equivalent von mises stress

The deformation shown in Figure 81 on the new version was 0.19 mm about 0.01 mm less than the original part.

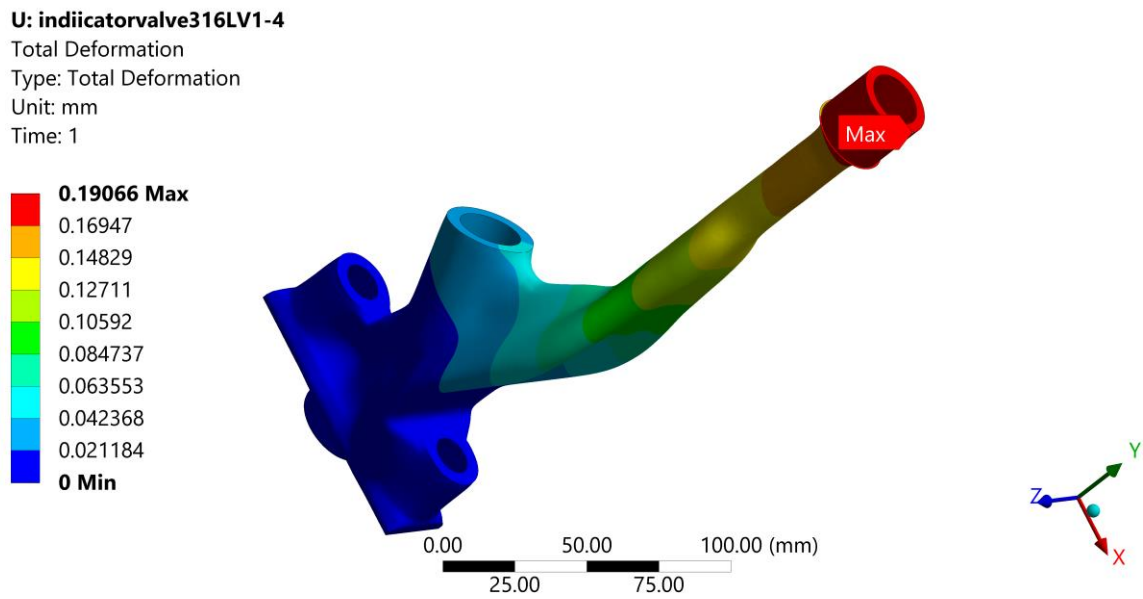


Figure 81. Redesigned Pressure Indicator Valve 316L deformation

Pressure Indicator valve Ti-6Al-4V

Because there was no time to redesign another geometry for Ti-6Al-4V, the model generated for 316L was tested in Ansys with the material properties of Titanium. This part naturally had very similar stresses to the 316L model as can be seen in Figure 82, with the highest stress of 136 MPa. This model was as expected much lighter, and weighed 0.95 kg, which is a weight saving of 58% compared to the original assembly. The Ti-6Al-4V version cost 2120 € to produce.

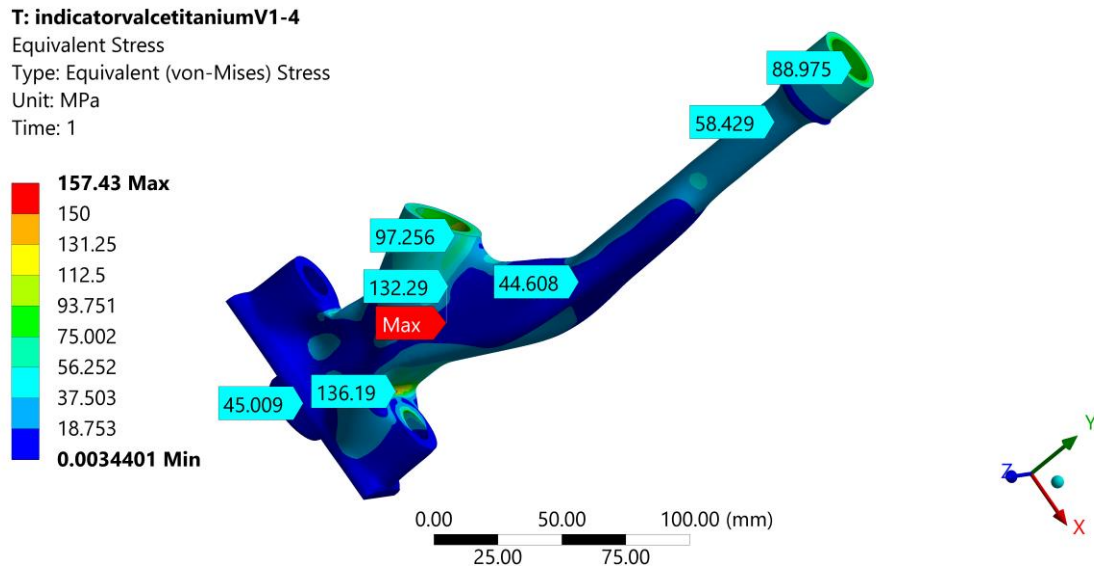


Figure 82. Redesigned Pressure Indicator Valve Ti-6Al-4V von mises stress

The lower Young's modulus naturally leads to a larger deformation of 0.29 mm, as can be seen in Figure 83.

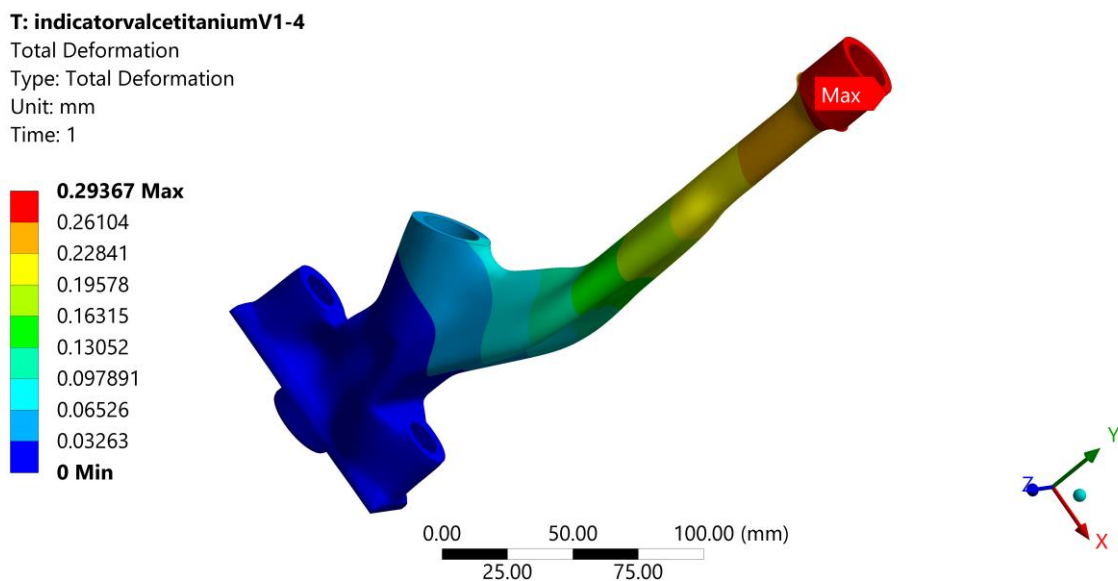


Figure 83. Redesigned Pressure Indicator Valve Ti-6Al-4V deformation

5.2 Experimental test

Because of the complex geometry of the topology optimized parts, it was decided to perform a destructive test on 50% scale plastic models of the parts. These tests we performed on an Instron 8801 linear load stress tester, which provides load and deformation at any given time during the test. As plastics have very different characteristics during a fracture than metals, the goal of these tests is to verify the deflection given a load in Ansys. The test started with calculating the material properties of the plastic with a given set of print settings, this was done with a standard stretch test.

5.2.1 Stretch Test

The plastic used in the tests is Addnorth E-PLA, the material properties provided by the manufacturer are shown in Table 3.

Table 3. Filament Properties from Addnorth

		<i>Standard</i>	<i>Unit</i>	<i>Typical value</i>
<i>Physical properties</i>	Density	ISO 537	g/cc	1.24
<i>Mechanical properties</i>	Tensile strength, Break	ISO 527	MPa	58
	Tensile Modulus	ISO 527	MPa	2870
	Tensile Elongation, Break	ISO 527	%	8
	Flexural Strength	ISO 178	MPa	120
	Flexural Modulus	ISO 178	MPa	3155

(AddNorth, 2022)

Anticipated values from testing using material properties from Table 3, the calculated values are as shown in Table 4.

Table 4. Anticipated test results on test rod given data provided by the manufacturer

<i>Parts</i>	Anticipated Force to break [N]	Anticipated Deflection at break [mm]
<i>Test rod</i>	13 000	1.50

The first test was performed using test rods printed in a horizontal direction, using the same filament and printer as the rocker arm and bracket test parts, mechanical drawings shown in Attachments B. The setup of the test rod can be seen in Figure 84. On the first test, the extensometer was not calibrated correctly, so the deflection on this test is invalid, but the load graphs were identical. The load to yield were lower than the theoretical values, as expected. The values obtained are shown in Table 5.

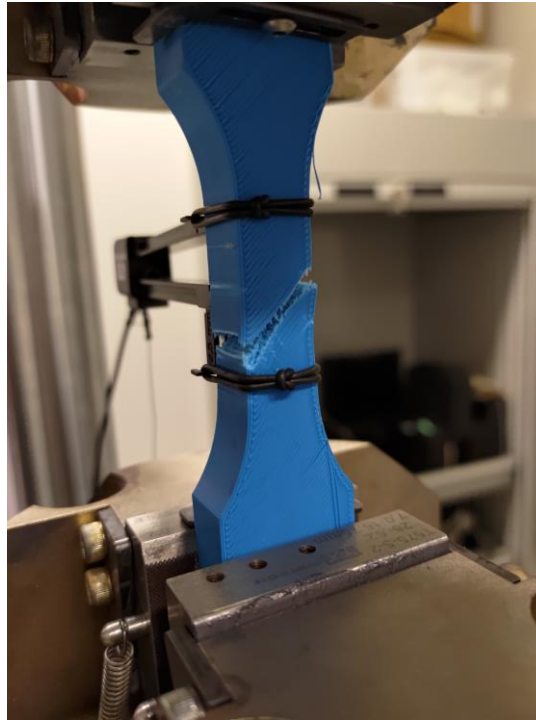


Figure 84. Test rod setup

Table 5. Test result from test rods.

<i>Parts</i>	Applied Force to break [N]	Deflection at yield [mm]
<i>Test rod #1</i>	6 900	N/A
<i>Test rod #2</i>	7 000	2.00

This test provided the information required to create custom real material properties which are used to anticipate the performance of the plastic test parts. The new corrected material properties are shown in Table 6 and were calculated using a MATLAB script written for this thesis, the Stress-Strain curve from the test is shown in Figure 85. Because of the limited time left, the same settings were used on all the prints. If more time was available, testing the mechanical properties of different print settings could give better results. The MATLAB script calculated all the material properties needed, this includes young modulus, yield strength, ultimate strength, real and engineering stress and strain. It also plots the graphs for visualization. The full MATLAB script is available in Attachments A.

Table 6. Adjusted mechanical properties from the test rod data.

	<i>Units</i>	<i>Adjusted Values</i>
<i>Tensile Strength</i>	MPa	31.5
<i>Tensile Elongation, Break</i>	%	15
<i>Young modulus</i>	MPa	2343

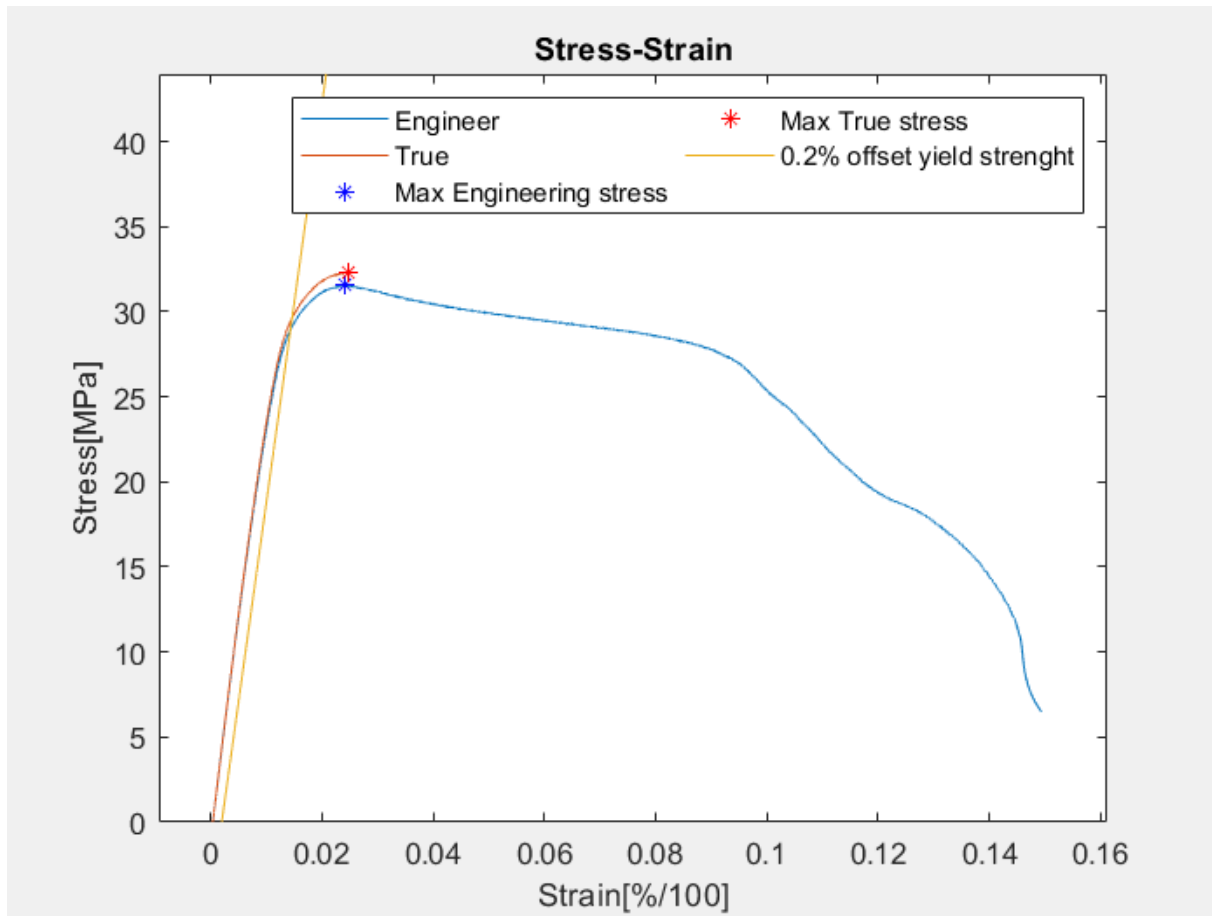


Figure 85. Stress-strain plot of test rods

5.2.2 Estimated results

Given these corrected values of material properties, new strength limits of the parts were estimated using ANSYS, the new anticipated values are shown in Table 7.

Table 7. Theoretical forces to break with the adjusted mechanical properties.

<i>Parts</i>	Anticipated Force to Break [N]	Anticipated Deflection at yield [mm]
<i>Original Rocker Arm</i>	1250	1.78
<i>Rocker Arm 316L</i>	775	1.45
<i>Original Bracket</i>	1300	0.40
<i>Bracket 316L</i>	1100	0.39

5.2.3 Test Set-up

During the test of the rocker arm and bracket, they were set up using custom made parts to make it possible to apply forces in the most realistic direction. These parts were made of steel as they needed to be stiff enough so that the extra deflection is negligible to the test results themselves.

The Rocker Arm support mechanism was made using a plasma cutter to create specific plates, which were welded together to create a holding tool, the part is mounted to the tool using a shaft turned in a lathe, the mechanical drawings are shown in Attachments D. It has a rod preventing movement around its axis counterclockwise. The force is applied downwards by a plate onto a bolt in the part, this is shown in Figure 86 (Left).

For the bracket, a plate with threads was made for mounting. A shaft was created with a radial groove to use a pulling plate on. The plate pulling had a cylindrical hole, to be able to apply force upwards in the groove as shown in Figure 86 (Right). Drawings for the test rig is available in Attachments C.

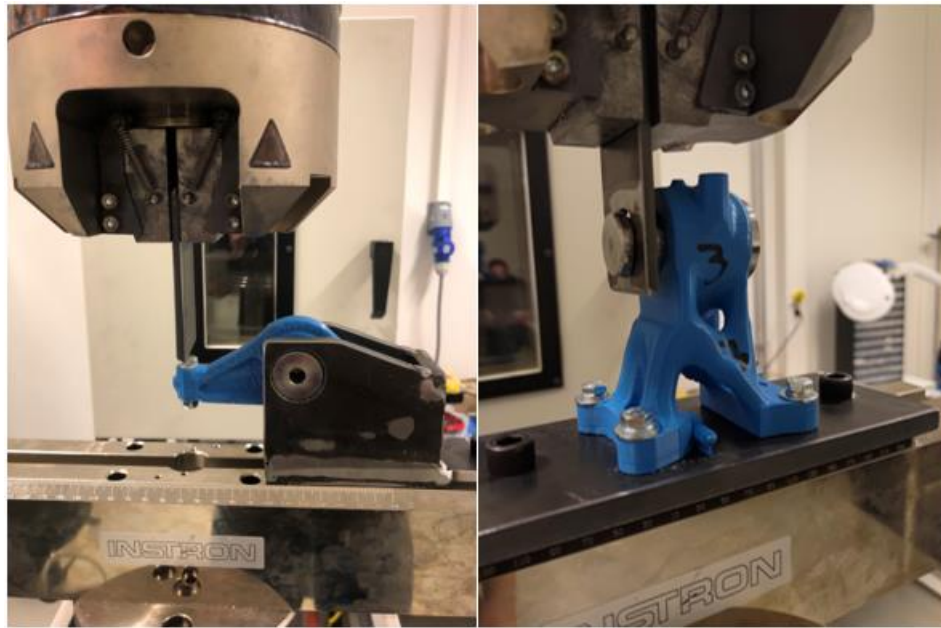


Figure 86. Setup of parts, Rocker Arm (Left) Bracket (Right)

5.2.4 Test results

Most of the test set-up went as planned, there was one issue on Bracket 316L #1 as the machine moved without recording the data, which led to this specific test being invalid. The data received from testing are shown in Table 8.

Table 8. Test results from physical test

<i>Parts</i>	Applied Force to yield [N]	Deflection at yield [mm]
<i>Original Rocker Arm</i>	2070	4.66
<i>Rocker Arm 316L #1</i>	2325	5.44
<i>Rocker Arm 316L #2</i>	2055	4.90
<i>Original Bracket</i>	520	0.55
<i>Bracket 316L #1</i>	N/A	N/A
<i>Bracket 316L #2</i>	900	1.32

The data from the test were also plotted using Excel. The plot of the bracket test can be seen in Figure 87.

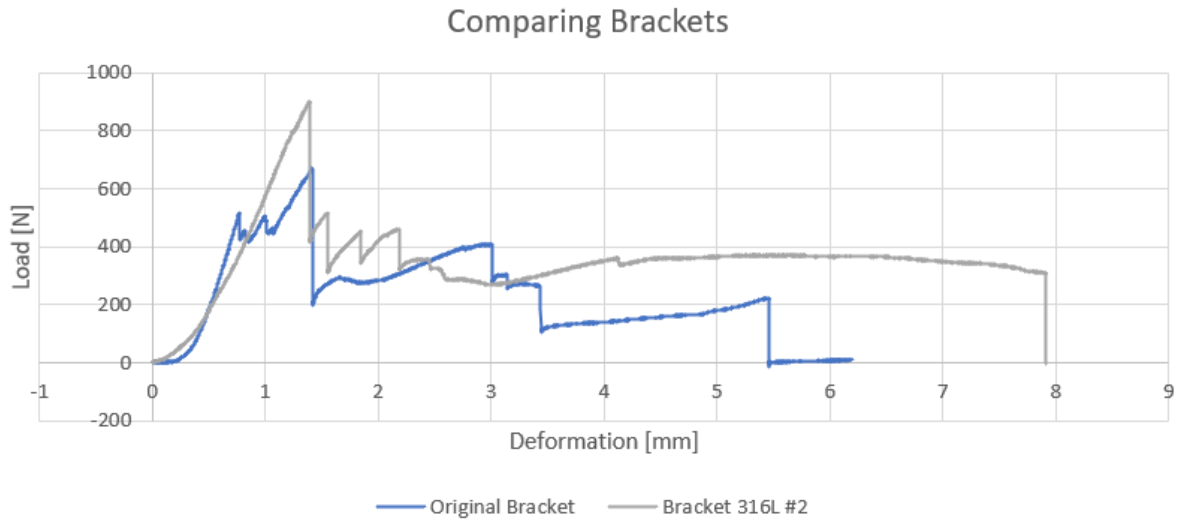


Figure 87. Plot of Bracket tests

The test on the rocker arm was much better, as expected, this can be seen in Figure 88.

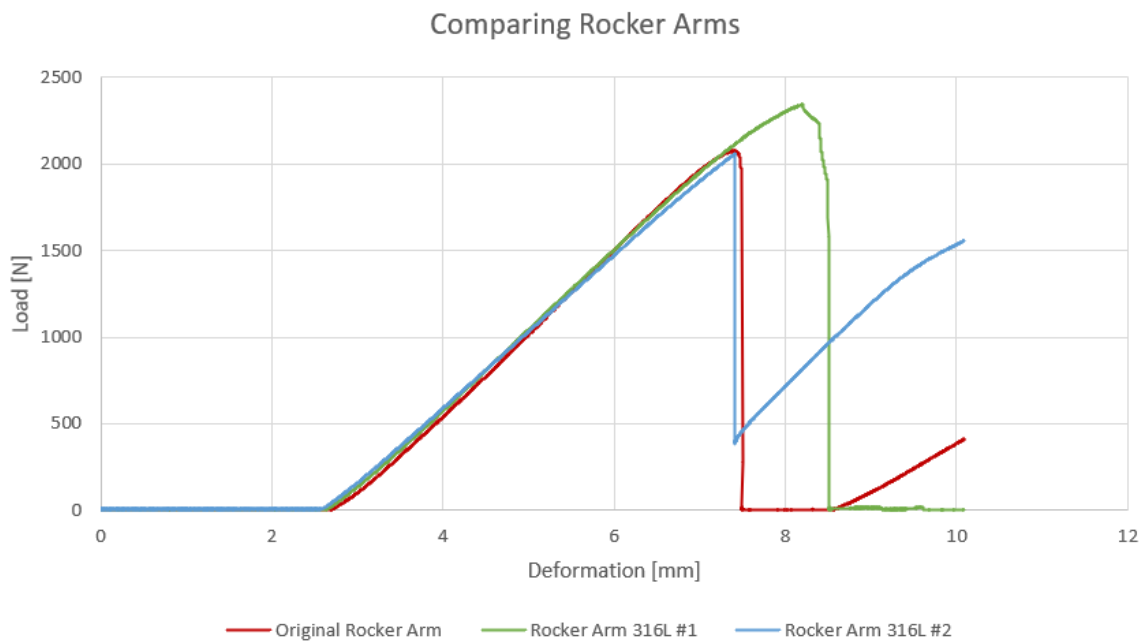


Figure 88. Plot of Rocker Arm tests

After plotting the data received by the tests, it was observed that the deflection on the original rocker arm and the 316L rocker arm were very similar given the same load at which the original rocker arm yielded. As expected, the results were not similar in the bracket. This can be seen in Table 9.

Table 9. Other values of interest obtained

<i>Parts</i>	Applied Force [N]	Deflection [mm]
<i>Rocker Arm 316L #1</i>	2070	4.65
<i>Bracket 316L #2</i>	520	0.86

Because of this, a new Ansys simulation was set up, where the redesigned rocker arm was simulated with a load of 2070, making it possible to compare the physical results with simulated results directly. The result of this analysis can be seen in Table 10.

Table 10. Simulated yield value in ANSYS

<i>Parts</i>	Applied Force [N]	Deflection [mm]
<i>Rocker Arm 316L #1</i>	2070	4.34

The FDM printer method of this test part creates a weakness in the layers of the print direction. This weakness is causing a shear break in the rocker arm, and an opening of layers in the bracket shown in Figure 89 (Right). The weakest points are at the cylindrical feature as shown in Figure 89 (Left).

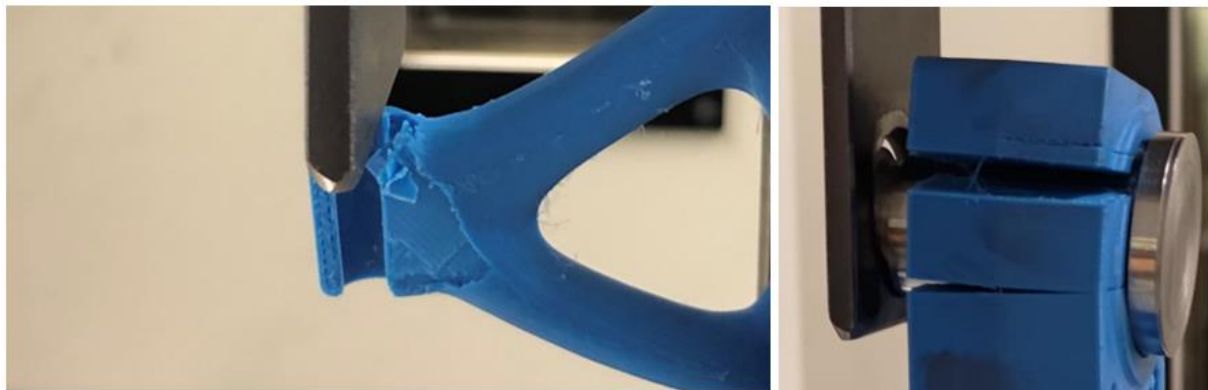


Figure 89. Test fractures, Rocker Arm for 316L (Left), Original Bracket (Right)

5.2.5 Sources of error

The main source of error in the physical tests is that the parts were designed for SLM metal production, and the parts were printed in FDM plastic. This is an issue because of the different characteristics of plastics, and the increased weakness in the print direction compared to SLM. Because of this, it was expected that the Bracket would break earlier than the simulation suggested. Inspecting the broken bracket, it is easy to see that the fracture was straight over a print layer, and not ductile. Another issue was warping in the test “sticks”, because of this, the load might be unevenly distributed in the parts.

The Rocker Arm was printed in a better direction given the force, but it did show signs of buckling before the break, this could have increased the deflection obtained. There was also very poor surface quality in the shaft hole of the bracket, this could dramatically skew the deformation results.

5.3 Discussion

The different case study designs benefited differently from the different materials. The optimal material for each part is discussed below, as well as comparing the properties achieved.

5.3.1 Comparing case 1, Bracket

Looking at the results from the case study shown in Table 11, the weight savings ranged from 40% to 55%. This clearly shows that the original part was poorly optimized, and that additive manufacturing can provide much better parts when combined with topology optimizations.

Table 11. Comparing Bracket properties

<i>Material</i>	<i>Weight [Kg]</i>	<i>Weight Saving [%]</i>	<i>Stress [MPa]</i>	<i>Safety factor</i>	<i>Deflection [mm]</i>	<i>Price [€]</i>
<i>Original</i>	10.62	N/A	95	3.4	0.151	N/A
<i>GJS-500-7</i>	6.38	40	130	2.5	0.124	N/A
<i>316L</i>	5.88	45	142	3.4	0.152	3141
<i>Ti-6Al-4V</i>	4.81	55	122	8.1	0.156	6522

The GJS-500-7 version clearly shows that even when the material used is the same, topology optimization greatly increases the stiffness while removing material at the same time. The 316L version removed 45% of the weight while making a stronger part with a higher safety factor. The Ti-6Al-4V model is the lightest, but considering that the part is over double the price of the 316L and that there is a risk of warping during the printing process, it is not the best version in general.

It is also important to mention that the prices shown in the tables do not include the price of post-processing, as the steering holes under the bracket and the shaft hole need to be machined to tight tolerances not achievable by additive manufacturing. There are also uneven thicknesses on all the parts, so recrystallization of all the parts is recommended to remove all internal stresses.

5.3.2 Comparing case 2, Rocker arm

The different material versions of the Rocker Arm are compared in Table 12, The version for Ti-6Al-4V titanium does save the most weight and has a very large safety factor. The deflection is 0.03mm larger than the original part, this would not increase cycle time much, and would most likely not be critical.

The 316L version was much cheaper to produce, but since the material density is higher than the others the weight savings were not as much as the titanium version. The cost to weight-saving percentage is still best for 316L at 49 € / % compared to 80 € / % for the titanium version.

The redesign in GJS-500-7 did show that just geometry changes would reduce the weight by 24%. With this method.

The limiting factor for most of these materials is the stiffness. If the requirement could be increased in the design, the weight savings of 316L and Ti-6Al-4V could be increased greatly while reducing the volume and cost of production.

Table 12. Comparing Rocker Arm properties

<i>Material</i>	<i>Weight [Kg]</i>	<i>Weight Saving [%]</i>	<i>Stress [MPa]</i>	<i>Safety factor</i>	<i>Deflection [mm]</i>	<i>Price [€]</i>
<i>Original</i>	3.0	N/A	132	2.42	0.29	N/A
<i>GJS-500-7</i>	2.2	23	185	1.73	0.29	N/A
<i>316L</i>	2.3	23	174	2.79	0.28	1127
<i>Ti-6Al-4V</i>	1.8	40	115	8.61	0.32	3225

5.3.3 Comparing case 3, Toolholder

The Toolholder is a tool designed to hold two parts together in a static position. The elastic deflection is not important, this increased the potential for titanium optimized parts greatly, as the young modulus is the limiting factor. The results in this case did provide considerable weight savings, as Table 13 shows the redesign saved 80% weight compared to the original part. For 1289 € or 16.2 € / % which is the lowest cost per weight saved of all the case studies.

Table 13. Comparing the Toolholder properties

<i>Material</i>	<i>Weight [Kg]</i>	<i>Weight Saving [%]</i>	<i>Stress [MPa]</i>	<i>Safety factor</i>	<i>Deflection [mm]</i>	<i>Price [€]</i>
<i>Original</i>	3.18	N/A	132	2.7	0.02	N/A
<i>Ti-6Al-4V</i>	0.63	80	660	1.4	0.24	1289

5.3.4 Comparing case 4, Pressure Indicator Valve

As can be seen in Table 14, using the same geometry in two different materials does not adjust the stresses a lot. However, there is a high increase in the safety factor and the deformation. Because of this, it is only recommended to use the Ti-6Al-4V version if the pressure tests are static, as dynamic loads can cause huge vibrations in the valve.

Table 14. Comparing the Pressure indicator valve properties

<i>Material</i>	<i>Weight [Kg]</i>	<i>Weight Saving [%]</i>	<i>Stress [MPa]</i>	<i>Safety factor</i>	<i>Deflection [mm]</i>	<i>Price [€]</i>
<i>Original</i>	2.25	N/A	107	2.2	0.20	N/A
<i>316L</i>	1.74	23	146	3.3	0.19	1397
<i>Ti-6Al-4V</i>	0.95	58	136	7.3	0.29	2120

It is also important to remember that the redesigned Pressure Indicator Valve lowers the number of parts in the assembly. Originally the assembly consisted of five parts and one sub-assembly, now it is only three parts and one sub-assembly, this makes assembly and logistics easier.

5.3.5 Experimental test result

Given the failed test of one of the brackets and the uncertainty because of the bad surface finish in the shaft hole, it is hard to draw any conclusions about stiffness from that test. However, the test showed that the part fractured in the shaft hole before any of the legs failed, and the redesigned brackets have changed very little around these holes. From this, it can be concluded that the removal of material between the legs did not weaken the structural integrity of the part.

More importantly, the results from the rocker arm test clearly show that the simulations in Ansys are trustworthy. Looking at the rocker arm data from Table 8, Table 9 and Table 10. The load on all parts is 2070 N, and the two physical tests had nearly identical deflections. The original rocker arm and the redesigned rocker arm had a deflection of 4.66 mm and 4.65 mm respectively. The same redesigned rocker arm was simulated in Ansys with the same load of 2070 N and the new material properties from the test had a deflection of 4.31 mm. This clearly shows that the simulations in Ansys are valid even though complicated topology optimized geometry was used.

6. Conclusion

The objective of this thesis was to redesign different parts made for traditional manufacturing so that they can be manufactured with additive manufacturing. The goal was to minimize the weight while keeping the stiffness of the parts. The parts being redesigned were a bracket, a rocker arm, a toolholder, and a pressure indicator valve, all drawings and data needed were provided by Bergen Engines.

Both the advantages and disadvantages of the different technologies and materials available were explored. As most of the parts were subject to cyclic dynamic loads and the fatigue properties of the parts were essential, SLM was selected as the best manufacturing method. Because of the low Young's modulus of Ti-6Al-4V, case studies were performed where the different materials were used in Creo's Generative Design tool. The general rules when designing for additive manufacturing were applied to all the new parts. Issues and limitations due to bugs in Creo Generative were discussed and solutions to these bugs were proposed. Physical tests in plastic were performed and these confirmed the accuracy of the Ansys simulations.

All the parts were lighter and had higher safety factors when being designed in Ti-6Al-4V, but the prices were almost double that of the 316L versions, which still had considerable weight savings compared to the original parts. The weight savings varied from 23 to 80% and prices vary from 1127 to 6522 Euros without post-processing. This shows that while one can obtain a major increase in performance, it is still a very costly manufacturing method.

For future projects, we would recommend looking at parts where lattices are more applicable, as this would lead to new challenges and learning outcomes.

List of figures

Figure 1. Michell structure (Picelli, 2015)	6
Figure 2. 2D Cell shapes	8
Figure 3. 3D Cells shapes.....	8
Figure 4. Rocker Arm design with lattice	9
Figure 5. Example mimicking Michell structure.....	9
Figure 6. Generative Design options	10
Figure 7. Different boundary conditions in Creo	10
Figure 8. Generative Design options	11
Figure 9. Generate options in Generative Design	12
Figure 10. Original Bracket.....	13
Figure 11. Bracket moment and bearing load	14
Figure 12. Bracket bolt pretention.....	14
Figure 13. Bracket friction surface.....	15
Figure 14. Original Bracket oil channel	15
Figure 15. Original Bracket von mises stress	16
Figure 16. Original Bracket maximum principal stress.....	16
Figure 17. Original Bracket deformation	16
Figure 18. Starting geometry of bracket, based on negative step file of free space.	17
Figure 19. The original conserved geometry, this was too complicated to generate.....	18
Figure 20. Bottom face of the available space	18
Figure 21. Initial results of generative design (Left). Fix to "seed" the geometry flow (Right).	19
Figure 22. Cut outs of sharp corners on the edges of the bracket feet.....	20
Figure 23. Design criteria used on redesigned Bracket.....	20
Figure 24. The internal oil channel is marked in red (Left). Notice the teardrop shape in the horizontal part of the channel (Right).....	21
Figure 25. The hollowing out of the bottom of the bracket.....	22
Figure 26. Rocker Arm boundaries	23
Figure 27. Original Rocker Arm highest stress	23

Figure 28. Original Rocker Arm von mises stress	24
Figure 29. Original Rocker Arm maximum Principal Stress	24
Figure 30. Original Rocker Arm deflection	25
Figure 31. Rocker Arm preserved geometry	26
Figure 32. Rocker Arm starting geometry.....	26
Figure 33. The slanted design of the Original Rocker Arm	27
Figure 34. Cross-section of Rocker Arm 316L, teardrop-shaped internal oil channel.....	27
Figure 35. Original Toolholder overview.....	28
Figure 36, Original Toolholder exploded view	28
Figure 37. Original Toolholder boundaries	29
Figure 38. Original Toolholder von mises stress.....	29
Figure 39. Original Toolholder total deformation.....	30
Figure 40. Toolholder starting geometry (Left). Toolholder preserved geometry (Right).....	30
Figure 41. Original Pressure Indicator Valve exploded assembly	31
Figure 42. Pressure Indicator Valve boundary conditions	32
Figure 43. Original Pressure Indicator Valve von mises stress	32
Figure 44. Original Pressure Indicator Valve deformation	33
Figure 45. Pressure Indicator Valve starting geometry	34
Figure 46. Pressure Indicator Valve conserved geometry	34
Figure 47. Bracket GJS-500-7.....	35
Figure 48. Bracket GJS-500-7 von mises stress.....	36
Figure 49. Bracket GJS-500-7 maximum principal stress.....	36
Figure 50. Bracket GJS-500-7 alternative load case maximum principal stress	37
Figure 51. Bracket GJS-500-7 deformation	37
Figure 52. Bracket 316L.....	38
Figure 53. Bracket 316L von mises stress.....	39
Figure 54. Bracket 316L maximum principal stress	39
Figure 55. Bracket 316L deformation	40

Figure 56. Bracket 316L maximum principal stress alternative load case	40
Figure 57. Bracket Ti-6Al-4V	41
Figure 58. Bracket Ti-6Al-4V von mises stress	42
Figure 59. Bracket Ti-6Al-4V maximum principal stress	42
Figure 60. Bracket Ti-6Al-4V deformation.....	43
Figure 61. Bracket Ti-6Al-4V alternative load maximum principal stress	43
Figure 62. Rocker Arm GJS-500-7 external and internal overview.....	44
Figure 63. Rocker Arm GJS-500-7 von mises stress	44
Figure 64. Rocker Arm GJS-500-7 maximum principal stress	45
Figure 65. Rocker Arm GJS-500-7 minimum principal stress.....	45
Figure 66. Rocker Arm GJS-500-7 deformation	46
Figure 67. Rocker Arm Ti-6Al-4V titanium external and internal overview.....	46
Figure 68. Rocker Arm Ti-6Al-4V von mises stress.....	47
Figure 69. Rocker Arm Ti-6Al-4V deformation	47
Figure 70. Rocker Arm 316L internal and external overview.....	48
Figure 71. Rocker Arm 316L von mises stress	48
Figure 72. Rocker Arm 316L maximum principal stress	49
Figure 73. Rocker Arm 316L minimum principal stress.....	49
Figure 74. Rocker Arm 316L deformation.....	49
Figure 75. Toolholder Ti-6Al-4V front and back view	50
Figure 76. Toolholder Ti-6Al-4V front von mises stress	50
Figure 77. Toolholder Ti-6Al-4V back von mises stress	51
Figure 78. Toolholder Ti-6Al-4V deformation	51
Figure 79. Redesigned Pressure Indicator Valve	52
Figure 80. Redesigned Pressure Indicator Valve 316L equivalent von mises stress.....	52
Figure 81. Redesigned Pressure Indicator Valve 316L deformation.....	53
Figure 82. Redesigned Pressure Indicator Valve Ti-6Al-4V von mises stress.....	54
Figure 83. Redesigned Pressure Indicator Valve Ti-6Al-4V deformation	54

Figure 84. Test rod setup 56

Figure 85. Stress-strain plot of test rods 57

Figure 86. Setup of parts, Rocker Arm (Left) Bracket (Right) 58

Figure 87. Plot of Bracket tests 59

Figure 88. Plot of Rocker Arm tests 59

Figure 89. Test fractures, Rocker Arm for 316L (Left), Original Bracket (Right) 60

List of tables

Table 1. Comparison of different alloys for additive manufacturing.....	4
Table 2. Simulation results of original STEP file Rocker Arm.....	25
Table 3. Filament Properties from Addnorth	55
Table 4. Anticipated test results on test rod given data provided by the manufacturer.....	55
Table 5. Test result from test rods.	56
Table 6. Adjusted mechanical properties from the test rod data.	56
Table 7. Theoretical forces to break with the adjusted mechanical properties.....	57
Table 8. Test results from physical test.....	58
Table 9. Other values of interest obtained.....	60
Table 10. Simulated yield value in ANSYS	60
Table 11. Comparing Bracket properties.....	61
Table 12. Comparing Rocker Arm properties	62
Table 13. Comparing the Toolholder properties	62
Table 14. Comparing the Pressure indicator valve properties.....	63

References

- AddNorth. (2022, april 29). *Technical data sheet*. Retrieved from Addnorth.fi/en:
<https://addnorth.fi/product/E-PLA/E-PLA%20-%201.75mm%20-%2020750g%20-%20Aurora%20Green>
- Desu, R. &. (2015). *Mechanical properties of Austenitic Stainless Steel 304L and 316L at elevated temperatures*. Journal of materials ressearch ang technology.
- Diegel, O., Nordin, A., & Motte, D. (2020). *A Practical Guide to Design for Additive Manufacturing*. Singapore: Springer.
- Dijkkamp. (2022, march 17th). www.dijkkamp.nl/en. Retrieved from Dijkkamp:
<https://www.dijkkamp.nl/en/materials/ggg50-en-gjs-500-7/>
- Fábio Gustavo Lima Pereiraa, J. M. (2018). *Fracture Behavior and Fatigue Performance of Inconel 625*. Norte, Brasil: bInstituto Federal de Educação Ciência e Tecnologia do Rio Grande do Norte.
- Galinak Asperovicha, J. H. (2015). *Improvement of fatigue resistance and ductility of TiAl6V4 processed by selective laser melting*. Kaiserslautern: ScienceDirect.
- Mauro M. de Oliveira, A. A. (2018). *Mechanical Behavior of Inconel 625 at elevated temperatures*. MDPI.
- Picelli, R. (2015, October). *Researchgate*. Retrieved from
https://www.researchgate.net/figure/Example-of-Michell-structure_fig4_286456911
- Picelly, R. (2022, april 29). *researchgate.net*. Retrieved from researchgate.net:
https://www.researchgate.net/figure/Example-of-Michell-structure_fig4_286456911
- Rakish Shrestha, J. S. (2021). *Fatigue behavior of additive manufactured 316L*. Auburn: ScienceDirect.
- Shunyu Liu, Y. C. (2019). *Additive manufacturing of Ti6Al4V alloy: A review*. Lafayette: ScienceDirect.
- Toyserkani, E., Sarker, D., Ibhadode, O. O., Liravi, F., Russo, P., & Taherkhani, K. (2022). *Metal Additive Manufacturing*. New Jersey: Wiley.
- Villa, S. D. (2019). *Machinability Evaluation of Ti-48Al-2Nb-0.7Cr-0.3Si in Finishing Operations by Milling*. Porto: Faculty of Engineering of the University of Porto-FEUP.
- Zhihua Tian, C. Z. (2019). *A Review on Laser Powder Bed Fusion of Inconel 625*. Shanghai: Shanghai Key Laboratory of Digital Manufacture for Thin-Walled Structures, School of Mechanical.

Attachments

A. MatLab Code for Stretch test

27/05/22 16:53 C:\Users\Marcus\Des...\ProevestavPLA.m 1 of 2

```

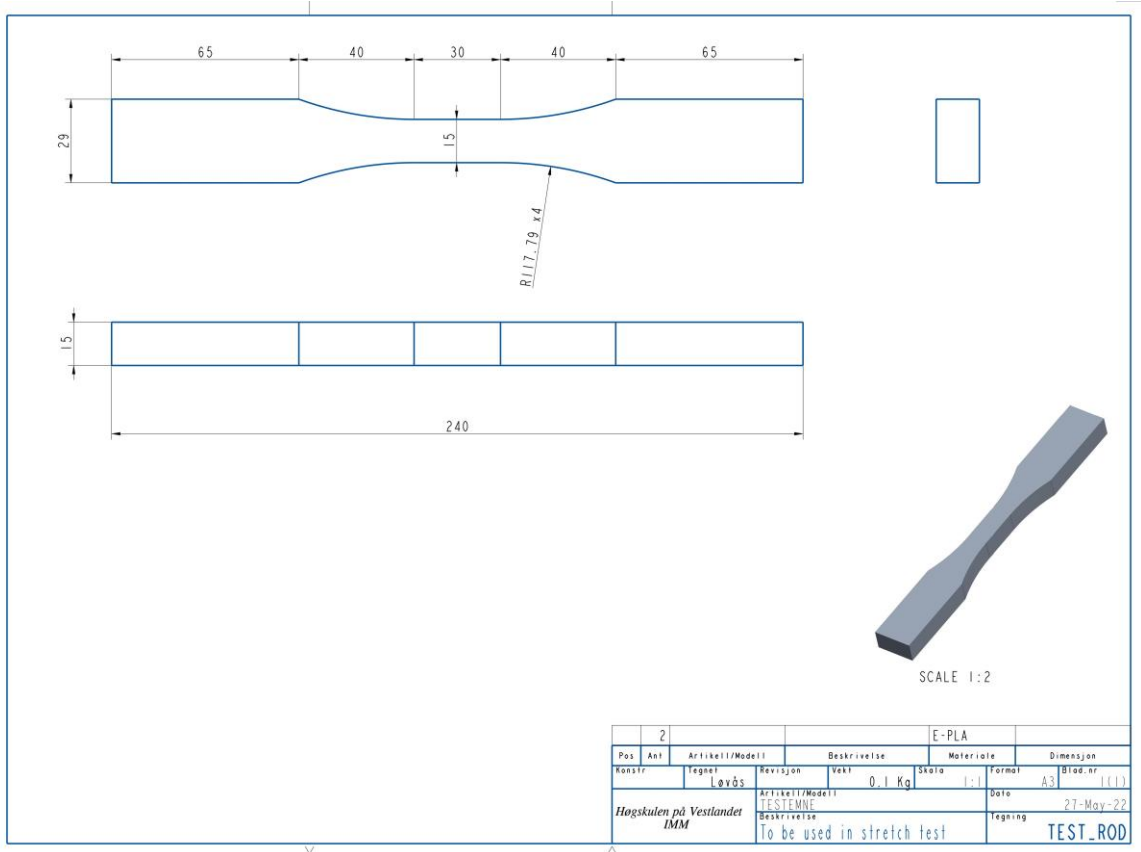
1 clear all
2 data=readtable("Testrod2v2.csv") ;
3
4 tidt = data(:,1);
5 lastt = data(:,2);
6 distanset = data(:,3);
7 lengdet = data(:,4);
8 tid=table2array(tidt);
9 last=table2array(lastt);
10 distanse=table2array(distanset);
11 lengde=table2array(lengdet);
12 startlengde=25.;
13 lengdetot=lengde+startlengde;
14
15 dybde=15; %Fyll inn
16 bredde=15 ; %Fyll inn
17 areal0=dybde*bredde; %Verifiser
18 deltalengde=[lengdetot-startlengde];
19 toeyning=[deltalengde./startlengde];
20 spenning=[last/areal0];
21 sannspenning=[spenning.*(1+toeyning)];
22 sanntoeyning=[log(1+toeyning)];
23
24
25 hold off
26 plot(toeyning,spenning,'DisplayName','Engineer');
27 hold on
28 sannspenningx=(~sannspenning==0);
29 sanntoeyningx=(~sanntoeyning==0);
30 sannspenning(4211:13387)=[] ; % sannspenning og toeyning er ikke gyldig etter
yield
31 sanntoeyning(4211:13387)=[] ;
32 sannspenningx(4211:13387)=[] ;
33 sanntoeyningx(4211:13387)=[];
34 plot(sanntoeyning(sanntoeyningx),sannspenning
(sannspenningx),'DisplayName','True')
35 xlabel('Strain[%/100]')
36 ylabel('Stress[MPa]')
37 title('Stress-Strain')
38 axis([0 0.155 0 40]) %situasjonsbestemt
39 plot(0.024238,max(spenning),'b*','DisplayName','Max Engineering stress') %
situasjonsbestemt
40 plot(0.024707,max(sannspenning),'r*','DisplayName','Max True stress') %
situasjonsbestemt
41 lgd = legend;
42 lgd.NumColumns = 2;
43 format shortG
44
45 sannspenning(4211:13387)=0;
46 sanntoeyning(4211:13387)=0;
47
48 %eksporterer resultater til csv-fil
49 tabell=[last lengde deltalengde toeyning spenning sannspenning sanntoeyning];

```

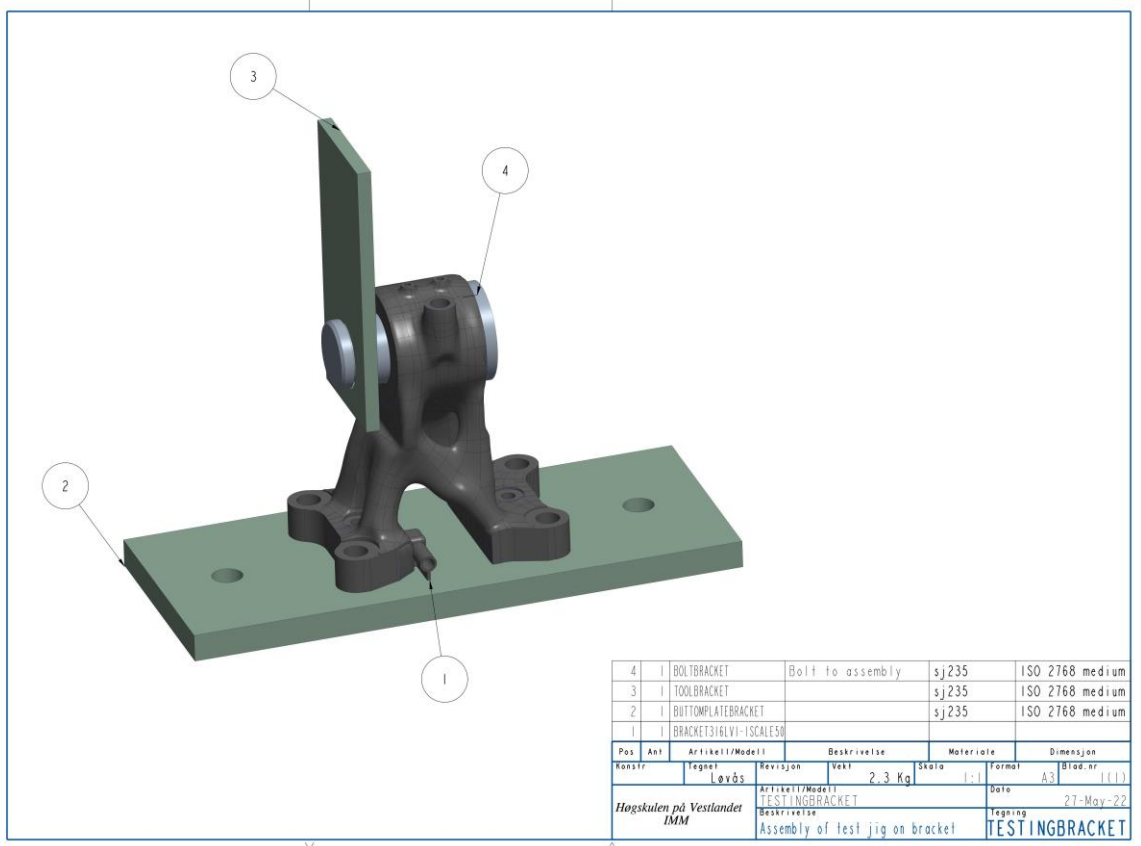
27/05/22 16:53 C:\Users\Marcus\Des...\ProevestavPLA.m 2 of 2

```
50 %T = array2table(tabell,'VariableNames',{'lastN','lengdemm ','deltalengdemm '
','toeyning','spenningMPa ','sannspenning','sanntoeyning'});
51 %writetable(T,'tabellfraplatest.csv')
52
53 %ser på graf når den slutter å være flat
54 emodul1=22.8787/0.0097277; %situasjonsbestemt
55 emodul2=15.0579/0.0061936; %situasjonsbestemt
56 emodul3= 5.3265/0.0023716; %situasjonsbestemt
57 Emodul=(emodul1+emodul2+emodul3)/3
58
59 % forskyver funksjon med Emodul som stigningstall
60 flytegrense0002=[(toeyning)*Emodul-Emodul*0.002];
61 plot(toeyning,flytegrense0002,'DisplayName','0.2% offset yield strenght');
62
63 %Strekfasthet [TS]
64 TS=max(spenning)
```

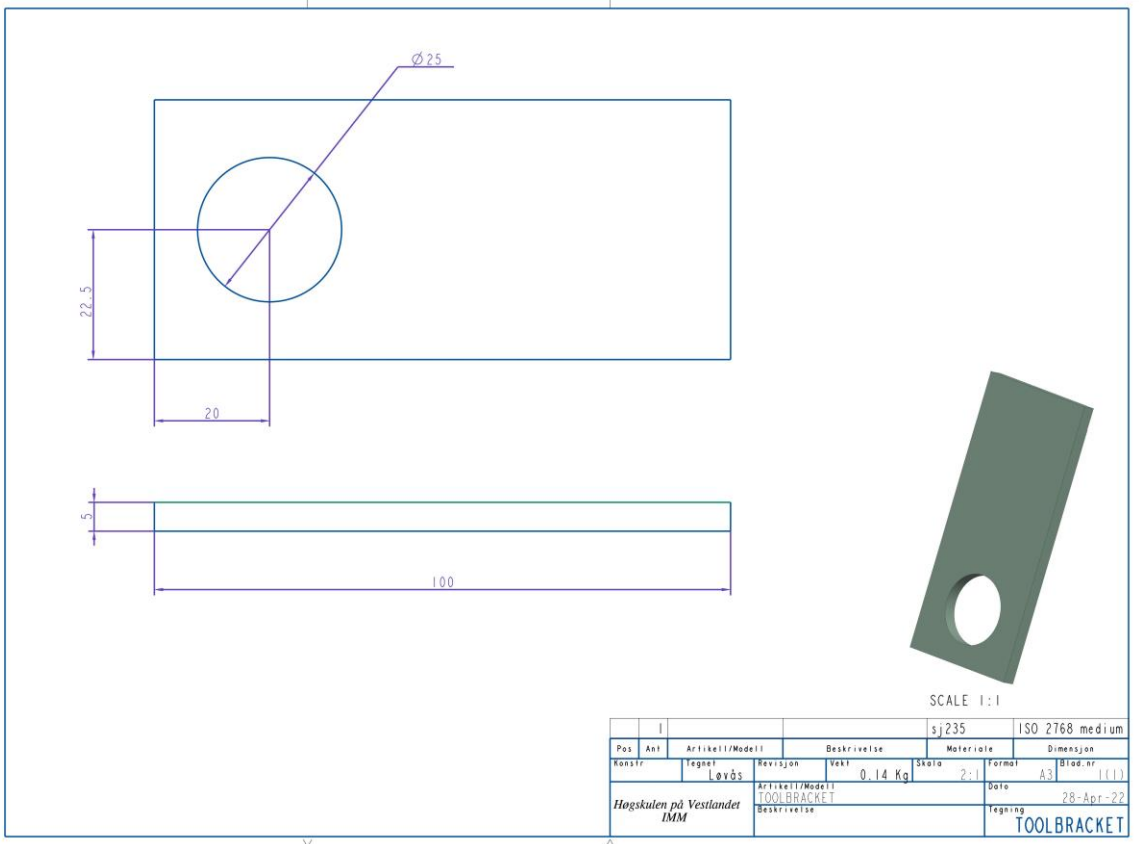
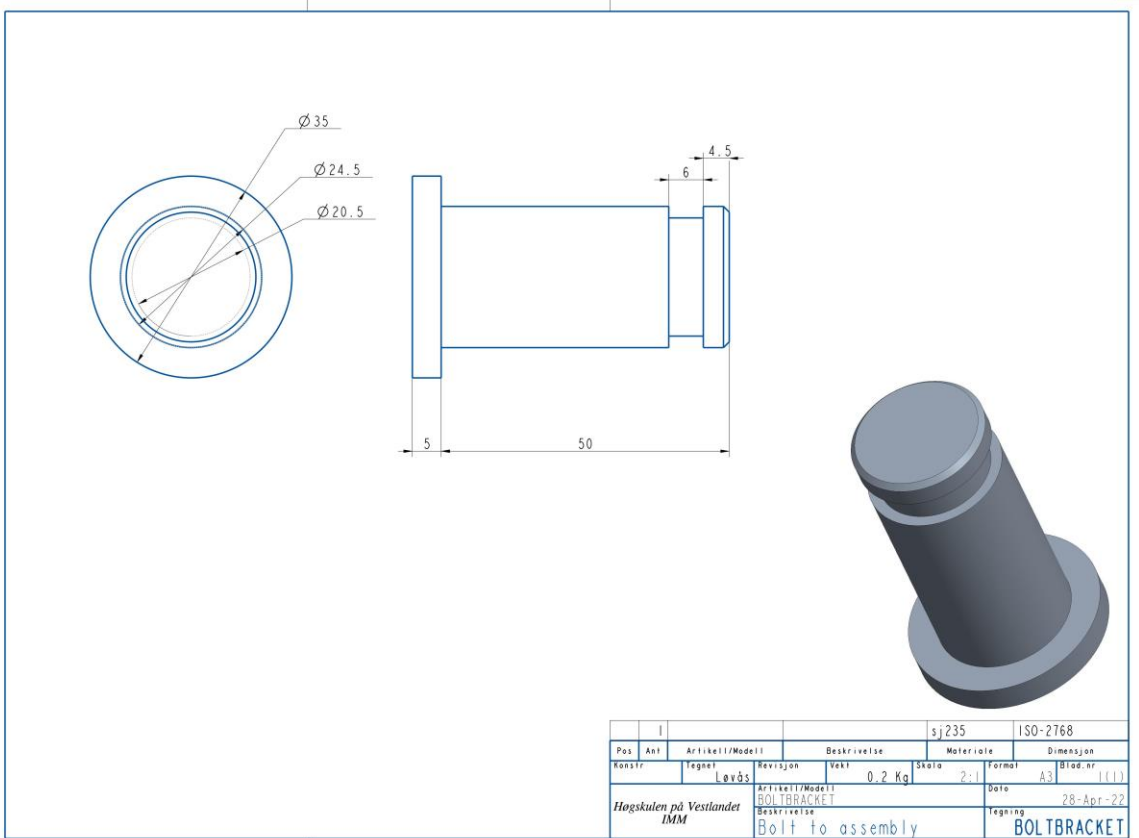

B. Testrod Drawings

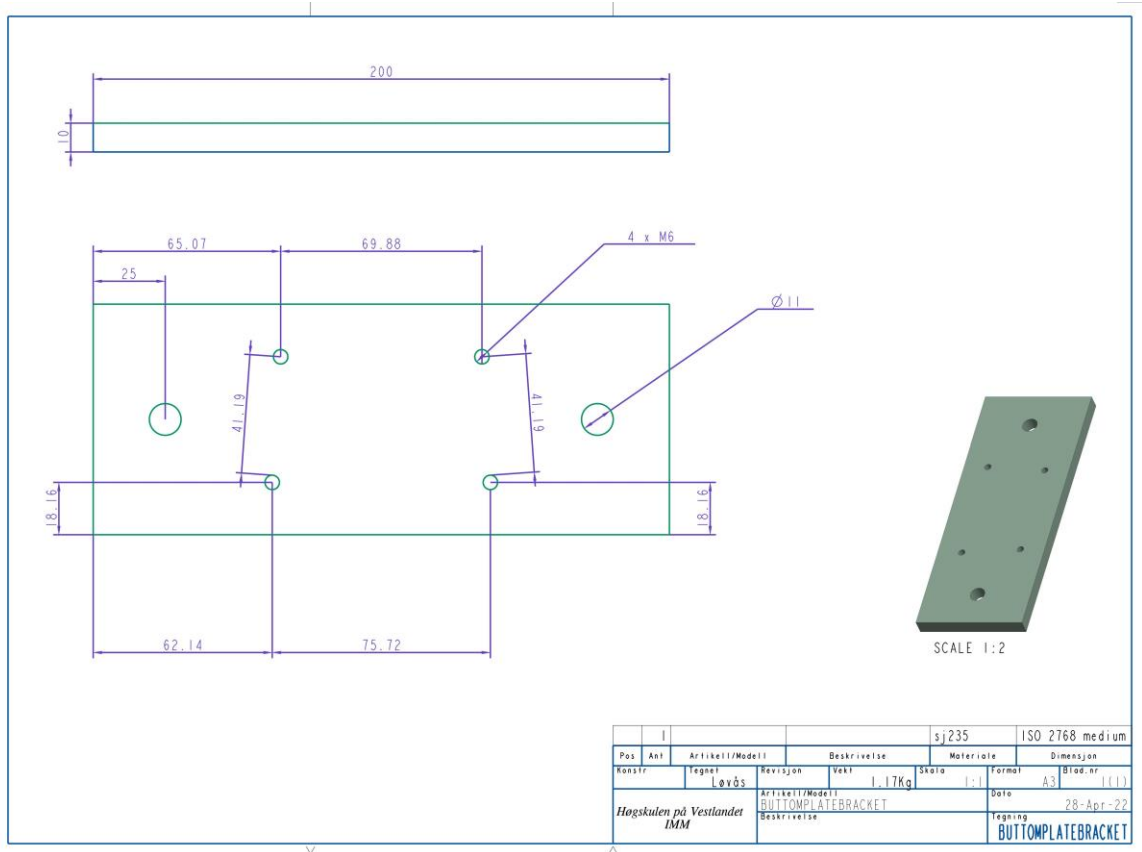


C. Bracket Test Rig Drawings

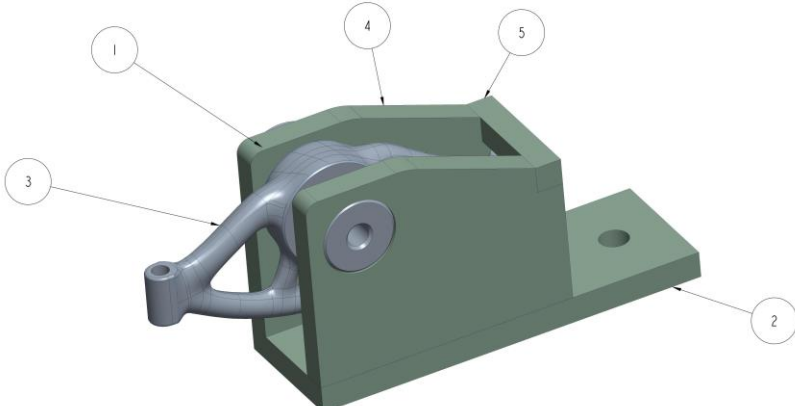


Design for Additive Manufacturing



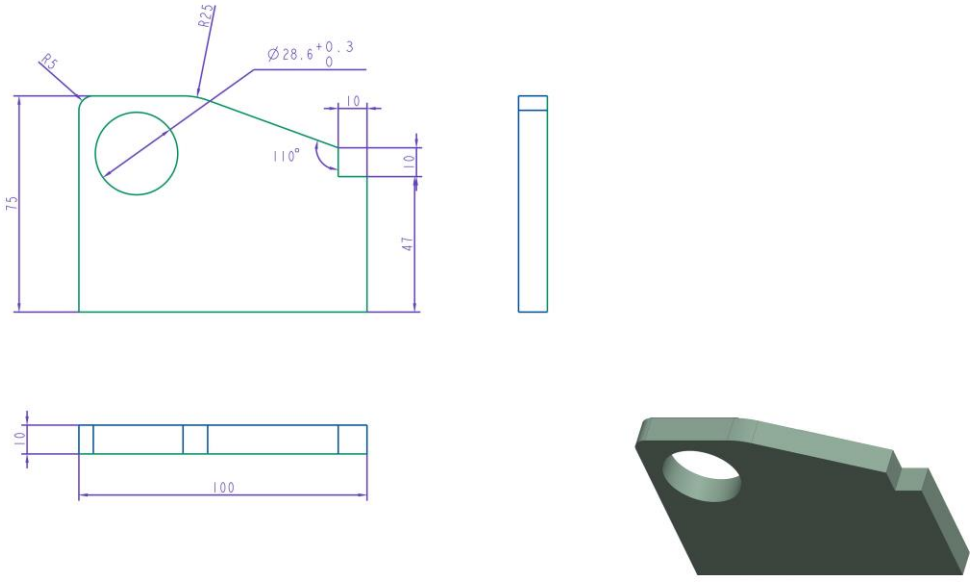


D. Rocker Arm Test Rig Drawings



5	1	TOPPLATE		sj235	ISO 2768	medium
4	2	SIDEPLATE I		sj235	ISO 2768	medium
3	1	ROCKERARM				
2	1	BOTTOMPLATE		sj235	ISO 2768	medium
1	1	BOLT		sj235	ISO 2768	medium

Pos	Ant	Artikkel/Modell	Beskrivelse	Materiale	Dimensjon
Konstr	Tegnet	Revisjon	Vekt	Skala	Formal
	LØVÅS		2,0 Kg	1:1	A3
Høgskulen på Vestlandet		Artikkel/Modell	Beskrivelse	Dato	Blad.nr
IMM		TESTING-ROCKERARM	Jig	28-Apr-22	1(1)
				Tegning	JIG-ROCKERARM



2				sj235	ISO 2768	medium
Pos	Ant	Artikkel/Modell	Beskrivelse	Materiale	Dimensjon	
Konstr	Tegnet	Revisjon	Vekt	Skala	Formal	
	LØVÅS		0,45 Kg	1:1	A3	
Høgskulen på Vestlandet		Artikkel/Modell	Beskrivelse	Dato	Blad.nr	
IMM		SIDEPLATE I		28-Apr-22	1(1)	
				Tegning	SIDEPLATE I	

